DYNAMICS OF POWER SYSTEMS WITH WIND POWER GENERATION AND THE FRACTIONAL FREQUENCY TRANSMISSION SYSTEM

by

JING LI

A thesis submitted to

The University of Birmingham

for the degree of

DOCTOR OF PHILOSOPHY

School of Electronic,

Electrical and System Engineering

University of Birmingham

January 2016

To my parents

ACKNOWLEDGEMENT

First and foremost, I would like to take this opportunity to express my sincere gratitude to my supervisor Prof. Xiao-Ping Zhang. With his invaluable guidance, support and encouragement, I was able to carry on with my research and finally finish this PhD thesis.

I also wish to express my appreciation to my colleagues Dr. Xuan Yang, Dr. Suyang Zhou, Dr. Jingchao Deng, Mr. Jianing Li, Mr. Puyu Wang, Ms. Na Deng, Mr. Zhi Wu, Mr. Ying Xue, Ms. Can Li, Mr. Hao Fu and all my other colleagues in the Power and Control Group for their selfless assistance and support over the last three years.

I am deeply grateful for the Li Siguang Scholarship from the University of Birmingham and the China Scholarship Council (CSC). Through this sponsorship, I have had the chance to pursue my PhD degree here.

Finally, I am indebted to my parents, Mr. Shuyi Li and Ms. Jianying Jing, for their love and unfailing support throughout all my life.

ABSTRACT

Under pressure for low carbon emissions and environmental protection, large scale wind farms are constructed and integrated into power systems to meet energy demands. On the other hand, the long distance transmission for large scale wind power and conventional power plants is another technical issue in modern power systems. These two challenges stimulate the research and development of wind energy and the fractional frequency transmission system (FFTS). With wide utilisation of wind energy and the FFTS, the dynamics of power systems will inevitably be influenced. Thus, the research of this thesis focuses on the small signal stability of power systems with wind generation and the FFTS.

The research of this thesis can be divided into the following three parts:

Firstly, the influence of wind farms on the subsynchronous resonance (SSR) of conventional power systems is systematically examined. Both eigenvalue analysis and time domain simulations are conducted to examine the influence of wind farms from torsional interaction (TI) and the induction generator effect (IGE).

Secondly, the FFTS is proposed to deliver the energy from large scale offshore wind farms. The small signal stability of the FFTS with wind farms is studied. To improve the damping performance of such a system, a proper controller for the FFTS is proposed.

Thirdly, the FFTS is also proposed to be applied in grid interconnections. The application of the FFTS can improve the damping of inter-area oscillations in a multi-area system. Furthermore, the power flow between different areas can also be controlled through the FFTS.

Table of Contents

List of Figures

List of Tables

List of Abbreviations

DDPMG   Direct Drive Permanent Magnet Generator

DFIG   Doubly Fed Induction Generator

EU   European Union

FBM   First Benchmark Model

FFTS   Fractional Frequency Transmission System

HVAC   High Voltage Alternating Current

HVDC   High Voltage Direct Current

IEEE   Institute of Electrical and Electronics Engineering

IGE   Induction Generator Effect

IGR   Intergroup Reactor

PI   Proportional-Integral

RMS   Root Mean Square

SMIB   Single Machine Infinite Bus

SSR   Subsynchronous Resonance

TA   Torsional Amplification

T-G   Turbine-Generator

TI   Torsional Interaction

WF   Wind Farm

WTG   Wind Turbine Generator

CHAPTER 1 INTRODUCTION

1.1 Background and Motivation

1.1.1 Development of Wind Energy

The progress and development of human society boosted the increasing demand for energy. Between 1971 and 2003, the primary energy demand around the world almost doubled, and it is expected to increase by another 40% by 2020 [1]. Currently, most energy consumption is extracted from fossil fuels, which causes air pollution and climate change. In particular, the global warming problem has become one of the greatest issues of concern for governments and civilians in recent years, and the reduction of carbon dioxide emissions has gained broad consensus around the world. Renewable energy, which is environmentally clean and safe, has become a necessary choice for substituting the fossil-based energy. In 2008, the European Union promotion proposed to improve energy efficiency by 20%, reduce greenhouse gas emissions by 20%, and had a target of 20% of energy consumption from renewable energy sources by 2020 [2]. Hence, renewable energy will play an irreplaceable role in energy supply around the world in the future.

In 2012 and 2013, renewable energy contributed 22% of global electricity generation and 19% of overall energy consumption [3]. The sources of renewable energy include

hydropower, solar, biomass, geothermal and wind, etc. The utilisation of hydro power has a long history and currently accounts for the largest share of electricity generation among all the renewable resources. Wave power and tidal power are two relatively new forms of hydropower, and they have not been widely utilised commercially. Solar is another important renewable energy resource, which is abundant and widely distributed around the world. Biomass is derived from living organisms and can be used to provide heat or be converted into other forms of bio-fuel. The geothermal energy is cost effective and clean, but its application is usually limited by geographic locations.

Currently, wind is one of the most popular renewable energy sources around the world. Wind energy is clean and environmentally safe, and more importantly, it can be used easily. With the maturity of wind technology, the world's wind energy capacity has experienced a rapid increase in the last decades. From 1990 to 2005, the wind energy capacity doubled approximately every three years, and 83 countries had applied wind energy on a commercial basis around the world by 2011 [4]. In June 2014, the wind energy capacity around the world had grown rapidly to 336 GW, and it accounts for about 4% of the overall world electricity usage [5]. In the EU, the installed capacity of wind energy reached 128.8 GW, and the electricity produced by installed wind power capacity was enough to cover 10.2% of the electricity consumption [6]. In 2012, the UK ranked as the 6th largest wind producer around the

world [7]. By mid-July 2015, wind power in the UK consisted of 6,536 wind turbines with a total installed capacity of over 13 GW [8]. From the above statistics, it can be anticipated that more and more wind energy will be integrated into the power grids, and thus the dynamics of the existing conventional power systems will inevitably by affected by wind generation.

Due to the low cost and easy installation, wind farms were constructed on land in the early stages. However, better wind energy resources are often located offshore. The sharply increasing consumption of energy and the pressure for low carbon emissions promotes the development of offshore wind farms. Although the construction and maintenance costs of offshore wind farms are considerable higher than those of onshore wind farms, the great potential encourages the further development of offshore wind farms. In many EU countries, the power produced by offshore wind farms comprises a large share of the total power generated by wind energy. In 2008, the UK overtook Denmark to become the world leader of offshore wind energy [9]. The largest offshore wind farm, which consists of 175 wind turbines, is located off the Kent coast in the UK [9]. It is also estimated that the UK has over a third of the offshore wind resources in Europe, and this promises a better future for the utilisation of offshore wind energy in the UK [11].

The wind turbine generators (WTGs) are used to convert the kinetic energy from wind into electricity. At present, there are mainly three popular WTGs: the squirrel cage of

induction generator (SCIG), the doubly-fed induction generator (DFIG), and the direct-driven permanent magnet generator (DDPMG). The above three WTGs can be divided into two categories: the fixed speed WTG and the variable speed WTG. The SCIG belongs to the fixed speed WTG, and the DFIG and the DDPMG are the variable speed WTGs.

Initially, the SCIG was the dominant WTG. In a SCIG, the stator of the induction machine is directly connected to the power grid. As the SCIG is designed to operate at a fixed speed, the maximisation of wind energy capture cannot be achieved. When the SCIG is subjected to a gust of wind, the rotor speed of the induction machine can only change slightly. The range for the rotor speed variation is 1% ~ 2% of the nominal speed. However, the SCIG can be operated at two different rotor speeds if the number of stator pole pairs is changed. Furthermore, SCIG naturally consumes a large amount of reactive power, and additional capacitor banks are needed to maintain the voltage level of the grid.

With the introduction of power electronic controls into the WTG, the speed range of the wind turbine can be extended significantly. The DDPMG is a wide-range variable speed wind turbine and is based on a synchronous generator. To achieve wide-range variable speed operation, the synchronous generator is connected to the grid via a full-scale PWM converter directly. The PWM converter completely decouples the synchronous generator from the grid. Compared with other types of WTGs, the

DDPMG can eliminate the gearbox if the generator applies the multi-pole synchronous machine designed for low speed. Without the gearbox and slip ring, the DDPMG has the advantage of lower power loss, lower maintenance costs and high reliability. Hence, the DDPMG has the potential to be widely installed in the future.

Due to the advantages of high capacity, low cost and flexible control, the DFIG is very popular among all the other types of wind generation [12]. In North America, most large wind farms employ the DFIG-base wind turbines [13]. The generator of DFIG is also the induction machine. The stator of the induction generator is directly connected to the power grid, and its rotor is linked to the grid through a back-to-back PWM converter. The PWM converter consists of the rotor side converter and the grid side converter connected by a DC-link capacitor. Through the PWM converter, the active and reactive power of DFIG can be controlled separately. The capacity size of the PWM converter is normally designed to be 20% ~ 30% of the rated capacity of DFIG. This means a certain amount of power can flow in or out from the rotor through this converter. There are two modes of operation for a DFIG: the super-synchronous mode and the sub-synchronous mode. These two modes depend entirely on the rotational speed of the induction generator. If the DFIG operates in the super-synchronous mode, the power will be transmitted from the rotor to the grid through the PWM converter. If the DFIG works under the sub-synchronous mode, the rotor of the induction generator will absorb power from the grid through the PWM converter.

Since the DFIG is the dominant type of WTG installed around the world, the wind farms in this thesis are proposed to be composed of DFIGs. The model and dynamic performance of DFIG will be further discussed in detail below.

1.1.2 Development of FFTS

Better wind energy resources are often located offshore, and this means that more productive wind farms need to be constructed away from the land. The next generation of offshore wind farms are expected to be installed 300 km away from the shore, and the individual capacity of each wind farm is likely to reach the gigawatt range [14]. Under such circumstances, the long distance delivery for offshore wind energy becomes a challenge.

To increase the transmission distance and capacity is always challenging in the power industry. Historically, in the AC transmission system, raising the voltage level is an approach to increase transmission distance and capacity. However, the voltage level of the AC transmission line has its limitations, and further up-grading will encounter material and environmental issues. Currently, the high voltage alternating current (HVAC) is still an option for the delivery system of offshore wind farms. From the economical perspective, the HVAC is suitable for short distance submarine cables (less than 50km). If the distance exceeds 50km, the capacitive charging current and power losses of AC submarine cables makes HVAC on longer cost effective.

The high voltage direct current (HVDC) system is another choice for increasing the transmission capacity. It can break through the bottleneck of the transmission distance and has no stability limit problems. Initially, the line-commutated HVDC was proposed to deliver offshore wind energy for its reliability and mature technology. Then, VSC-HVDC, which can perform independent control of active and reactive power, becomes another feasible solution. The converters at the two ends of HVDC are very expensive and difficult to maintain, especially for offshore wind farms [15]. In addition, the multi-terminal operation of the HVDC is still difficult today.

As an alternative approach to HVAC and HVDC, a relatively new electricity transmission system, the fractional frequency transmission system (FFTS), is proposed. It multiplies the transmission capacity through the reduction of the transmission frequency. Initially, the FFTS was proposed to transmit the hydro power from the west region to the east region in China where the delivery distance ranges from 1000 to 2500km [16]. This novel transmission system is also very suitable to transmit power from remote offshore wind farms. Firstly, because the speed of the wind generation remains in the range from 12Hz-18Hz [17] [18], wind turbines are able to generate power directly at this frequency without a gearbox [17]. Secondly, compared with HVAC and HVDC, the FFTS costs less considering the investment, maintenance and losses. The Power Systems Engineering Research Centre (PSERC) [19] performed a comprehensive evaluation between FFTS, HVAC and HVDC, and their final report can

support the above facts. Thirdly, the FFTS can easily form a network as the conventional AC system. Finally, the implementation of FFTS faces no special technical difficulty. The key power electronic equipment-cycloconverter, which acts as the frequency changer, is mature [20]. Comprehensive knowledge is available from the development of the single phase FFTS railway grid in Austria, Switzerland and etc. [18].

1.2 Research Focus and Contributions

The low carbon emissions and efficient energy transmission are two major challenges for modern power systems. These challenges stimulate the development and research in wind energy and the fractional frequency transmission system (FFTS). The wide utilisation of wind energy and the FFTS will bring changes to the dynamics of power systems. So, the aim of this thesis is to study the damping performance of power systems under the utilisation of wind power generation and the fractional frequency transmission system. The research objectives and contributions of this thesis can be summarised as follows,

1) When traditional power plants are gradually replaced by wind power generation, the dynamics of power systems will inevitably be influenced. One research objective of this thesis is to systematically investigate the impacts of the increased DFIG-based wind farm on the SSR of T-G units from the perspectives of torsional interaction (TI)

and the induction generator effect (IGE). Both eigenvalue analysis and dynamic simulations are conducted to demonstrate the influences of DFIG-based wind farms on the SSR of power systems and how the control parameters of wind farms can affect the SSR.

2) The fractional frequency transmission system (FFTS) is a relatively new technology to deliver power from remote offshore wind farms. However, the dynamics of the FFTS with wind farms may be different from that of the standard AC transmission system with wind farms. So, one research objective of this thesis is to study the damping performance of the FFTS with wind farms. The mathematical models for the FFTS with wind farms and the key component (cycloconverter) are established. The small signal stability of the FFTS with wind farms is evaluated through eigenvalue analysis and time domain simulations. Furthermore, this thesis also proposes a solution to improve the damping of the FFTS with wind farms through the frequency changer-cycloconverter.

3) The FFTS is proposed to interconnect power systems in different areas. The objective of this research is to study the dynamic performance of the FFTS in system interconnections. The mathematical model of the FFTS in the two-area system is established. Both eigenvalue analysis and dynamic simulations are carried out to investigate the damping performance of the FFTS in system interconnections. Finally,

a power flow controller for the FFTS is proposed, and its effectiveness is verified through time domain simulation.

The main contributions of this thesis are provided in Chapter 4, 5 and 6. Chapter 4 investigates the SSR of power systems with wind energy integration. Chapter 5 and Chapter 6 study the applications of FFTS. Chapter 5 proposes to deliver offshore wind energy through FFTS and studies the damping performance of this system. The application of FFTS in system interconnections is presented in Chapter 6.

1.3 Thesis Outline

The utilisation of wind energy and the FFTS will inevitably influence the dynamics of power systems. So, this thesis studies the damping performance of power systems with wind generation and FFTS. The contents of each chapter are summarised as follows,

Chapter 2: A literature review is presented. Previous researches on dynamics of wind farms and power systems are reviewed in detail. The research progress of the FFTS is also introduced.

Chapter 3: The SSR and small signal models for the major electrical components in this thesis are presented. These models include the DFIG-based wind turbine, the

conventional T-G unit and the transmission network. The procedures to form overall state space model and conduct eigenvalue analysis are also introduced.

Chapter 4: This chapter systematically investigate the influence of the increased wind energy on the subsychronous resonance (SSR) of the T-G units. A new test system for research scenario is proposed, and its detailed mathematical model is also presented. The eigenvalue analysis and time domain simulation are carried out to evaluate the impacts of DFIG-based wind farms from torsional interaction (TI) and induction generator effect (IGE).

Chapter 5: The fractional frequency transmission system is chosen to deliver the power from offshore DFIG-based wind farms. The small signal stability model of the studied system is represented. The eigenvalue analysis and time domain simulation are conducted to evaluate the damping performance of the FFTS with wind farms. The damping performance of the FFTS is also compared with that of the standard AC system. In addition, a feedback control loop is proposed to improve the damping performance of the FFTS.

Chapter 6: The FFTS is applied in system interconnections. Both eigenvalue analysis and time domain simulations are conducted to demonstrate that the FFTS can improve the damping of inter-area oscillations. Furthermore, the power flow control through the FFTS is also proposed.

Chapter 7: The conclusion of this thesis is summarised, and future research topics are discussed.

CHAPTER 2 LITERATURE REVIEW

2.1 Dynamics of Power systems and Wind Farms

2.1.1 Stability Analysis of Power Systems

Power system stability has been an important and complex problem that has challenged power system operation since the 1920s [21]. Severe damages caused by power system instability illustrated the importance of this problem. Although the definition of power system stability has a long history, its definition is continuous evolving with the development of power systems from theory to practical engineering. In 2004, the IEEE/CIGRE Joint Task Force on Stability Terms and Definitions proposed a precise understanding. In their report, power system stability was defined as the ability to regain operating equilibrium after a physical disturbance [21]. Power system stability is not a single problem, and the instability of power systems may happened in different forms and be caused by a wide range of factors. Consequently, it is necessary to classify the stability into several appropriate types for further study. In general, power system stability can be divided into three main categories:

1) Rotor angle stability: this kind of stability includes the study of electromechanical oscillations in power systems. It refers to the ability of synchronous machines in an interconnected power system to maintain synchronism when being subjected to a disturbance.

2) Frequency stability: it can be defined as the ability of a power system to regain the steady frequency with minimum loss of loads after a significant imbalance between the generations and loads. The instability of frequency may lead to continuous frequency swing and finally cause the tripping of generator units or loads.

3) Voltage stability: it refers to the capacity of a power system, under normal operating conditions, to maintain steady voltages at all buses after a disturbance. If the voltage of a power system is unstable, this may lead to the loss of loads in an area or tripping of the transmission lines and other elements in this system.

The rotor angle stability of a power system can be further classified into the following two subcategories:

1) Transient stability: it is the ability of a power system to keep synchronism after being subjected to a severe or large disturbance. This phenomenon is a nonlinear dynamics and involves large excursion of the states in power systems. It mainly depends on the initial conditions of power systems and the severity of disturbances.

2) Small signal stability: it is related with the steady state of the power system, and it can be defined as the ability to maintain synchronism when subjected to small disturbances [21]. The analysis of small signal stability can provide useful information about the dynamics of power systems and assist system designs.

The dynamics of power system discussed in this thesis mainly focus on the small signal stability. So, the following introduction will emphasise on the mathematical theories and methods in the analysis of small signal stability.

The small signal stability of a power system is affected by several factors including the initial system operating conditions, the strength of electrical connections between power components and different control devices [23]. Since power systems are inevitable to experience small disturbances, any power system in operation should be stable in the term of small signal stability. In practice, the small signal stability of power systems is mainly a problem of insufficient damping of oscillation. In the process of small signal stability analysis, it is critical to determine the electromechanical oscillation modes of power systems. The categories of electromechanical oscillation can be summarised as follows,

1) Local modes, also named machine modes, are related with the swing of generating units in one station against the rest of the overall power system. This kind of oscillation exists locally at one station or a small portion of a power system. Typically, the oscillation frequency of local mode ranges from 0.7 Hz to 2 Hz [23].

2) Inter-area modes are associated with the swing of machines in one area of the power system with respect to the machines in other areas. They are normally caused by several groups of closely coupled machines being linked by weak tie lines [106].

3) Torsional modes involve the shaft system of the turbine-generator unit. The oscillation frequency is usually from 10-50 Hz [23]. It is an oscillation mainly being discussed in subsychronous resonance (SSR) analysis. More details about torsional oscillation will be introduced and discussed later in this thesis.

4) Control modes are associated with the speed governors, exciters, HVDC converters and other control devices and components.

In the small signal stability, a power system is subjected to small disturbances. These disturbances are supposed to be sufficiently small for the linearization of system models. So, small signal stability is suitable to be carried out on the system's nonlinear equations linearizing around a chosen operating point.

At present, eigenvalue analysis and frequency domain analysis are the two main methods to analyse the small signal stability of power systems. Eigenvalue analysis has been recognised as most widely used method. It is based on the linear system theory and Lyapunov stability theory [23]. In this method, the complex power systems are initially modelled by nonlinear differential equations, and then these nonlinear models are linearized around a chosen stable operating point. The procedure of eigenvalue analysis is summarised as the following.

The nonlinear model of the power system is often described as [22],

$$\dot{x} = f(x,u) \tag{2.1}$$

$$y = g(x,u) \tag{2.2}$$

where x is the vector of system states, u is the vector of system inputs, y is the vector of system outputs, $f()$ and $g()$ are the nonlinear functions.

Then, the above nonlinear equations are linearized around an equilibrium point. The equilibrium point is an operating point where the derivative of state vector x is simultaneous zero. If x_0 is the equilibrium point of state vector x, the following is obtained,

$$\dot{x} = f(x_0, u_0) = 0 \tag{2.3}$$

$$y_0 = g(x_0, u_0) \tag{2.4}$$

If the system is perturbed from the above state, the following is obtained,

$$x = x_0 + \Delta x \tag{2.5}$$

$$y = y_0 + \Delta y \tag{2.6}$$

$$u = u_0 + \Delta u \tag{2.7}$$

where Δ denotes a small deviation from the equilibrium point.

Based on equation (2.1) and (2.2), the nonlinear system can be linearized as

$$\Delta \dot{x} = A\Delta x + B\Delta u \tag{2.8}$$

$$\Delta y = C\Delta x + D\Delta u \tag{2.9}$$

17

where A is the state matrix, B is the input matrix, C is the output matrix and D is the forwarding matrix which describes the direct connection between the input and output of the system.

According to the Lyapunov's first method, the stability of system can be analysed by calculating the eigenvalue of the state matrix A. The locations of all the eigenvalues of the system determine the dynamic responses under small disturbance, and the law is expressed as follows,

1) When the real parts of all the eigenvalues are negative, the system is asymptotically stable.

2) When the eigenvalues (at least one) have positive real parts, the system is unstable

3) When the eigenvalues have real parts equal to zero, the stability of system can be decided by this method.

Each eigenvalue of the state matrix A can be expressed as

$$\lambda = \delta \pm j\omega \qquad (2.10)$$

The real part of the eigenvalue determines the damping of oscillation, and the damping ratio is given by,

$$\zeta = -\sigma \big/ \sqrt{\sigma^2 + \omega^2} \qquad (2.11)$$

18

The imaginary part of a eigenvalue gives the frequency of oscillation. When $\omega=0$, the corresponding mode has non-oscillatory response. When $\omega \neq 0$, the corresponding mode has a oscillatory response. The frequency of mode oscillation in Hz is expressed by,

$$f = \frac{\omega}{2\pi} \tag{2.12}$$

From the above eigenvalue analysis, the left and right eigenvector can also be calculated. Based on the left and right eigenvector, the participation factor, which identifies the contribution of each state variable to a particular eigenvalue, can also be determined.

2.1.2 Stability Analysis of Wind Farm

Wind energy, among all the renewable energy resources, is one of the most widely utilized worldwide. As the share of wind power increases to a certain amount, the dynamics of power systems may be affected by wind farms. In general, the characteristics of wind farms are different from conventional power plants. Therefore, the influences of wind energy on existing power systems need further study.

The first step to evaluate the influence of wind farms is to establish the models for various wind farms. Currently, most wind farms are composed of three popular wind turbine generators: the squirrel cage of induction generator (SCIG), the doubly-fed

induction generator (DFIG), and the direct-driven permanent magnet generator (DDPMG).

The SCIG is a fixed-speed wind turbine. The simple model [24] of fixed speed wind turbine was developed to investigate the dynamics of wind farm, and this model was compared with the high-order model. Reference [25] discussed the dynamic modelling of fixed speed induction generator wind turbine in large (MW) capacity. The reduced-order model of SCIG was proposed for transient stability simulation [26].

The DDPMG is a variable speed wind turbine. The small signal model of the DDPMG was presented in [27], and the influences of DDPMG on the stability of power systems were also studied. Reference [28] proposed the reduced order model, which could reduce the simulation time and the complexity of model.

DFIG is also a variable speed wind turbine, and it is widely applied in most large wind farms worldwide. The research on the model of DFIG has been conducted for many years. Initially, [29] described the engineering and design model of DFIG using back-to-back PWM converter. Reference [30] derived the dynamic model of DFIGs and their associated control and protection circuits, and this model was very suitable for transient stability analysis of DFIGs. A simple wind turbine model was developed to facilitate the integration in power system simulation [31]. Reference [32] proposed a reduced model of the DFIG and its converter for stability studies. The small signal

stability model of the DFIG and the corresponding controllers were analysed in [33] and [35], and the optimization methods for the control parameters of DFIG was proposed and verified through eigenvalue analysis and dynamic simulations.

After extensive studies on the modelling of wind turbines, research focus began to concentrate on the impact of increased large scale wind power on the dynamics of existed power systems. In 2003, [37] initiated the study on the influence of wind turbines, including constant speed and variable speed wind turbines, on the small signal stability of power systems. It was concluded that the impacts of wind farms depended on the types of wind turbines and the penetration level, and the constant speed wind turbines can provide better damping for power systems than the variable speed wind turbines. Reference [38] investigated the influence of wind power integration on the damping of inter-area oscillation in the Nordic grid, and various types of wind turbines were also tested. The results showed that the SCIG improved the damping of inter-area oscillation, while the DFIG and DDPMG decreased the damping. Through using the sensitivity of the eigenvalues, the transient and small signal stability of DFIG were investigated in [41]. Both beneficial and detrimental impacts of increased penetration of DFIG were found. Under the circumstances of a weak area of the grid, [39] found that the DFIG wind turbines can provide a good damping performance.

In general, based on different types of wind turbines, the impact of the large scale wind farm can be summarised as Table 2.1. The SCIG has a positive impact on power

systems due to its asynchronous nature. The DFIG and DDPMG have both positive and

negative impacts on the damping performance of power systems according to different

types of oscillations, the capacity of wind farms and the location of connecting points

[42].

Table 2.1 Influences of different WTGs on damping performance [42]

	Positive	Negative
SCIG	√	
DFIG	√	√
DDPMG	√	√

2.2 SSR of Power System and Wind Farm

2.2.1 SSR of Conventional T-G Unit

Series capacitive compensation is a common means to increase the capacity of

transmission lines and improve transient stability. However, series capacitors in the

transmission lines may expose power systems to the potential risk of subsynchronous

resonance (SSR), which can cause turbine-generator (T-G) shaft failure or electrical instability at subsynchronous frequency [43]. Therefore, the mechanism of SSR needs to be fully understood when power systems are designed and operated with series capacitors.

Early in the 1930s, the "self-excitation" phenomenon was found in the synchronous generators with the capacitive load or series capacitive compensated transmission line under certain circumstances [44]. This "self-excitation" oscillation was treated as a purely electrical phenomenon until the 1970s. In 1970 and 1971, the Mohave generating station in Southern Nevada experienced two shaft failures, and the failures happened in the shaft section between the generator and the exciter [45]. The analysis of these failures indicated that the "self-excitation" caused by series compensated transmission line can not only excite the electrical oscillation but also a novel interaction between the transmission line and the shaft of T-G unit. This lead to the further research and development of the theory of the interaction between the series compensated transmission line and the mechanical system of the T-G unit. The oscillation frequency of this kind of interaction was much higher than that of the well-known "low frequency oscillation" of power systems, and it was lower than synchronous frequency. Hence, this interaction was defined as subsynchonous resonance (SSR).

After the two shaft failures at Mohave, the severe damage caused by SSR attracted the attention both from the academia and power industry. The discussion and research on SSR become a hot topic. Much work has been done on the analysis and suppression method of SSR [46]-[48]. In 1973, the IEEE established the Subsynchronous Resonance Working Group to organise and coordinate the research in this field. This working group recommended two benchmark models for SSR analysis [49][50] and also dedicated to provide the terminologies and definitions of SSR [51]-[54]. According to the IEEE's definition, SSR is an abnormal operating condition of electric power system. Under this condition, significant energy exchanges between the electric network and a turbine generator at one or more of the natural frequencies of the combined system below the synchronous frequency of the system [53]. It encompasses the oscillatory attributes of electrical and mechanical variables associated with turbine-generators when coupled to a series capacitor compensated transmission system where the oscillatory energy interchange is lightly damped, undamped, or even negatively damped and growing [51].

If the transmission line is uncompensated, disturbances and faults in the system will result in DC offset components in the stator winding of generator. In a series compensated transmission line, the result under faults or disturbances is quite different. Fig. 2.1 shows a simple radial system to explain the basic theory of SSR. The natural electrical frequency f_n of this radical system can be written by [55]

$$f_n = f_0 \sqrt{\frac{X_c}{X'' + X_E + X_T}} \qquad (2.13)$$

where f_0 is the synchronous frequency; X'' is the subtransient reactance of the synchronous machine; X_T and X_E are the reactance of the transmission line; X_c is the reactance of the series compensated capacitor. In Fig. 2.1, R_E is the resistance of the transmission line; E'' is the voltage before the subtransient reactance of the synchronous machine; E_B is the voltage of the infinite bus.
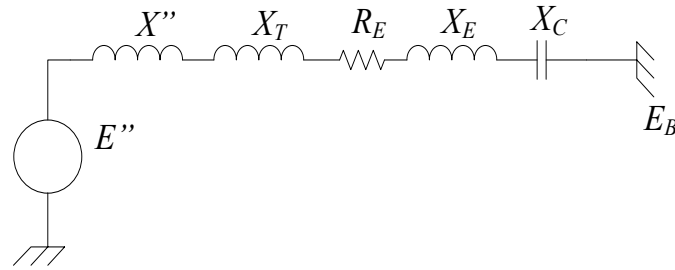
Fig. 2.1. A simple radial series compensated system

Any disturbances or faults in such a system will cause offset alternating current, and the frequency of the alternating current is f_n. The offset alternating current will flow into the stator of generator and induce the rotor currents of slip frequency $f_0 - f_n$. The rotor currents at the slip frequency may excite the system or interact with one of the natural torsional modes of the turbine-generator shaft.

Typically, the SSR interaction is divided into three categories: torsional interaction (TI), induction generator effect (IGE) and torsional amplification (TA) [56].

1) Torsional interaction (TI) is an unstable state that the mechanical system of a turbine-generator (T-G) unit interacts with the series capacitor-compensated network. This phenomenon happens when the frequency of the induced torque in the generator is close or coincides with one of the torsional frequencies of the T-G shaft system [22].

2) Induction Generator Effect (IGE) is a purely electrical phenomenon and not involved with the mechanical system of T-G unit [57]. It is mainly caused by self-excitation of the electrical part of power systems. The rotor resistance to the subsynchronous currents is negative when viewed from the armature terminals. If the negative resistance of generator surpasses the positive resistance of the network at the subsynchronous frequency, the electrical system will become self-excited.

3) Torsional Amplification (TA) is caused by significant system disturbances. In a series capacitor-compensated transmission system, if the complement of the natural oscillatory frequency of the network is close with one of the torsional frequencies, torques in the shaft system may be induced [55]. The shaft response not only includes a single frequency component, but contains all the torsional modes.

The TI and IGE are related with steady state of power systems [58], and they are supposed to be considered in the small disturbance conditions. Hence, the TI and IGE can be analysed through linear models. The TA is a nonlinear transient dynamics, and

the analysis is complex and can be done through simulations. In this thesis, the research focuses on the TI and IGE, and the TA will not be discussed in details.

To systematically analyse the problem of SSR, several methods are proposed as follows,

1) Eigenvalue analysis [59]-[61]: this method can provide the dynamic information of the entire power system in a single calculation. The general procedures are the same as the described in the small signal stability analysis. The generators and networks are modelled by linear equations. However, the stator circuits of the generator and the network in SSR study cannot be treated as steady-state algebraic equations in the small signal stability analysis. Besides, the mechanical dynamics of shaft system need to be modelled in the TI analysis. Consequently, the system model for the SSR study is of high order and contains more information compared with the model in the small signal stability analysis.

2) Frequency scanning [62]: this method has been widely used for a preliminary analysis of SSR analysis in North America [56], and it is particularly suitable for the study of IGE. The frequency scanning technique calculates the equivalent resistance and inductance, as a function of frequency, viewed from the stator winding of a particular generator looking into the network. If the resistance is negative and the

inductance is zero at a certain frequency, there is potential risk of IGE. The frequency scanning methods can also be used to obtain the information about possible TI and TA.

3) Time domain simulation [63] [64]: the electromagnetic transient program (EMTP) is widely utilized in the SSR analysis to compute the transient responses. Unlike the transient stability program, the three-phase detailed models are used. Furthermore, the EMTP can model the nonlinearity of complex power system components, and is particularly suitable to analyse the transient torque of SSR problem.

When the potential risk of SSR problem is identified, the appropriate protection need to be selected and implemented to avoid the severe damage caused by SSR [65]. Depending on the problem and protection level, the cost of some countermeasures for SSR may be very high. So, the selection process for countermeasures should consider the probability of SSR events and the amount of expected damage. One method to prevent SSR is to avoid the series compensation levels that may induce the SSR. However, this method usually needs to decrease the transmission capacity, and thus it is not cost effective. Another option is to trip the relevant unit. This choice is suitable for the occurrence of SSR at low probability. The various countermeasures can be classified into the following categories: modifications of generator and system, tripping of generator and system, protective relaying and filtering, etc [66]-[72].

2.2.2 SSR of Wind Farm

The SSR problem of the T-G units interconnected with a series compensated transmission line has been long recognized and extensively studied [56]. With the rapid development of wind energy, it provides a substantial amount of the electricity demand at present. As the increasing scale of wind farms, the energy generated by wind farm also needs the series compensated transmission line for long-distance delivery. Under this circumstance, the wind farms are exposed to the potential risk of SSR.

As mentioned previous, there are three popular types of wind turbines. Due to their different structures and dynamic performances, the SSR problem of each wind turbine may happen under different conditions and be caused by different factors. In the following, the SSR of each wind turbine will be introduced briefly.

Early work of the SSR analysis of fixed speed wind generations was done in [73]. The results demonstrated that the SSR phenomenon of this kind of wind turbine is primarily attributed to IGE. The SSR conditions of fixed speed wind generation connected with series compensated transmission line was investigated in [74], and the time domain simulations were carried out to demonstrate the TI and IGE. This paper concluded that greater power from the fixed-speed wind generations leads to the less damping of the system. Reference [74] and [75] also proposed to mitigate the potential TI and IGE of fixed speed wind generation by FACTS devices.

The DDPMG is connected to the grid through the back-to-back converter, which isolates the wind turbines from the grid. So, the DDPMG is immune to SSR [77]. Reference [77] studied the SSR condition of synchronous machine connected to the grid through HVDC, which is similar to the DDPMG. It pointed out that there was no risk of SSR if the grid-side converter operated as an inverter.

Due to the popularity of DFIG, extensive studies have been done on the SSR analysis of DFIG. Reference [79] modelled the DFIG based wind farm with a series compensated transmission line. The controller for converters, the flux observer and phase-locked loop were included in this detailed mathematical model. The developed model was also validated through simulation in both Matlab/Simulink and PSCAD/EMTDC. Reference [58] also established the SSR model for DFIG-based wind farm, and it further differentiated the SSR phenomenon from IGE and TI. In [80], impedance-based Nyquist criterion was used to analyse the SSR of DFIG-based wind farm, and it concluded that the interaction between the controller of the DFIG converters and the electric network was the main cause for SSR. Reference [81] presented a comprehensive analysis of SSR in wind integrated systems and proposed procedures to study and mitigate the SSR problem.

However, the above publications have not studied the impacts of the DFIG-based wind farm on the SSR of conventional T-G units. Thus, one research objective of this

thesis is to investigate the influences of the DFIG-based wind farm on the SSR of T-G units.

2.3 FFTS

To increase power transmission capacity is always a technical challenge in power industry. In the AC power system, the power transmission capacity is related with two basic parameters: voltage and frequency. Due to the invention of transformer, different voltage levels can be tuned flexibly in power systems. So, raising voltage level is the most utilized method to increase the transmission capacity. However, this method inevitably faces the limitations of material and environmental issues.

The fractional frequency transmission system (FFTS), or named low frequency transmission system, changes the transmission frequency to increase the capacity of the transmission line. Fractional frequency means the frequency of power is lower than the standard frequency (60/50 Hz). This kind of AC transmission system usually uses 1/3 of the nominal frequency, which 20/16.66 Hz for 60/50Hz systems respectively [82]. The power frequency of the FFTS is limited by the harmonics caused by cycloconverter, and the output frequency is better to be no more than 1/3 of the standard frequency [124]. However, lower frequency means a slower time response for a system. So, 1/3 of the standard frequency is an appropriate frequency for the FFTS.

The basic principle of the FFTS will be introduced in the following.

The active power transmitted via the AC transmission line is [22]:

$$P = \frac{V_S V_R}{X} \sin \delta \qquad (2.14)$$

where P is the positive power; V_S and V_R are the sending and receiving end voltage, respectively; δ is the transmitting angle; X is the transmission line reactance and it is proportional to the transmission frequency f,

$$X = 2\pi f L \qquad (2.15)$$

where L is the total inductance of the transmission line.

According to equation (2.14) and (2.15), voltage level and transmission frequency are the two fundamental factors that affect the transmission capacity. Either the increase of voltage level or the reduction of transmission frequency could achieve the objective of multiplying the transmission capacity.

In the FFTS, the transmission frequency is usually chosen to be 1/3 of the standard frequency, and the reactance of the transmission line also correspondingly reduces to 1/3 of the original one. Consequently, the capacity of active power delivered through the AC transmission line will increase three times. Besides, the voltage drop of the transmission line can be decreased to 1/3 of voltage drop in the standard AC transmission line. The voltage drop of a transmission line can be obtained by,

$$\Delta V\% = \frac{QX}{V^2} \times 100 \qquad\qquad (2.16)$$

where Q is the reactive power of the transmission line. According to the above equation, the voltage drop of the transmission line is proportional to the reactance of the transmission line. Reducing the transmission frequency will obviously improve the voltage drop.

During the late 19th and early 20th century, the electricity transmission system used many frequencies, such as 50/3, 25, 50, 60 and 133 Hz. In 1896, the transmission line between Niagara and Buffalo chose the 25 Hz transmission frequency [83]. The choice of frequency in an AC system should consider several factors, including motors, lighting, generators, transformers and transmission lines. These factors interact with each other, and thus the selection of a suitable power frequency is a compromise between these contradictory factors [129]. Finally, the 50/60 Hz frequency was accepted as the standard power frequency worldwide. After the standardization of transmission frequency, changing the transmission frequency was rarely considered. This was mainly attributed to that transforming frequency is more difficult than changing the voltage level.

However, low power frequency and high power frequency have been utilised in some specific system until now. In railway traction power networks, Germany, Switzerland, Austria, Sweden and Norway use 50/3 or 16.7 Hz single-phase AC power [132], and

the United States chooses 25 Hz for its traction power system [133]. High power frequency is usually used in spacecraft, telecommunication, electric vehicle and computer device, etc. [134] [136].

With the development of new materials and power electronic techniques, the change of power frequency is much easier today. Low transmission frequency regains the attention in the application of long distance transmission. In 1994, the Fractional Frequency Transmission System (FFTS) was proposed to cope with the long distance transmission of Hydro power in China [84]. The FFTS applied 50/3 Hz frequency to decrease the electrical length of the AC transmission line and thus remarkably multiply the transmission capacity and improve the operating performance. Then, the feasibility of FFTS was analysed in details, and a mathematical model and computer simulation were also developed for the purpose of evaluation [16]. The results indicated that the FFTS was a promising novel transmission system. Reference [20] introduced the establishment of the experimental FFTS. In this experimental platform, the AC synchronous generator directly produced 50/3 Hz electric power, and then the power was delivered through a simulated 1200 km 50 kV transmission line. The power was feed into the main grid through a phase-controlled cycloconverter, which can step up the frequency to the standard 50 Hz. The results of this experiment showed that the FFTS was rather smooth during the grid synchronization process, and the transmission capacity could be increased 2.5 times compared with that of the standard AC

transmission system. From engineering practice, the FFTS faced no essential technique difficulties and had great potential for practical implementation in future [18]. Reference [85] emphasised the economic advantage of the FFTS compared conventional AC transmission system when it was used to transmit hydro and wind power.

The key component in the FFTS is the frequency changer, which is responsible for stepping up the power from the low frequency to the nominal frequency. Basically, there are three options for the frequency changer: saturable transformer [16], AC-DC-AC converter [90] and cycloconverter [20]. The saturable transformer has simpler structure, lower cost and more reliable operation. Power electronic type is superior in higher efficiency and more flexible in installation. Until now, the cycloconverter is most widely applied in the FFTS. Conventionally, it is used to drive motors in high power application. Reference [20] proposed to operate cycloconverter in its inversion mode in the FFTS for the first time. Then, the most common fault of cycloconverter, non-condition of bridge arms, was analysed, and some suggestions were proposed for the fault identification [92]. Reference [93] simulated the cycloconverter in PSCAD/EMTDC and investigated the dynamic response of cycloconverter under three-phase short-circuit fault on the low frequency bus. The advanced time domain model of a three-phase cycloconverter in the FFTS was

presented in [94]. The proposed model was accurate and reliable, and it was expected to be applied in transient stability and harmonic studies.

Wind power, especially those located in remote or offshore areas, is also very suitable to apply FFTS for long distance transmission. In 2009, [15] investigated the feasibility of integrating large offshore wind farms through FFTS. It concluded that the competitive transmission distance for the FFTS was about 30-150 km. [17] and [95] conducted the FFTS experiment for wind power integration and verified the practical feasibility. The advanced time domain model for FFTS with wind farms was established in [96], and the performance of such system was also presented. [18] provided the preliminary basic design of FFTS with offshore wind farms, and discussed the pros and cons from technical feasibility and operational respects. From the aspect of reliability and cost, [19] conducted a comprehensive evaluation of integrating wind energy through FFTS. Reference [85] applied a case study to emphasize the advantages of integrating wind power through the FFTS, and it can be summarised as: 1) The gearbox of wind turbine can be simplified; 2) Compared with traditional AC system, the investment for transmission line can be reduced; 3) Compared with HVDC, investment and maintenance cost for converters was greatly reduced; 4) voltage fluctuation of transmission line may be reduced, etc.

Since the FFTS is proposed again in the application of long distance transmission in recent years, the above research works have been done from several aspects, including

feasibility study, preliminary design, economic evaluation and simulations, etc. However, the dynamics of the FFTS has rarely discussed. With vast utilization of the FFTS, the dynamics of FFTS, especially the damping performance, needs further research. So, this thesis will study the damping of the FFTS in the application of wind power integration and system interconnections.

2.4 Summary

This chapter has reviewed previous research related to the topic of this thesis. With the rapid development of wind technology, wind energy becomes an indispensable source for the world's energy supply. The increased penetration level of wind energy will influence the dynamics of power systems. So, this chapter first reviewed the basic concept and research in the field of stability analysis of power systems and wind farms, especially the small signal stability analysis. Then, the theory of subsynchronous resonance (SSR) was introduced, and the recent research progress in the SSR study of the conventional power systems and wind farms was presented.

On the other hand, the long distance transmission for large scale offshore wind farms also becomes a challenge. The FFTS provides another solution to cope with this problem. The history and development of the FFTS were introduced, and the recent research was reviewed in this field. Furthermore, the advantages of the FFTS for offshore wind energy delivery were compared with the HVDC and HVAC.

Based on previous research in wind power and the FFTS, this thesis will conduct further studies on the dynamics of power systems with utilization of wind generation and the FFTS. In the following, each research result will be introduced chapter by chapter.

CHAPTER 3 MODELLING OF WIND FARM AND CONVENTIONAL POWER SYSTEM

3.1 Introduction

In general, the research on power system dynamics, including small-signal stability and subsynchronous resonance (SSR), starts with understanding the dynamic characteristics of each electrical component. Based on the principle and dynamic performance, the mathematical model of each electrical component can be established through differential and algebraic equations. Then, the mathematical model of each part is connected together to represent the dynamic performance of the overall power system.

One single electrical component in a power system needs at least one or several differential equations to describe its dynamics. A large scale power system includes tens of thousands of electrical components, and the mathematical model for such a system is very complex. Regardless of how complex the power system is, it can ultimately be demonstrated through a certain number of differential equations. According to different types of stability analysis, the mathematical model for an electrical component can be very different. The appropriate model for a power system

should include the important components and closely related information, and it is better to exclude some irrelevant components and information.

In this thesis, the research focuses on the small signal stability and subsynchronous resonance (SSR). In the small signal stability analysis, low frequency oscillation is the main research objective, and the oscillation frequency range is between 0.1~2 Hz. So, the stator transients of the synchronous machines and the fast electromagnetic transients of the transmission lines and transformers have been ignored. The SSR is an interaction between the mechanical and electrical system, and the oscillation of this interaction lies in the range between 10~50 Hz. In the SSR model, the stator transients of the synchronous machines and the fast electromagnetic transients of the transmission lines and transformers should all be included. Besides, the shaft system of the turbine-generator unit also needs to be modelled in detail.

The main electrical components in this thesis include the DFIG-based wind turbine, the turbine-generator (T-G) unit and the transmission line. The mathematical model of each component will be introduced in the following section. Then, the linearisation and integration of the mathematical models are carried out to form the state-space representation. Based on the state-space equation of a system, the small signal stability and SSR can be analysed further.

The structure of this chapter is constructed as follows. Section 3.2 divided the DFIG-based wind turbine into several parts, and the mathematical model of each part will be introduced in detail. This model for the DFIG-based wind turbine is suitable for both the small signal stability and the SSR analysis. Section 3.3 introduces both the small signal stability and SSR models of the conventional T-G unit, and the differences between both models are indicated. In section 3.4, the small signal stability and SSR model for the network are presented, and their differences are compared.

3.2 Model of DFIG-based Wind Turbine

Due to its high capacity, low cost and flexible control, the DFIG-based wind turbine is the most employed wind turbine. In this thesis, wind farms are supposed to be composed of DFIG-based wind turbines. So, the mathematical model for this type of wind turbine needs an in-depth study. The typical configuration of a DFIG-based wind turbine is shown as Fig. 3.1. It includes a drive train, an induction machine, a DC-link capacitor, a rotor-side converter (RSC) and a grid-side converter (GSC). The induction machine is a wound rotor induction generator with slip rings. The variable speed operation is achieved through controlling current into or out of the slip rings. The stator winding of the induction machine is directly connected to the grid. The RSC is connected to the slip ring of the induction machine, and it imposes a voltage on the slip ring which allows the machine to operate over a large speed range. The GSC is connected to the grid and responsible to maintain a constant voltage of the DC

capacitor. The RSC, GSC and DC-link capacitor constitute an AC-DC-AC converter, which allows the power to flow directly from the slip ring of induction machine to the grid.
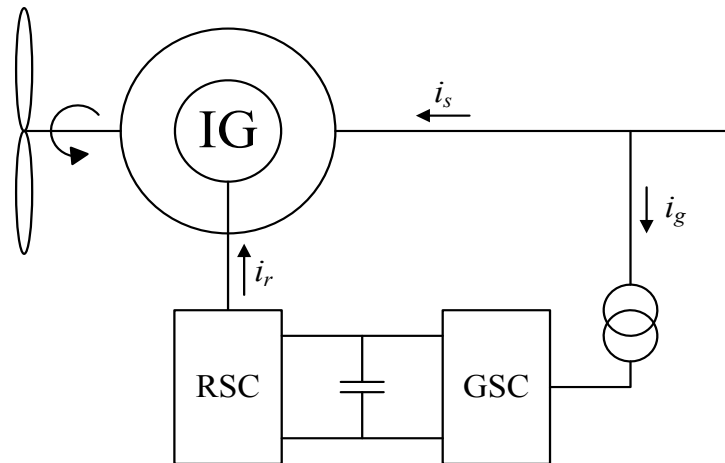
Fig. 3.1 Configuration of DFIG-based wind turbine

In a DFIG-based wind turbine, the power can be delivered to the grid through both stator and rotor. The rotor can generate or absorb power, and this depends on the rotational speed of induction generator. When the rotational speed of generator is above the synchronous speed, power will be transmitted from rotor to the grid through the AC-DC-AC converter. When the rotational speed is under the synchronous speed, the power will be delivered from the grid to the rotor. The maximum power delivered through converter is 20% ~ 30 % of the nominal rating of the generator [1].

Under the steady state, the relationship of the stator electrical power, the rotor electrical power and the mechanical power in a DFIG-based wind turbine is shown as Fig. 3.2. This power relationship ignores the power losses of the stator and rotor.
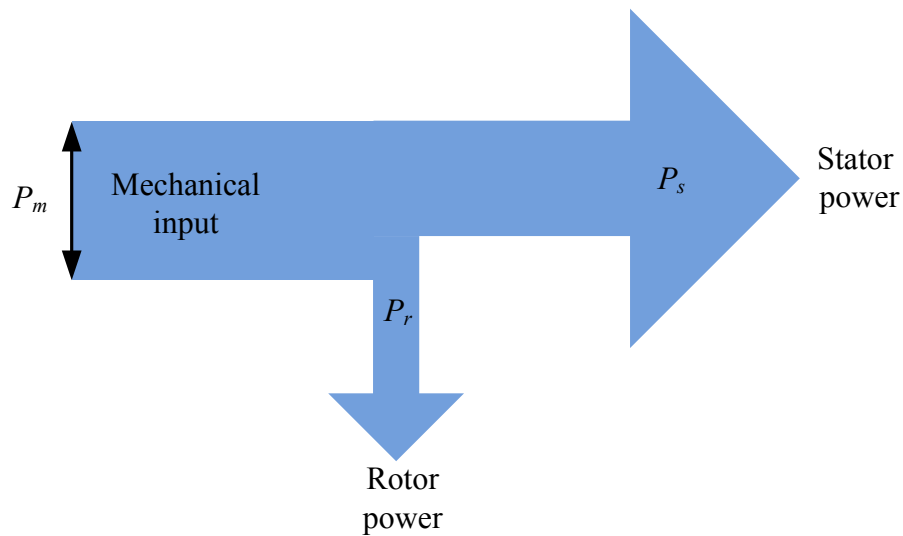
Fig. 3.2 Power relationship of DFIG

The relationship of the stator power P_s, the mechanical power P_m and the rotor power P_r can be expressed as

$$P_s = P_m - P_r \tag{3.1}$$

Equation (3.1) can be rewritten in the terms of the generator torque T as

$$T\omega_s = T\omega_r - P_r \tag{3.2}$$

where ω_s is the synchronous speed and ω_r is the rotor speed.

Based on (3.2), the rotor power can be obtained as

$$P_r = -T(\omega_s - \omega_r) = -sP_s \tag{3.3}$$

where s is the slip and $s = (\omega_s - \omega_r)/\omega_s$.

According to the above equations, the mechanical power can be expressed as

$$P_m = P_s + P_r = (1 - s)P_s \tag{3.4}$$

When the losses of the stator and rotor are both neglected, the power delivered to the grid is expressed by

$$P_g = P_s + P_r \tag{3.5}$$

In the following, each part of the DFIG-based wind turbine will be introduced separately.

3.2.1 The Drive Train

The drive train has been modelled as six-mass, three-mass, two-mass and lumped-mass system in [86]. To study the dynamics of DFIG, the drive train is usually represented by a two-mass model, including wind turbine, gearbox, shafts and other mechanical components [33]. The two-mass model of the drive train can be written as (3.5)-(3.8)

$$2H_t \frac{d\omega_t}{dt} = T_m - T_{sh} \tag{3.5}$$

$$\frac{d\theta_{tw}}{dt} = \omega_b (\omega_t - \omega_r) \tag{3.6}$$

$$2H_g \frac{d\omega_r}{dt} = T_{sh} + T_e - B\omega_r \tag{3.7}$$

$$T_{sh} = K_{sh}\theta_{tw} + D_{sh}\omega_b(\omega_t - \omega_r) \tag{3.8}$$

where H_t is the inertia constant of the wind turbine; ω_t is the angle speed of the wind turbine; T_m is the torque of the wind turbine; T_{sh} is the shaft torque; θ_{tw} is the shaft twist angle; H_g is the inertia constant of the generator; B is the friction coefficient of the generator; T_e is the electromagnetic torque; K_{sh} is the shaft stiffness coefficient of the wind turbine; D_{sh} is the damping coefficient of the wind turbine.

T_e and T_m are demonstrated as

$$T_e = \frac{P_s}{\omega_s} \tag{3.9}$$

$$T_m = \frac{0.5\pi\rho R^2 C_p V_w^3}{\omega_r} \tag{3.10}$$

where P_s is the active power of stator; ρ is the air density; ω_s is the synchronous angle speed; R is the blade radius of the wind turbine; C_p is the power coefficient; V_w is the wind speed; ω_r is the rotor angle speed.

When the wind speed is lower than the rated speed, the power coefficient C_p maintain at an optimal constant to extract the maximum power. When the wind speed is higher than the rated speed, C_p is adapted to limit the over-speed of the induction generator.

3.2.2 Induction Generator

The generator of DFIG is a wound rotor induction machine. In this type of induction machine, the stator windings are connected to the grid, and the rotor windings are connected with outside circuits through the slip ring. In the *d-q* reference frame, the stator voltage equations of an induction machine are written as follows,

$$v_{ds} = \frac{d\psi_{ds}}{dt} - \omega_s \psi_{qs} + R_s i_{ds} \tag{3.11}$$

$$v_{qs} = \frac{d\psi_{qs}}{dt} + \omega_s \psi_{ds} + R_s i_{qs} \tag{3.12}$$

where v_{ds} and v_{qs} are the *d* and *q* axis stator voltages, respectively; ψ_{ds} and ψ_{qs} are the *d* and *q* axis stator flux linkage, respectively; i_{ds} and i_{qs} are the *d* and *q* axis stator currents, respectively; R_s is the stator resistance.

The rotor voltage equations in the *d-q* reference frame is as follows

$$v_{dr} = \frac{d\psi_{dr}}{dt} - s_r \omega_s \psi_{qr} + R_r i_{dr} \tag{3.13}$$

$$v_{qr} = \frac{d\psi_{qr}}{dt} + s_r \omega_s \psi_{dr} + R_r i_{qr} \tag{3.14}$$

where v_{dr} and v_{qr} are the *d* and *q* axis rotor voltages, respectively; ψ_{dr} and ψ_{qr} are the *d* and *q* axis rotor flux linkage, respectively; i_{dr} and i_{qr} are the *d* and *q* axis rotor currents, respectively; R_r is the rotor resistance.

The flux linkage equations of the stator and the rotor is given by

$$\psi_{ds} = L_{ss} i_{ds} + L_m i_{dr} \tag{3.15}$$

46

$$\psi_{qs} = L_{ss}i_{qs} + L_{m}i_{qr} \tag{3.16}$$

$$\psi_{dr} = L_{rr}i_{dr} + L_{m}i_{ds} \tag{3.17}$$

$$\psi_{qr} = L_{rr}i_{qr} + L_{m}i_{qs} \tag{3.18}$$

where L_{ss} is the stator self-inductance; L_{rr} is the rotor self-inductance; L_m is the mutual inductance.

According to (3.17) and (3.18), the rotor current can be written as,

$$i_{dr} = \frac{\psi_{dr} - L_m i_{ds}}{L_{rr}} \tag{3.19}$$

$$i_{qr} = \frac{\psi_{qr} - L_m i_{qs}}{L_{rr}} \tag{3.20}$$

Substituting (3.19) and (3.20) into (3.13) and (3.14), the rotor voltage equations is transformed as,

$$\frac{dE'_d}{dt} = s_r\omega_s E'_q - \omega_s \frac{L_m}{L_{rr}}v_{qr} - \frac{1}{T'_0}\left[E'_d + (X_s - X'_s)i_{qs}\right] \tag{3.21}$$

$$\frac{dE'_q}{dt} = -s_r\omega_s E'_d + \omega_s \frac{L_m}{L_{rr}}v_{dr} - \frac{1}{T'_0}\left[E'_q - (X_s - X'_s)i_{ds}\right] \tag{3.22}$$

where $E'_d = -\frac{\omega_s L_m}{L_{rr}}v_{qr}$, $E'_q = \frac{\omega_s L_m}{L_{rr}}v_{dr}$, $X_s = \omega_s L_{ss}$, $X'_s = \omega_s(L_{ss} - \frac{L_m^2}{L_{rr}})$, $T'_0 = \frac{L_{rr}}{R_r}$.

Similarly, substituting (3.15) and (3.16) into (3.11) and (3.12), the stator voltage equations can be obtained as,

$$\frac{X'_s}{\omega_s}\frac{di_{ds}}{dt} = v_{ds} - \left[R_s + \frac{1}{\omega_s T'_0}(X_s - X'_s) \right] i_{ds} - (1 - s_r)E'_d$$
$$- \frac{L_m}{L_{rr}} u_{dr} + \frac{1}{\omega_s T'_0} E'_q + X'_s i_{qs} \tag{3.23}$$

$$\frac{X'_s}{\omega_s}\frac{di_{qs}}{dt} = v_{qs} - \left[R_s + \frac{1}{\omega_s T'_0}(X_s - X'_s) \right] i_{qs} - (1 - s_r)E'_q$$
$$- \frac{L_m}{L_{rr}} u_{qr} - \frac{1}{\omega_s T'_0} E'_d - X'_s i_{ds} \tag{3.24}$$

The (3.21)-(3.24) form the fourth-order model of the DFIG generator, and it can be simplified as,

$$\dot{x} \quad x\ z, u) \tag{3.25}$$

where $x=[i_{ds},\ i_{qs},\ E'_d,\ E'_q]^T$, $z=[v_{dr},\ v_{qr}]^T$, $u=[v_{ds}, v_{qs}]^T$.

3.2.3 DC-link Capacitor

As shown in Fig. 3.1, the DC-link capacitor connects the rotor side converter (RSC) and the grid side converter (GSC). The active power is fed back from the stator to the rotor through the DC-link capacitor. The energy is balanced in this capacitor, and the power balance equation can be written as

$$P_r = P_g + P_{DC} \tag{3.26}$$

where P_r is the active power at the AC side of RSC; P_g is the active power at the AC side of GSC; P_{DC} is the active power of the DC-link capacitor. These can be obtained as,

$$P_r = v_{dr}i_{dr} + v_{qr}i_{qr} \tag{3.27}$$

$$P_g = v_{dg}i_{dg} + v_{qg}i_{qg} \tag{3.28}$$

$$P_{DC} = -Cv_{DC}\frac{dv_{DC}}{dt} \tag{3.29}$$

where v_{dg} and v_{qg} are the d and q axis voltages of the grid-side converter; i_{dg} and i_{qg} are the d and q axis currents of the grid-side converter; v_{dr} and v_{qr} are the d and q axis rotor voltages; i_{dr} and i_{qr} are the d and q axis rotor currents; v_{DC} is the DC capacitor voltage; C is the capacitance of the DC capacitor.

Based on the above equations, the following equation can be derived as,

$$Cv_{DC}\frac{dv_{DC}}{dt} = v_{dg}i_{dg} + v_{qg}i_{qg} - (v_{dr}i_{dr} + v_{qr}i_{qr}) \tag{3.30}$$

3.2.4 Rotor-side Converter

The RSC adopts the decoupling control strategy. Its objective is to control the electromagnetic torque and the reactive power of DFIG in this thesis. The DFIG-based wind turbine is a nonlinear and complex system and very difficult to control in the static reference frame. However, if it is controlled in the stator-flux oriented reference frame with the d-axis oriented along the vector position of the stator-flux ψ_s, the active and reactive component of the rotor current can be decoupled. Then, the decoupled control for the electromagnetic torque and reactive power of the DFIG can be achieved through regulating the active and reactive component of rotor current.

When the wind speed is less than the rated speed, the reference for the electromagnetic torque is obtained through the maximum power tracking point (MPT). Above the rated wind speed, the reference torque is a constant value. According to different requirements, the reference for the reactive power is set to a constant value or to be zero. The control block diagram of the rotor-side converter is shown as Fig. 3.3. Under the stator-flux oriented reference frame, the electromagnetic torque is proportional to i_{qr} and can be controlled through v_{qr}. The reactive power is proportional to i_{dr} and can be regulated through v_{dr}. The controller for the RSC applies the cascade control. The inner control loops apply the PI control to regulate the rotor currents i_{dr} and i_{qr}, and the outer control loops also use the PI control to manipulate the electromagnetic torque and reactive power, respectively.
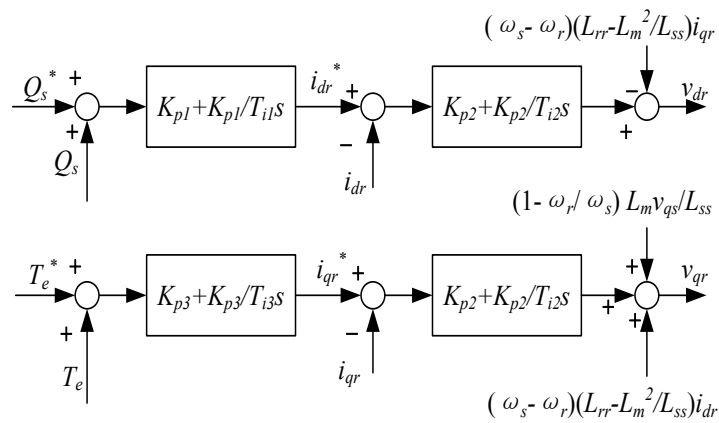
Fig. 3.3 Control block diagram of rotor-side converter

According to the control block diagram, the control equations are demonstrated as,

$$\frac{dx_1}{dt} = Q_s^* + Q_s \tag{3.31}$$

$$\frac{dx_2}{dt} = K_{p1}(Q_s^* + Q_s) + \frac{K_{p1}}{T_{i1}} x_1 - i_{dr} \tag{3.32}$$

$$\frac{dx_3}{dt} = T_e^* + T_e \tag{3.33}$$

$$\frac{dx_4}{dt} = K_{p3}(T_e^* + T_e) + \frac{K_{p3}}{T_{i3}} x_3 - i_{qr} \tag{3.34}$$

$$v_{dr} = K_{p2}\frac{dx_2}{dt} + \frac{K_{p2}}{T_{i2}} x_2 - (\omega_s - \omega_r)\delta L_{rr} i_{qr} \tag{3.35}$$

$$v_{qr} = K_{p2}\frac{dx_4}{dt} + \frac{K_{p2}}{T_{i2}} x_4 + (\omega_s - \omega_r)\left(\frac{L_m}{L_{ss}}\psi_s + \delta L_{rr} i_{dr}\right) \tag{3.36}$$

where Q_s and Q_s^* are the actual and reference reactive power, respectively; T_e and T_e^* are the actual and reference electromagnetic torque; x_1, x_2, x_3 and x_4 are the intermediate variables; i_{dr}^* and i_{qr}^* are the control reference for the d and q axis current of the rotor-side converter, respectively; K_{p1} and K_{i1} are the proportional and integrating gains of the reactive power regulator, respectively; K_{p2} and K_{i2} are the proportional and integrating gains of the current regulator of the rotor-side converter, respectively; K_{p3} and K_{i3} are the proportional and integrating gains of the electromagnetic torque regulator, respectively.

3.2.5 Grid-Side Converter

The GSC is controlled in the grid-voltage oriented reference frame with d-axis oriented along the grid-voltage vector position. It is supposed to maintain the DC link voltage

and control the reactive power of the terminal. The reference for i_{dg} is usually set to zero, which means that the reactive power for the grid-side converter is set to zero. The reference for the DC-link voltage depends on the modulation factor and the size of the back-to-back converter.

The control block diagram of the grid-side converter is shown as Fig. 5. Under the grid-voltage oriented reference frame, the DC-link voltage can be regulated via i_{dg}. The reactive power of GSC is proportional to i_{qg} and can be controlled through v_{qg}. The controller for GSC also adopts the cascade control. The inner control loops regulate i_{dg} and i_{qg} through the PI controller, and the outer control loop maintains the DC-link voltage through the PI controller.

The control equations of the grid side converter are given by,

$$\frac{dx_5}{dt} = v_{DC}^* - v_{DC} \tag{3.37}$$

$$\frac{dx_6}{dt} = K_{p4}(v_{DC}^* - v_{DC}) + \frac{K_{p4}}{T_{i4}} x_4 - i_{dg} \tag{3.38}$$

$$\frac{dx_7}{dt} = i_{qg}^* - i_{qg} \tag{3.39}$$

$$v_{dg} = \omega_s L_g i_{qg} + v_{ds} - K_{p5} \frac{dx_6}{dt} - \frac{K_{p5}}{T_{i5}} x_6 \tag{3.40}$$

$$v_{qg} = v_{qs} - \omega_s L_g i_{dg} - K_{p5} \frac{dx_7}{dt} - \frac{K_{p5}}{T_{i5}} x_7 \tag{3.41}$$

where $v_{DC}{}^*$ is the control reference of the DC-link voltage; $i_{dg}{}^*$ and $i_{qg}{}^*$ are the control

reference for the d and q axis current of the grid-side converter, respectively; x_5, x_6 and

x_7 are the intermediate variables; K_{p4} and K_{i4} are the proportional and integrating gains

of the DC bus voltage regulator, respectively; K_{p5} and K_{i5} are the proportional and

integrating gains of the grid-side converter current regulator.
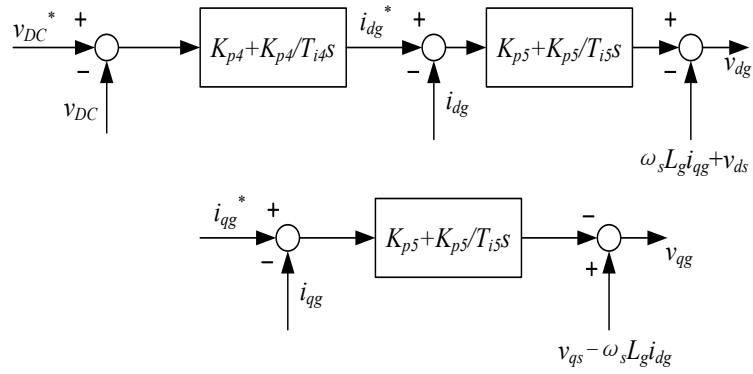
Fig. 3.4 Control block diagram of grid-side converter

The dynamic model of the grid-side converter is given by,

$$L_g \frac{di_{dg}}{dt} = v_{ds} - R_g i_{dg} + \omega_s L_g i_{qg} - v_{dg} \tag{3.42}$$

$$L_g \frac{di_{qg}}{dt} = v_{qs} - R_g i_{qg} - \omega_s L_g i_{dg} - v_{qg} \tag{3.43}$$

where L_g is the inductance of the grid-side transformer; R_g is the resistance of the

grid-side transformer.

53

3.3 Model of Turbine-Generator Unit

The turbine-generator (T-G) unit is composed of a synchronous machine and a shaft system. Synchronous machine is the major source for electric energy in power systems. The power system stability problems are related with synchronism of interconnected synchronous machines. Therefore, understanding the dynamics and mathematical model of synchronous machine is the fundamental basis to study the stability of power systems.

The synchronous machine is a nonlinear and strong coupling system, and the modelling of it has always been a challenge since the 1920s [22]. After the proposal of Park's transformation [22], the mathematical model of synchronous machine can be decoupled under *d-q* frame reference and widely applied in the analysis of power system stability. According to different usage of model, the synchronous machine can be modelled with varying degree of complexity. In this section, the mathematical models of the synchronous machine for small signal stability and SSR analysis will be introduced respectively.

The shaft system represents the mechanical dynamics of the T-G unit. The model complexity of this system is quite different for small signal stability and SSR analysis. This section will introduce the mathematical models for both analysis and compare their difference in modelling.

3.3.1 Model of Synchronous Machine

The model for the synchronous machine is established in the *d-q* reference frame. The direct (*d*) axis is oriented along the centre of north pole of the rotor. The quadrature (*q*) axis is ahead of the *d*-axis with 90 electrical degrees. The direction of *d-q* axis can be arbitrary, and the above selection is based on the IEEE standard definition [22].

To derive the mathematical model of synchronous machine, the following ideal assumptions are made [22] [56].

(1) The stator windings have a sinusoidal distribution with 120 electrical degrees apart.

(2) Magnetic hysteresis is ignored.

(3) Magnetic saturation effect is also neglected for the convenience in stability analysis.

The model of synchronous machine includes the stator windings and the rotor circuits. The stator windings carry alternating currents. The rotor circuits consist of a field winding and several damper windings. The field winding is connected to a direct current source. The damper windings have different forms and may not physically exist. In this thesis, the damper windings are represented by the equivalent damper circuits in the *d* and *q* axis: *1d* on the *d*-axis, *1q* and *2q* on the *q*-axis. The equivalent circuits of SM are shown in Fig. 3.5, and the voltage equations are as follows.
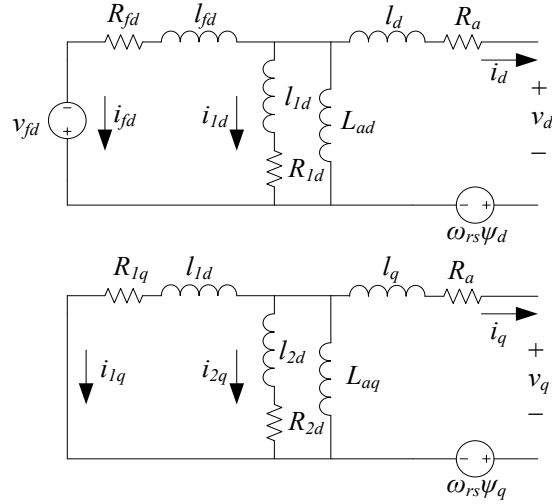
Fig. 3.5 Equivalent circuits of the synchronous machine (above: *d*-axis circuit; below: *q*-axis circuit)

The voltage equations of a synchronous machine in the *d*-axis are given by

$$v_d = \frac{1}{\omega_b} \frac{d\psi_d}{dt} - \psi_q \omega_{rs} - R_a i_d \qquad (3.44)$$

$$v_{fd} = \frac{1}{\omega_b} \frac{d\psi_{fd}}{dt} + R_{fd} i_{fd} \qquad (3.45)$$

$$0 = \frac{1}{\omega_b} \frac{d\psi_{1d}}{dt} + R_{1d} i_{1d} \qquad (3.46)$$

The voltage equations of a synchronous machine in the *q*-axis are demonstrated as

$$v_q = \frac{1}{\omega_b} \frac{d\psi_q}{dt} + \psi_d \omega_{rs} - R_a i_q \qquad (3.47)$$

$$0 = \frac{1}{\omega_b} \frac{d\psi_{1q}}{dt} + R_{1q} i_{1q} \qquad (3.48)$$

$$0 = \frac{1}{\omega_b} \frac{d\psi_{2q}}{dt} + R_{2q} i_{2q} \qquad (3.49)$$

56

where v_d and v_q are the d and q axis voltages of the stator, respectively; ψ_d and ψ_q are the d and q axis flux linkages of the stator, respectively; i_d and i_q are the d and q axis currents of the stator, respectively; R_a is the stator resistance; v_{fd} is the voltage of the field winding; ψ_{fd} is the linkage of the field winding; i_{fd} is the current of the field winding; R_{fd} is the resistance of the field winding; ψ_{1d} and ψ_{1q} are the flux linkages of the 1st d and q axis amortisseur, respectively; i_{1d} and i_{1q} are the currents of the 1st d and q axis amortisseur, respectively; R_{1d} and R_{1q} are the resistances of the 1st d and q axis amortisseur, respectively; ψ_{2q} is the flux linkage of the 2nd q axis amortisseur; i_{2q} is the current of the 2nd q axis amortisseur; R_{2q} is the resistance of the 2nd q axis amortisseur; ω_{rs} is the rotor angle speed.

(1) The model for SSR analysis

In the SSR analysis, the high frequency components of the dynamic response influence the SSR of the T-G unit greatly. Therefore, the stator transients of the synchronous machine cannot be neglected in the model. Equation (3.44)-(3.49) can fully represent the mathematical model of synchronous machine for SSR analysis.

(2) The model for small signal stability analysis

In the small signal stability analysis, the transients of the transmission line mainly contain high frequency components and decay rapidly. For the sake of simplicity, the transients of transmission line can be neglected. Due to the mathematical limitation, if

the transients of transmission line need to be ignored, the transients of the machine stator should also be neglected. Only both these transients are neglected, the various electrical components can be interconnected to represent the overall power system.

When the stator transients are ignored, (3.44) and (3.47) can be rewritten as,

$$v_d = -\psi_q \omega_{rs} - R_a i_d \tag{3.50}$$

$$v_q = \psi_d \omega_{rs} - R_a i_q \tag{3.51}$$

Then, the small signal stability model of synchronous machine can be represented by the algebraic equation (3.50) (3.51) and differential equation (3.45) (3.46) (3.48) (3.49).

The above mathematical model is usually written in another form [87] as the following.

The four differential equations of the synchronous machine:

$$\frac{dE'_{qs}}{dt} = \frac{1}{T'_{d0}} \left(-E'_{qs} - \left(X_d - X'_d \right) \left(-i_d - \frac{X'_d - X''_d}{\left(X'_d - X_L \right)^2} \left(\varphi_{1d} - \left(X_d - X_L \right) i_d - E'_{qs} \right) \right) + v_{fd} \right) \tag{3.52}$$

$$\frac{dE'_{ds}}{dt} = \frac{1}{T'_{q0}} \left(-E'_{ds} - \left(X_q - X'_q \right) \left(i_q - \frac{X'_q - X''_q}{\left(X'_q - X_L \right)^2} \left(-\varphi_{2q} - \left(X_q - X_L \right) i_q - E'_{ds} \right) \right) \right) \tag{3.53}$$

$$\frac{d\varphi_{1d}}{dt} = \frac{1}{T''_{d0}} \left(-\varphi_{1d} + E'_{qs} + \left(X'_d - X_L \right) i_d \right) \tag{3.54}$$

58

$$\frac{d\varphi_{2q}}{dt} = \frac{1}{T''_{q0}} \left(\varphi_{2q} + E'_{ds} + \left(X'_q - X_L \right) i_q \right) \tag{3.55}$$

where E'_{ds} and E'_{qs} are the d and q axis induced transient electromagnetic force, respectively; φ_{1d} and φ_{2q} are the subtransient induced electromagnetic force; X_d, X'_d and X''_d are the d-axis synchronous, transient and subtransient reactance, respectively; X_q, X'_q and X''_q are the q-axis synchronous, transient and subtransient reactance, respectively; T'_{d0} and T''_{d0} are the d-axis transient and subtransient time constant, respectively; T'_{q0} and T''_{q0} are the q-axis transient and subtransient time constant, respectively; X_L is the armature leakage reactance.

The two algebraic equations of the stator voltage:

$$v_d = \frac{X''_q - X_L}{X'_q - X_L} E'_{ds} - \frac{X'_q - X''_q}{X'_q - X_L} \varphi_{2q} - R_a i_d + X''_q i_q \tag{3.56}$$

$$v_q = \frac{X''_d - X_L}{X'_d - X_L} E'_{qs} + \frac{X'_d - X''_d}{X'_d - X_L} \varphi_{1d} - R_a i_q - X''_d i_d \tag{3.57}$$

3.3.2 Shaft System

The shaft system of a T-G unit is a complex mechanical system. According to different purpose of studies, the shaft system may be divided into several segments. In the small signal stability analysis, the mechanical dynamics of the shaft system is not the focus of study. The shafts and their coupling are assumed to be very stiff, and the overall shaft system can be regarded as a rigid body. Therefore, the shaft system is usually modelled

as a lumped mass. In practice, the couplings between shaft segments have finite stiffness, and each segment is slightly displaced to its adjacent segments. Especially, in the SSR analysis, the lumped mass model of the shaft system does not include all the necessary information. The SSR of power systems involve both electrical and mechanical interaction, so the shaft system should be modelled in detail.

(1) Shaft model for SSR analysis

As shown in Fig. 3.6, the overall shaft system of the T-G unit is modelled as a number of torsional masses connected together by springs. When the mechanical damping is assumed to be zero, the motion equations of the shaft system are as follows,

$$\frac{d\delta_i}{dt} = \omega_b \Delta\omega_i \tag{3.58}$$

$$\frac{d\Delta\omega_i}{dt} = \frac{1}{2H_i}\left[T_i + K_{i-1,i}(\delta_{i-1} - \delta_i) - K_{i,i+1}(\delta_i - \delta_{i+1})\right] \tag{3.59}$$

where $i=1,2, ...,6$; δ_i is the angular position of mass i; $\Delta\omega_i$ is the speed deviation of mass i; $K_{i-1,i}$ and $K_{i,i+1}$ are the shaft stiffness; T_i is the mechanical torques of each turbine section; H_i is the inertia constant of each turbine section; ω_b is the base speed (377 *rad/s*).
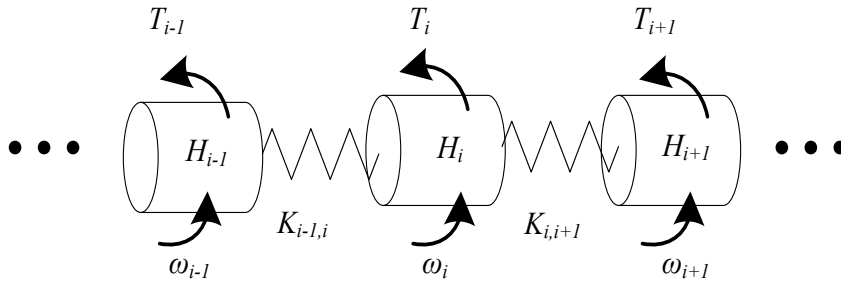
Fig. 3.6 Shaft system of the T-G unit

(2) Shaft model for small signal stability analysis

The shaft model for small signal stability analysis is much simpler than that for SSR. The shaft system can be modelled as a lumped mass. The motion equations of such shaft system are given by,

$$\frac{d\delta}{dt} = \omega_b \Delta\omega \tag{3.60}$$

$$\frac{d\Delta\omega}{dt} = \frac{1}{2H}(T_m - T_e) \tag{3.61}$$

where δ is the angular position of the entire rotor; $\Delta\omega$ is the speed deviation of the entire rotor; T_m is the mechanical torque of the entire rotor; H is the inertia constant of the entire rotor.

3.4 Model of Networks

In small signal stability analysis, the low frequency electromagnetic oscillations of power system are of concern [23]. However, the network transients mainly contain comparatively high frequency oscillations. So, the ignorance of network transients will not affect the analysis results of small signal stability. On the other hand, in the SSR analysis, the oscillation frequencies usually range from 5 to 55 Hz. The network transients should be considered in the model for SSR analysis.

In this thesis, the model of network is simplified as a lumped RLC circuit, as shown in Fig. 3.7. In Fig. 3.7, v_1 and v_2 are the terminal voltage of buses; X_L is the reactance of the inductance; X_C is the reactance of the inductance; R_N is the combined resistance of the transmission line. The simplified network model for small signal stability and SSR analysis will be introduced in the following.
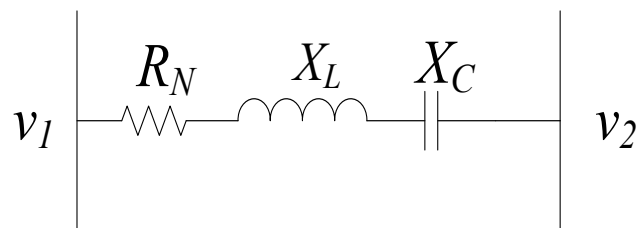
Fig. 3.7 Configuration of the network

(1) Network model for small signal stability analysis

In small signal stability analysis, the transients of the inductance and capacitor in the network are neglected. The mathematical model of network can be demonstrated by algebraic equations.

In the *d-q* reference frame, the voltage equation of network is given by

$$v_{1d} - v_{2d} = R_N i_{dL} - X_{LC} i_{dL} \tag{3.62}$$

$$v_{1q} - v_{2q} = R_N i_{qL} + X_{LC} i_{qL} \tag{3.63}$$

where v_{1d} and v_{1q} are the *d* and *q* axis voltage of v_1, respectively; v_{2d} and v_{2q} are the *d* and *q* axis voltage of v_2, respectively; i_{dL} and i_{qL} are the *d* and *q* axis current of network; X_{LC} is the combined reactance of the inductance and capacitor; R_N is the combined resistance of the transmission line.

(2) Network model for SSR analysis

The model of network should include the transients of inductance and capacitor in the SSR analysis. So, the dynamics of network is represented by differential equations. In the *d-q* axis reference frame, the mathematical model of the network can be described by,

$$\frac{1}{\omega_b} \frac{dv_{cd}}{dt} - \omega_s v_{cq} = X_C i_{dL} \tag{3.64}$$

$$\frac{1}{\omega_b} \frac{dv_{cq}}{dt} + \omega_s v_{cd} = X_C i_{qL} \tag{3.65}$$

63

$$R_N i_{dL} - X_L i_{qL} + \frac{X_L}{\omega_b} \frac{di_{dL}}{dt} + v_{cd} = v_{1d} - v_{2d} \qquad (3.66)$$

$$R_N i_{qL} + X_L i_{dL} + \frac{X_L}{\omega_b} \frac{di_{qL}}{dt} + v_{cq} = v_{1q} - v_{2q} \qquad (3.67)$$

where v_{cd} and v_{cq} are the d and q axis voltages across the capacitor; X_c is the reactance of the compensation capacitor; X_L is the reactance of the inductance.

3.5 State Space Model and Eigenvalue Analysis

The small signal stability and SSR of power systems are supposed to be evaluated under the condition that power systems are subjected to small disturbances. Under such assumption, the nonlinear model of every electrical component in a power system can be linearized at an operating point, and then the linearized models are interconnected together to form the state space model of the overall power system. Based on the state space model, the steady-state dynamics of a power system can be analysed by eigenvalue analysis.

3.5.1 State Space Model

In previous section, the mathematical models are represented by differential equations and algebraic equations. These models are nonlinear and need to be linearized to conduct further analysis. In general, the original mathematical model of an electrical component (excluding the network) can be written as the following,

$$\dot{x} \quad \quad x, u_i)$$ (3.68)

where x_i is the state vector of an electrical component; u_i is the input vector of an electrical component.

If x_{i0} is the initial state vector and u_{i0} is the initial input vector at an equilibrium point, we have

$$\dot{x} \quad \quad x_{i0}, u_{i0}) = 0$$ (3.69)

As the disturbances of the electrical component is small, the linearized model at this equilibrium can be obtained as,

$$\Delta\dot{x} \quad x + B_i \Delta u_i$$ (3.70)

where A_i is the state matrix; B_i is the input matrix; the prefix Δ denotes a small deviation.

The input vector u_i usually contains the terminal voltages of an electrical component. The mathematical model of each electrical component in a power system is represented in its own *d-q* reference frame. For the purpose of system interconnection, all the terminal voltages must be expressed in a common reference frame. The common reference frame is usually defined as *R-I* reference frame, which rotating at the synchronous speed [22]. The relationship of the terminal voltages in its own *d-q* axis and common *R-I* reference frame is expressed by

$$v_{di} = v_{Ri} \sin \delta - v_{Ii} \cos \delta \qquad (3.71)$$

$$v_{qi} = v_{Ri} \cos \delta + v_{Ii} \sin \delta \qquad (3.72)$$

where v_{di} and v_{qi} are the d and q axis terminal voltages, respectively; v_{Ri} and v_{Ii} are the R and I axis terminal voltages, respectively; δ is the angle difference between the its own d-q axis and R-I axis reference frame.

In the common R-I reference frame, the state space equations including all the electrical devices can be obtained as,

$$\Delta \dot{x}_c = A_c x_c + B_c \Delta u_c \qquad (3.73)$$

The electrical components in a power system are interconnected via networks. To form the overall state space model of a power system, the nonlinear model of networks also need to be linearized at the operating point first and then connect all the existed electrical components. As all the transients of networks are neglected in small signal stability analysis, the model of networks is represented via algebraic equations. However, the model of networks in the SSR analysis should include all the transients and can only be demonstrated by differential equations. Therefore, the procedures of forming the overall state-space model in small signal stability and SSR analysis are quite different, and these procedures will be introduced briefly in the following.

(1) State space model in small signal stability analysis

The model of network in small signal stability analysis ignores the transients of inductances and capacitors, and its linearized model may be expressed as the following form,

$$\Delta \boldsymbol{x}_c = Y_N \Delta \boldsymbol{u}_c \tag{3.74}$$

where Y_N is the transfer matrix.

Based on (3.73) and (3.74), the state-space model of the overall power system can be written as,

$$\Delta \dot{\boldsymbol{x}} \qquad B_c Y_N^{-1} \Big) \Delta \boldsymbol{x}_c \tag{3.75}$$

(2) State space model in SSR analysis

The model of network in the SSR analysis contains the all the transients of inductances and capacitors. So, the linearized model of network may be written in the general form as,

$$\Delta \dot{\boldsymbol{x}} \qquad \boldsymbol{x}_N + D_N \Delta \boldsymbol{x}_c \tag{3.76}$$

$$\Delta \dot{\boldsymbol{x}} \qquad \boldsymbol{x}_c + F_N \Delta \boldsymbol{x}_N + G_N \Delta \boldsymbol{u}_c \tag{3.77}$$

where $\boldsymbol{x}_N$ is the states of the network; C_N is the state matrix of the network; D_N, E_N, F_N and G_N are the transfer matrices.

According to (3.73), (3.76) and (3.77), the state space model of the overall power system can be obtained as,

$$\begin{bmatrix} \Delta \dot{x}_c \\ \Delta \dot{x}_N \end{bmatrix} = \begin{bmatrix} A_c + B_c \left(B_c - G_N \right)^{-1} \left(E_N - A_c \right) & B_c \left(B_c - G_N \right)^{-1} F_N \\ D_N & C_N \end{bmatrix} \begin{bmatrix} \Delta x_c \\ \Delta x_N \end{bmatrix} \qquad (3.78)$$

In conclusion, the state space model of the overall power system in small signal stability and SSR analysis can be written in the general form as

$$\Delta \dot{x} = A \Delta x \qquad (3.79)$$

3.5.2 Eigenvalue analysis

If the state space model of a power system is obtained, the steady state dynamics of this system can be analysed by eigenvalue analysis.

The general form of state space model is as (3.79), and A is the state matrix, which includes the dynamic information of all the related states in a power system. The objective of eigenvalue analysis is to calculate the eigenvalues of state matrix A and finally obtain the dynamic information of power systems. The eigenvalue of state matrix A is defined as the following.

For a scalar parameter λ, if the equation

$$Av = \lambda v \qquad (3.80)$$

has non-trivial solutions, λ is the eigenvalues of matrix A. $\boldsymbol{v}$ is the right eigenvector of matrix A.

To calculate the eigenvalues, equation (3.81) can be transformed in the following form,

$$(A - \lambda \boldsymbol{I})\boldsymbol{v} = 0 \tag{3.81}$$

Then, the eigenvalues of matrix A can be obtained by the following,

$$\det(A - \lambda \boldsymbol{I}) = 0 \tag{3.82}$$

The eigenvalues of matrix A may be real or complex, and the complex eigenvalues always appear in conjugate pairs. The steady state dynamics of a power system is determined by the eigenvalues. The real eigenvalue represents a non-oscillatory mode. If the real eigenvalue is negative, its corresponding mode will decay without oscillation after small disturbances. The positive real eigenvalue represents the aperiodic instability of this mode. A pair of complex eigenvalues corresponds to an oscillatory mode. The real part of the complex eigenvalue indicates the damping of the corresponding oscillatory mode, and the imaginary part gives the oscillation frequency. A negative real part means a damped oscillation, and a positive real part indicates oscillation with increasing amplitude. A pair of complex eigenvalues can be written as,

$$\lambda_i = \sigma_i \pm j\omega_i \tag{3.83}$$

Based on (3.83), the frequency of oscillation is expressed as

69

$$f_i = \frac{\omega_i}{2\pi} \tag{3.84}$$

The damping ratio determines the decaying rate of the oscillation amplitude, and it can be given by,

$$\zeta_i = \frac{-\sigma_i}{\sqrt{\sigma_i^2 + \omega_i^2}} \tag{3.85}$$

The relationship of the modes and the states in a power system is also of concern in eigenvalue analysis. The participation matrix is a solution to determine the relationships, and it is obtained by combining right and left eigenvectors of matrix A. The element in the participation matrix is termed as participation factor. It measures the relative participation of state variables in a certain mode. Through the participation factor, the dominate states in a mode can be distinguished, and further analysis of the system dynamics can be done.

3.6 Summary

This chapter has described the modelling of major electrical components in this thesis. These models were represented by the differential equations or algebraic equations. According to the different purposes of study, the mathematical model for the same electrical component can differ. In this thesis, the dynamic performance of power systems focused on the small signal stability and subsynchronous resonance (SSR).

Consequently, the mathematical models for both small signal stability and subsynchronous resonance analysis were demonstrated in this chapter.

The mathematical models in this chapter included the DFIG-based wind turbine, the conventional T-G units and the networks. The model for the DFIG-based wind turbine was divided into five parts: the drive train, the induction generator, the DC-link capacitor, the rotor side converter and the grid side converter. This model was suitable for both small signal stability and subsynchronous resonance analysis. The T-G unit consisted of the shaft system and the synchronous machine. The model of T-G units was quite different in the small signal and subsynchronous resonance analysis. Both models were presented in this chapter, and their differences were compared. Regarding the networks, the small signal stability model was demonstrated by algebraic equations, and the SSR model was given by differential equations.

The state space equation of each electrical component can be obtained through linearizing the above models at an operating point. Then, the state space model of each electrical component can be integrated together to represent an overall power system. The procedures for the integration of the overall state space model were introduced in this chapter. Based on the state space model of the overall power system, the small signal stability and SSR analysis can be conducted through eigenvalue analysis. The basic concept and principle of eigenvalue analysis were also introduced in this chapter.

CHAPTER 4 IMPACT OF INCREASED WIND ENERGY ON THE SSR OF TURBINE-GENERATOR UNIT

4.1 Introduction

When increased wind power generations are integrated into power grids to replace the conventional Turbine-Generator (T-G) units, the dynamics of power systems will be affected. Previous researches have studied the influences of wind power on the small signal stability of power systems [37][38][39][41][42]. However, the influences of wind power on the subsynchronous resonance (SSR) of power systems also need further study. This chapter will analyse the influences of DFIG-based wind farm on the SSR of the T-G unit from the torsional interaction (TI) and the induction generator effect (IGE). Both eigenvalue analysis and time domain simulations will be conducted to investigate the SSR influences on the T-G unit and how the control parameters of wind farms can affect the SSR.

This chapter is organized as follows. In Section 4.2, the IEEE first benchmark model for SSR analysis is introduced, and then the modified test system is proposed to evaluate the impact of wind power on the SSR of the T-G unit. The model of the modified test system, which includes two groups of T-G units, the DFIG-based wind

farm and the series compensated transmission lines, are established in Section 4.3.

Section 4.4 describes the eigenvalue analysis and time domain simulations of the

modified test system. The results of torsional interaction (TI) and induction generation

effect (IGE) are demonstrated through eigenvalue analysis and time domain

simulations in Section 4.5 and 4.6. Section 4.7 summarises this chapter.

4.2 Research Scenario

4.2.1 IEEE First Benchmark Model

The IEEE First Benchmark Model (FBM) was prepared by the IEEE Subsynchronous

Resonance Task Force in 1977 to facilitate the comparison of calculations and

simulations [49]. It was simplified from the Navajo Project and consisted of an 892.4

MW turbine-generator and 500 kV series compensated transmission line. With proper

tuning, it can reproduce both transient and self-excitation problems as in the analysis of

the actual system.

As shown in Fig. 4.1, the IEEE first benchmark model is a simple radial RLC circuit. It

consists of a synchronous generator being connected to a large power system through a

series capacitor-compensated transmission line. In this benchmark, only one interaction

exists in this system, and this interaction happens between the synchronous machine

and the transmission line.
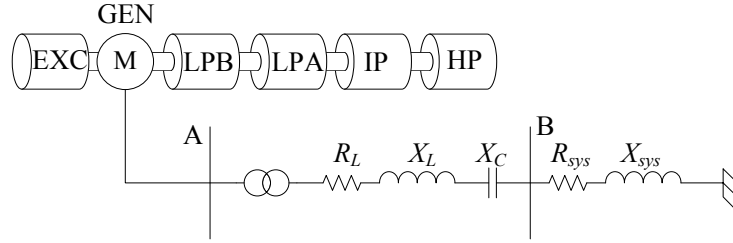
Fig. 4.1 IEEE first benchmark model for SSR analysis

In the original IEEE FBM, the value of the capacitive reactance is 0.371 per unit. So, the total impedance of this radical power system can by written by,

$$Z = R_L + R_{sys} + j(X_T + X_L + X_{sys}) - jX_C$$
$$= 0.02 + j0.70 - j0.371 = 0.02 + j0.329 \ (\text{p.u.})$$

Since the inductive reactance X_L of the transmission line is 0.5 p.u., the 0.371 p.u. capacitive reactance means the 74.2% compensation level [55]. In practice, this compensation level is almost the upper limit for long transmission line with series compensation.

In the dynamic analysis of power systems, the rotor of a T-G unit is usually assumed to be a single lumped mass. Such a model can only represent the oscillation of the entire rotor of the T-G unit against other generators. However, in reality, the rotor of T-G unit is a very complex mechanical system, which is composed of several predominant masses. In the IEEE FBM, the shaft system of the T-G unit consists of six torsional masses: a high-pressure turbine section (HP), an intermediate-pressure turbine section (IP), two low-pressure turbine section (LPA and LPB), a rotor of generator (GEN) and

a rotating exciter (EXC). Since six masses are considered in the shaft system, there are corresponding six modes of oscillation, which is usually named from Mode 0 to Mode 5. The Mode 0 represents the oscillation of the entire six masses against the power system, and it is often considered in system stability studies [22]. The other five modes are the torsional oscillation modes, and their mode shapes can be found in [49].

4.2.2 Modified Test Benchmark

To evaluate the influence of wind power generations on the SSR of the T-G unit, a modified test system, which is shown as Fig. 4.2, is derived from the IEEE first benchmark model (FBM). The IEEE FBM is widely accepted as a standard test case to study the SSR phenomenon of the T-G unit, and it can produce SSR as severe as any observed in the actual system. The IEEE FBM also provides flexible extension for new test cases and the models are sufficiently detailed for further studies in the SSR problems.

On the other hand, this chapter studies the interaction between the DFIG-based wind farm and the traditional AC system, especially from the SSR perspective. Although the modified test system has a simple system topology, which is a simple radial RLC circuit, it can demonstrate the basic influence of wind farm on the SSR of power systems. This research based on the new test system can give a preliminary insight into the influence of wind farms on the SSR of traditional power systems.

The modified test system includes GEN 1, GEN 2, a DFIG-based wind farm, and two series capacitive compensated transmission lines. GEN 1 only contains one T-G unit, and it is the same as T-G unit in the IEEE FBM. The power factor and the output power (803.16MW) of the synchronous machine in GEN 1 are also kept unchanged. GEN 2 consists of ten 75 MW T-G units. The capacities of these T-G units are comparatively small, and they are supposed to be exempt of the SSR phenomenon. The DFIG-based wind farm is composed of a certain number of 1.5-MW, 0.69-kV DFIG-based wind turbines. Due to the increased transmission capacity in modified test system, the single series capacitive compensated transmission line in the IEEE FBM is doubled to meet the transmission capacity. GEN 1, GEN 2 and the DFIG-based wind farm are connected to an infinite bus through these series compensated transmission lines.

In the modified test system, the per-unit base values and the parameters for two series compensated transmission lines are all the same as those in the IEEE FBM. GEN 1 is also the same as the T-G unit in the IEEE FBM, which means the shaft system in GEN 1 also consists of six torsional masses. Thus, the torsional oscillation modes and shapes of the six masses in GEN1 also remain the same. The parameters for GEN2 and DFIG-based wind farm are obtained from available cases, which can be referred to Appendix A.1.

Although two series compensated transmission lines exist in the new test system, the compensation level for each transmission line is never changed. So, the same torsional mode (Mode 2) as in the IEEE FBM will be excited when the modified test system experiences disturbances. The natural frequency of Mode 2 is 21.21 Hz [49]. According to the mode shapes, Mode 2 includes two polarity reversals, and these two polarity reversal happen between the LPA-LPB section and GEN-EXC section, respectively. In the time domain simulation, when Mode 2 is excited, it can be observed through the torsional response of LPA-LPB and GEN-EXC. In GEN 2, the shaft systems of T-G units are treated as a lumped mass.
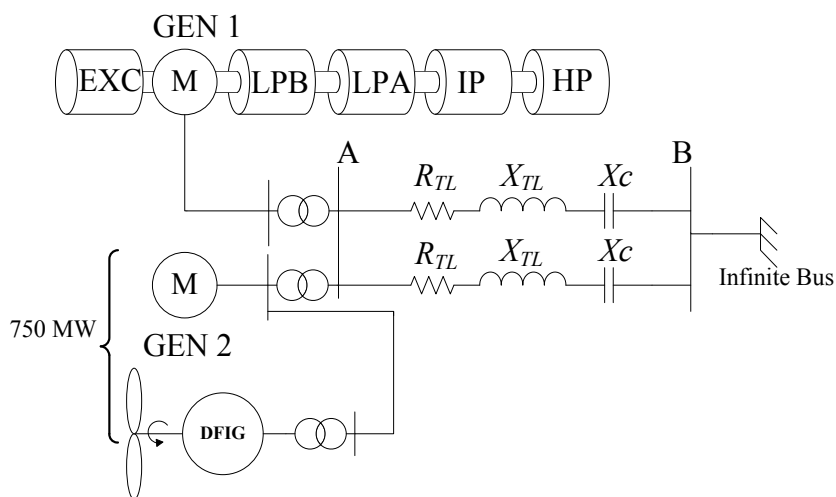
Fig. 4.2 Diagram of the new test benchmark system

In the following study, the DFIG-based wind farm is supposed to replace the conventional T-G units in GEN 2 gradually. This means the number of wind turbines in the DFIG-based wind farm will increase, and the number of the T-G units in GEN

2 will decrease accordingly. However, the total output power from GEN 2 and the DFIG-based wind farm is supposed to remain at 750 MW. Based on the above scenario, the influence of wind farm on the SSR phenomenon of GEN 1 will be systematically investigated in the following research.

4.3 Modelling of Test Benchmark

In previous section, the structure of modified test system has been introduced. For further analysis, the mathematical model for the modified test system needs to be established. The modified test system can be divided into T-G units in GEN 1 and GEN 2, the DFIG-based wind farm and two series capacitive compensated transmission lines. The DFIG-based wind farm is aggregated by a single DFIG-based wind turbine. So, the model of the wind farm can also be represented by the model of a DFIG-based wind turbine. In this section, each electrical component in the test benchmark will be modelled separately. Based on the following model, the eigenvalue analysis can be conducted.

4.3.1 Turbine-Generator Units

There are two types of T-G units in the proposed test benchmark system. In GEN 1, the shaft system of the T-G unit modelled as six torsional masses. Each T-G unit in GEN 2 only has a lumped shaft system. The synchronous machine in GEN 1 and GEN 2 has the same model.

1) Shaft System

The shaft system of the T-G unit in GEN 1 consists of six torsional masses. The general model of the shaft system has been introduced in Section 3.3, Chapter 3. Specifically, the model of the shaft system in GEN 1 can be demonstrated as,

HP section:

$$\frac{d\delta_1}{dt} = \omega_b \Delta\omega_1 \tag{4.1}$$

$$\frac{d\Delta\omega_1}{dt} = \frac{1}{2H_1}\left[T_{HP} - K_{12}\left(\delta_1 - \delta_2\right)\right] \tag{4.2}$$

IP section:

$$\frac{d\delta_2}{dt} = \omega_b \Delta\omega_2 \tag{4.3}$$

$$\frac{d\Delta\omega_2}{dt} = \frac{1}{2H_2}\left[T_{IP} + K_{12}(\delta_1 - \delta_2) - K_{23}\left(\delta_2 - \delta_3\right)\right] \tag{4.4}$$

LPA section:

$$\frac{d\delta_3}{dt} = \omega_b \Delta\omega_3 \tag{4.5}$$

$$\frac{d\Delta\omega_3}{dt} = \frac{1}{2H_3}\left[T_{LPA} + K_{23}(\delta_2 - \delta_3) - K_{34}\left(\delta_3 - \delta_4\right)\right] \tag{4.6}$$

LPB section:

$$\frac{d\delta_4}{dt} = \omega_b \Delta\omega_4 \tag{4.7}$$

$$\frac{d\Delta\omega_4}{dt} = \frac{1}{2H_4}\left[T_{LPB} + K_{34}(\delta_3 - \delta_4) - K_{45}(\delta_4 - \delta_5)\right] \qquad (4.8)$$

GEN section:

$$\frac{d\delta_5}{dt} = \omega_b\Delta\omega_5 \qquad (4.9)$$

$$\frac{d\Delta\omega_5}{dt} = \frac{1}{2H_5}\left[-T_e + K_{45}(\delta_4 - \delta_5) - K_{56}(\delta_5 - \delta_6)\right] \qquad (4.10)$$

EXC section:

$$\frac{d\delta_6}{dt} = \omega_b\Delta\omega_6 \qquad (4.11)$$

$$\frac{d\Delta\omega_6}{dt} = \frac{1}{2H_6}\left[K_{56}(\delta_5 - \delta_6) - T_{exc}\right] \qquad (4.12)$$

where δ_1, δ_2, δ_3, δ_4 and δ_5 are the angular positions of the HP, IP, LPA, LPB, GEN and EXC section, respectively; $\Delta\omega_1$, $\Delta\omega_2$, $\Delta\omega_3$, $\Delta\omega_4$ and $\Delta\omega_5$ are the speed deviations of the HP, IP, LPA, LPB, GEN and EXC section, respectively; H_1, H_2, H_3, H_4 and H_5 are the inertia constants of the HP, IP, LPA, LPB, GEN and EXC section, respectively; T_{HP}, T_{IP}, T_{LPA}, T_{LPB}, T_{EXC} are the mechanical torques of the HP, IP, LPA, LPB and EXC section, respectively; T_e is the electromagnetic torque of generator; K_{12} is the shaft stiffness between HP and IP section; K_{23} is the shaft stiffness between IP and LPA section; K_{34} is the shaft stiffness between LPA and LPB section; K_{45} is the shaft stiffness between LPB and GEN section; K_{56} is the shaft stiffness between GEN and EXC section; ω_b is the base speed (377 *rad/s*).

80

2) Synchronous Machine

The models for the synchronous machines in GEN 1 and GEN 2 are the same. These models are established in the *d-q* reference frame. The direct (*d*) axis is centred magnetically in the centre of the north pole, and the quadrature (*q*) axis is 90 electrical degree ahead of the d-axis. For a single synchronous machine, the model for SSR analysis includes two rotor circuits in the *d* and *q* axis, respectively [3], and the rotor consists of a field winding and the damper windings.

The detailed model of a synchronous machine for SSR study has been introduced in previous chapter, and it will not be further discussed here. The detailed model can be also written in a compact form as follows,

$$\dot{x}_{sm} = f_{sm}(x_{sm}, z_{sm}, u_{sm}) \tag{4.13}$$

where $x_{sm} = [\psi_d, \psi_{fd}, \psi_{1d}, \psi_q, \psi_{1q}, \psi_{2q}]^T$ $z_{sm} = [\omega_5]^T$, $u_{sm} = [v_d, v_q]^T$; v_d and v_q are the *d* and *q* axis voltages of the stator, respectively; ψ_d and ψ_q are the *d* and *q* axis linkages of the stator, respectively; ψ_{fd} is the linkage of the field winding; ψ_{1d} and ψ_{1q} are the linkages of the 1st *d* and *q* axis amortisseur, respectively; ψ_{2q} is the linkage of the 2nd *q* axis amortisseur; ω_5 is the rotor angle speed.

4.3.2 Model of DFIG-based Wind Farm

The DFIG-based wind farm is composed of a certain number of DFIG-based wind turbines. So, the model of wind farm can be represented by aggregating several wind turbines into a single DFIG-based wind turbine.

A single DFIG-based wind turbine includes a drive train, an induction machine, a DC-link capacitor, a rotor side and a grid side converter. The mathematical model for each part of the DFIG-based wind turbine has been discussed in previous chapter. The overall mathematical model of a DFIG-based wind turbine can be summarised as the following,

$$\dot{x}_{...} \quad_{- ...} \quad x_{wt}, z_{wt}, u_{wt})\tag{4.14}$$

$$z_{wt} = g_{wt}(x_{wt}, u_{wt})\tag{4.15}$$

where $x_{wt} = [\omega_t, \theta_{tw}, \omega_r, i_{ds}, i_{qs}, E'_d, E'_q, x_1, x_2, x_3, x_4, v_{DC}, x_5, x_6, x_7, i_{dg}, i_{qg}]^T$, $z_{wt} = [v_{dr}, v_{qr}, v_{dg}, v_{qg}]^T$, $u_{wt} = [v_{ds}, v_{qs}]^T$; ω_t is the angle speed of the wind turbine; θ_{tw} is the shaft twist angle; ω_r is the angle speed of induction machine, and $\omega_r = \omega_5$; i_{ds} and i_{qs} are the d and q axis stator currents, respectively; E'_d and E'_q are the d and q axis voltages behind the transient reactance, respectively; x_1, x_2, x_3 and x_4 are the intermediate variables of the controller for rotor side converter; v_{DC} is the DC capacitor voltage; x_5, x_6 and x_7 are the intermediate variables of the controller for grid side converter; i_{dg} and i_{qg} are the d and q axis currents of the grid-side converter, respectively; v_{dr} and v_{qr} are the d and q axis

rotor voltages, respectively; v_{dg} and v_{qg} are the d and q axis voltages of the grid-side converter, respectively; v_{ds} and v_{qs} are the d and q axis stator voltages, respectively.

4.3.3 Model of Series Compensated Transmission Line

In the modified test system, two transmission lines include two series capacitors respectively. For SSR analysis, the transients of the capacitors and inductances of the transmission lines cannot be neglected. The general SSR model for the series compensated transmission line has been presented in Section 3.4, Chapter 3. The specific model of the transmission line in the proposed test benchmark system can be written in the d-q axis reference frame as follows,

$$\frac{1}{\omega_b}\frac{dv_{cd}}{dt} - \omega_r v_{cq} = X_c i_{dL} \tag{4.16}$$

$$\frac{1}{\omega_b}\frac{dv_{cq}}{dt} + \omega_r v_{cd} = X_c i_{qL} \tag{4.17}$$

$$R_{TL}i_{dL} - \omega_r X_{TL}i_{qL} + \frac{X_{TL}}{\omega_b}\frac{di_{dL}}{dt} + v_{cd} = v_d - v_{1d} \tag{4.18}$$

$$R_{TL}i_{qL} + \omega_r X_{TL}i_{dL} + \frac{X_{TL}}{\omega_b}\frac{di_{qL}}{dt} + v_{cq} = v_q - v_{1q} \tag{4.19}$$

where v_{cd} and v_{cq} are the d and q axis voltages across the compensation capacitor; v_{1d} and v_{1q} are the d and q axis voltages of the infinite bus; i_{dL} and i_{qL} are the d and q axis currents through the transmission line; X_c is the reactance of the compensation

capacitor; X_{TL} is the combined reactance of the transmission line; R_{TL} the combined resistance of the transmission line.

4.4 Eigenvalue Analysis and Time Domain Simulation

In this section, the eigenvalue analysis and time domain simulation are conducted to evaluate the impact of increased DFIG-based wind farm on the SSR of the T-G units. The eigenvalue analysis is based on the state-space model of the proposed test benchmark system. The simulation platform for the modified test system is established in PSCAD/EMTDC, and the time domain simulations are conducted on this platform. For comparison, the eigenvalue analysis and time domain simulations are divided into the following two cases.

Case 1: The DFIG-based wind farm is not included in this case. The configuration of this case is as Fig. 4.1 without the wind farm. There are 10 T-G units in GEN 2, and the output power of each T-G unit is 75 MW.

Case 2: The configuration of this case is the same as the proposed test benchmark. The T-G units in GEN 2 are gradually replaced by the DFIG-based wind farm with equivalent capacity. The total output power of the DFIG-based wind farm and GEN 2 remain 750 MW during the above replacement.

4.4.1 Eigenvalue Analysis

The mathematical model of each electrical component in the test benchmark system has been introduced in section 4.3. These models are nonlinear, and they should be linearized to form the overall state space model of the test benchmark system. Based on equation (4.1)-(4.15), the linearized differential equations of GEN 1, GEN 2 and the DFIG-based wind farm can be derived at an operating point. These linearized equations, which include GEN 1, GEN 2 and DFIG-based wind farm, can be written in the following state space form as,

$$\Delta \dot{X}_1 = A_1 \Delta X_1 + B_1 \Delta U \tag{4.20}$$

where $\Delta X_1 = [\Delta X_{GEN1}, \Delta X_{GEN2}, \Delta X_{wt}]^T$. ΔX_{GEN1} represents the state variables of GEN1. These state variables includes the 6 rotating speeds of torsional masses, 6 relative angles between the torsional masses and 6 flux linkages of the synchronous machine in GEN1. ΔX_{GEN2} represents the state variables of GEN 2. The GEN 2 includes several T-G units, and these T-G units are modelled by an aggregated synchronous machine. So, state variables of ΔX_{GEN2} consists of the rotating speed of the lumped mass, the rotor angle and 6 flux linkages of the aggregated synchronous machine in GEN 2 . The ΔX_{wt} represents the state variables in the DFIG-based wind farm, and it contains 3 states of the drive train, 4 states of the induction generator in the DFIG-based wind turbine, 4 intermediate states of the rotor-side controller, the voltage of the DC-link capacitor, 3

intermediate states of the grid-side converter, and 2 current states for the grid-side converter. The ΔU is the input of the state space model, and it includes the d and q axis voltages of bus A.

The mathematical model for the series compensated transmission line in the test benchmark system can be demonstrated by (4.16)-(4.19). Then, the above mathematical model is linearized at an operating point, and the state space model of the series compensated transmission line can be demonstrated by

$$\Delta \dot{X}_{net} = A_{net}\Delta X_{net} + C_1\Delta X_1 \tag{4.21}$$

$$\Delta U = C_2\Delta X_1 + C_3\Delta X_{net} + D_1\Delta \dot{X}_1 \tag{4.22}$$

The state variable vector ΔX_{net} includes the d and q axis voltages of compensated capacitor.

The state space model of the GEN1, GEN 2, DFIG-based wind farm and the series compensated transmission lines have been derived previously. The overall state space of the proposed test benchmark system can be obtained by eliminating the inputs in (4.20). Based on (4.20)-(4.22), the state space model of the proposed test benchmark system can be represented by the following eqaution,

$$\Delta \dot{X} = A\Delta X \tag{4.23}$$

where $\Delta X=[\Delta X_1, \Delta X_{net}]^{T}$.

According to (4.23), the eigenvalues of Case 2 can be calculated based on the system parameters (as shown in Appendix) and the operating point. In Case 1, the DFIG-based wind farm is not included in the system. The eigenvalues of Case 1 can be obtained through removing the state variables of DFIG-based wind farm in ΔX_1.

4.4.2 Time Domain Simulation

Time domain simulations are conducted to verify the results of the eigenvalue analysis. The time domain simulation platform is established in PSCAD/EMTDC. For both Case 1 and Case 2, dynamics of the excitation and governor systems in GEN 1 and GEN 2 are not included in this simulation. The compensation level of the series compensated transmission lines is 74.2%. Under this compensation level, the second torsional mode is excited.   In the following simulations, a three-phase fault is applied at bus B, and the duration of this fault is 0.075s, which is four and a half cycles at 60 Hz [13]. According to the torsional mode shape, the second torsional mode happens between the LPA-LPB section and GEN-EXC section. When the torsional oscillation of Mode 2 is excited in the time domain simulation, it can be observed through the responses of LPA-LPB and GEN-EXC. Fig. 4.3 (a) shows the torsional responses of LPA-LPB and GEN-EXC in Case 1. When the fault happens at Bus B, the Mode 2 torsional oscillation is excited in Case 1. From dynamic responses of LPA-LPB and GEN-EXC, the torsional oscillation of Mode 2 exhibits slightly instability after the three phase fault.

4.5 Impact on Torsional Interaction

In this section, the study focuses on the torsional interaction of GEN1. In the following, the DFIG-based wind farm will gradually replace several T-G units in GEN 2 with equivalent capacity. The influence of the above replacement on GEN 1 will be investigated from the aspect of torsional interaction (TI).

In the proposed test benchmark system, torsional oscillations of the T-G units in GEN 1 mainly depend on the dynamics of the DFIG-based wind farm and the compensation level of the series compensated transmission lines. In this section, the compensation level remains the same to excite the same mode of torsional oscillation. As for the dynamics of the DFIG-based wind farm, it is attributed to three major factors: the scale of the DFIG-based wind farm, the control parameters of converters and the operating point of the DFIG-based wind turbines. In the following, these three factors of the DFIG-based wind farm will change respectively, and their impacts on the torsional interaction of the GEN 1 will be investigated in detail.

4.5.1 Impact of Wind Farm Scale

The TI of the T-G unit in GEN 1 may be affected by the scale of DFIG-based wind farm. When some T-G units in GEN 2 are substituted by the increased DFIG-based wind farm, the torsional mode of GEN 1 will change accordingly. In the following study, initially, the wind farm is assumed to contain 100 DFIG-based wind turbines, and the
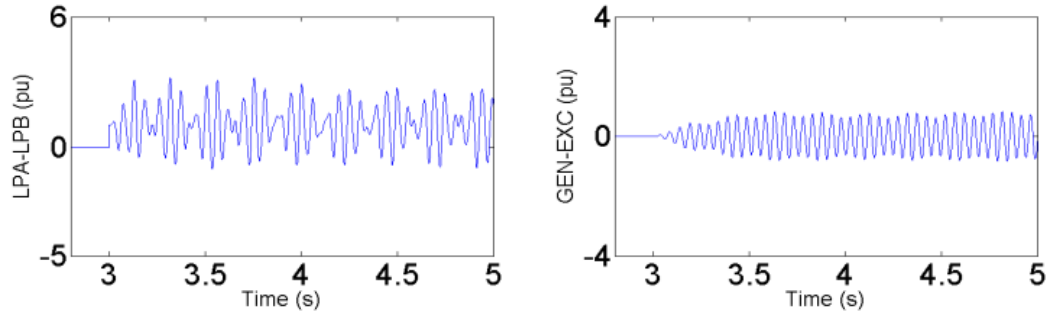
(a) 0 MW
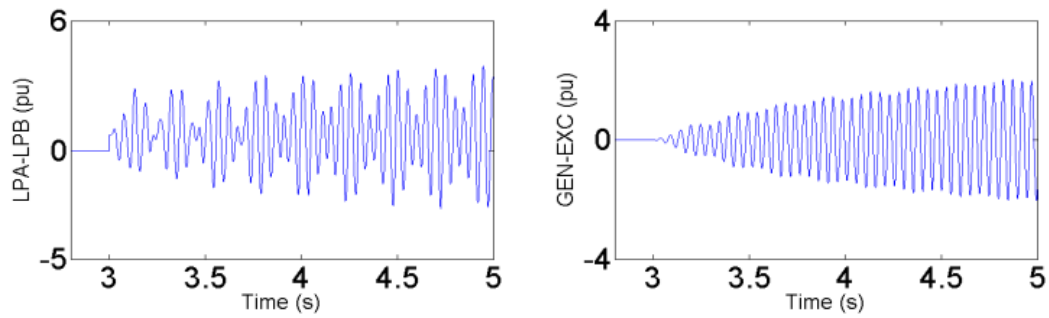
(b) 150 MW
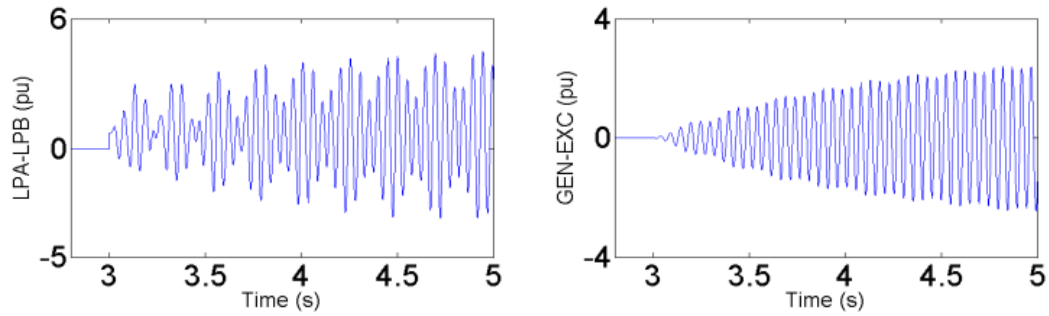
(c) 225 MW
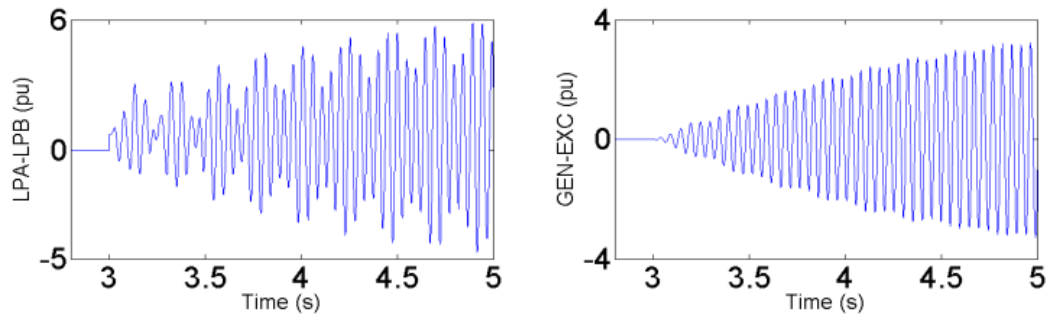
(d) 300 MW

Fig. 4.3 Torsional response of Mode 2 with (a) 0 MW, (b) 150 MW, (c) 225 MW and (d) 300 MW wind farm

output power of each DFIG-based wind turbine is 1.5 MW. Consequently, two 75 MW conventional T-G units in GEN 2 is replaced by the 150 MW DFIG-based wind farm. Then, as the number of wind turbines in the DFIG-based wind farm increases from 100 to 200, the number of T-G units in GEN 2 decreases from 8 to 6.

Fig. 4.3 (a) demonstrates the torsional oscillation of Mode 2 in Case 1 after the three phase fault. Fig. 4.3 (b) - (d) shows the torsional responses of LPA-LPB and GEN-EXC in Case 2 with increased wind farm scale. According to torsional responses of Mode 2 in Case 1 and Case 2, it is found that the replacement of conventional T-G units by DFIG-based wind farm will have a negative influence on the damping of TI. As the scale of DFIG-based wind farm increase gradually, more conventional T-G units in GEN2 are substituted. Meanwhile, the torsional responses of LPA-LPB and GEN-EXC become more severe, which means the damping of TI in GEN1 is even worse.

Table 4.1 Torsinal Mode 2 under increased wind farm scale

Wind Farm Scale (MW)	Eigenvalue (Mode 2)	Damping	Frequency (*Hz*)
0	0.29±127.95i	-0.227%	20.364
150	0.56±127.84i	-0.438%	20.351
225	0.71± 127.17i	-0.558%	20.240
300	0.78 ±127.19i	-0.613%	20.243
375	0.82 ±127.21i	-0.645%	20.246
450	0.85 ±127.23i	-0.668%	20.249
525	0.87 ±127.25i	-0.684%	20.252
600	0.89 ±127.26i	-0.699%	20.254

To confirm the results of time domain simulation, the eigenvalues of Mode 2 under different wind farm scales are listed in Table 4.1. From this table, all the eigenvalues of Mode 2 have positive real parts, which indicate that the SSR of the T-G unit is excited under different wind farm scale. As the scale of the DFIG-based wind farm increased from 0 MW to 600 MW, the real part of the eigenvalue for Mode 2 becomes larger, and the oscillation frequency changes slightly. This means the increased wind farm scale has a negative effect on the damping of Mode 2, which verifies the results of time domain simulation. Meanwhile, the change rate of damping ratio slows down with increased wind farm scale. This phenomenon attributes to that the damping provided by the wind farm changes nonlinearly with the wind farm scale.

4.5.2 Impact of DFIG Converter Control

A single DFIG-based wind turbine includes a rotor-side converter and a grid-side converter, and both converters have their corresponding controllers. The parameters of these controllers have a significant influence on the dynamics of wind turbines, and they may also affect the TI of the conventional T-G unit. In this part, the impact of the DFIG converter control on the TI of conventional T-G unit will be studied. During the following study, the number of wind turbines in the DFIG-based wind farm is fixed at 100. Each wind turbine generates 1.5 MW output power, and the total output power from the DFIG-based wind farm is 150 MW.

The controllers for both rotor-side and grid-side converter adopt cascade control. From the time domain simulation, it is found that the inner control loop of rotor-side controller has a significant influence on the TI of GEN 1. The control configuration of the rotor-side controller has been demonstrated in Fig. 3.3. According to Fig. 3.3, K_{p2} is the proportional gain of PI controller for the inner current control loop.

To evaluate the impact of proportional gain K_{p2} (as shown in Fig. 3.3), the eigenvalues of Mode 2 under different K_{p2} are listed in Table 4.2. From Table 4.2, all the eigenvalues have positive real parts, which mean Mode 2 is unstable under different control parameters of DFIG. Meanwhile, as the proportional gain K_{p2} decreases, the damping of Mode 2 will increase correspondingly. The result of eigenvalue analysis can also be confirmed by the time domain simulations under different K_{p2} as shown in Fig. 4.4.

Table 4.2 Torsional Mode 2 under different control parameters

Control Parameter K_{p2}	Eigenvalue (Mode 2)	Damping	Frequency (*Hz*)
0.025	0.56±127.84i	-0.438%	20.346
0.015	0.51 ± 127.79i	-0.399%	20.338
0.005	0.45 ±127.77i	-0.352%	20.335
0.0025	0.41 ±127.76i	-0.321%	20.334
0.001	0.39 ±127.76i	-0.305%	20.334
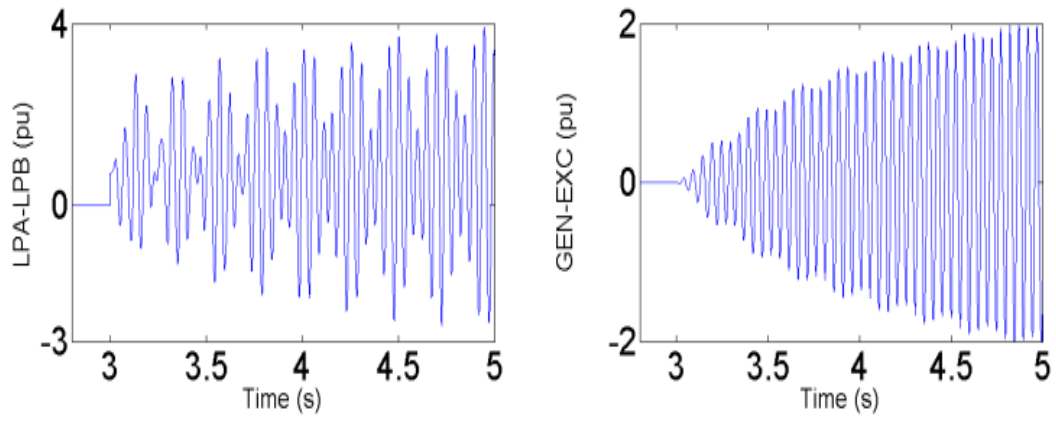
(a) K_{p2}= 0.025
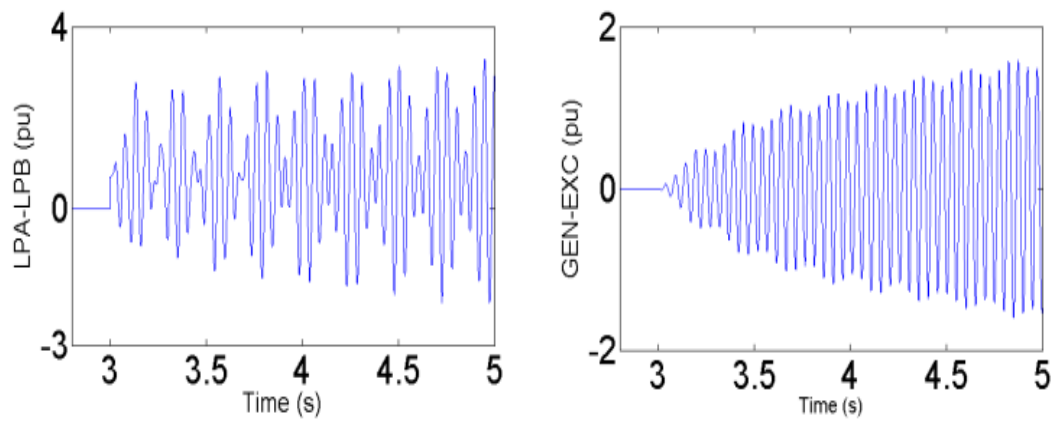
(b) K_{p2}= 0.005
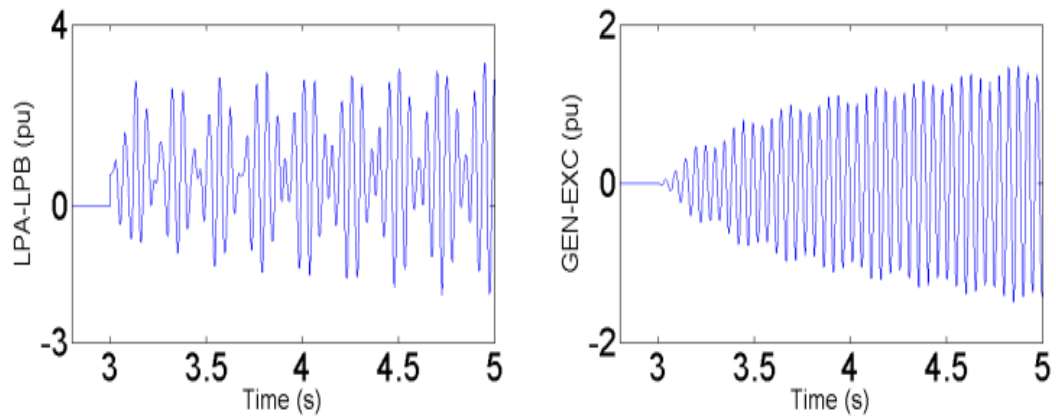
(c) K_{p2}= 0.001

Fig. 4.4 Torsional response of Mode 2 under different K_{p2}

4.5.3 Impact of Operating Points

The DFIG-based wind turbines will work at various operating points when they are under different wind speeds. The generator in a DFIG-based wind turbine is an induction machine, and the slip range of this machine may reach 30% to achieve the variable wind speed operation. Due to the large slip range of induction machine in DFIG, the dynamics of the DFIG-based wind farm is largely dependent on the operating point, and the operating point may also influence the TI of GEN 1. Table 4.3 demonstrates the relationship between the active power produced by a DFIG-based wind turbine and the wind speed. The data in Table 4.3 are obtained and calculated from the Appendix A.1. When the wind speed is comparatively low, the DFIG-based wind turbine operates in the range of sub-synchronous speed. Higher wind speed will make the DFIG-based wind turbine operate in the range of super-synchronous speed.

To exclude the influence of wind farm scale, the total number of DFIG-based wind turbines in the wind farm remains 100. Consequently, two T-G units in GEN 2 will be replaced. In the following study, the output power of each DFIG-based wind turbines increases from 0.75 MW to 1.5MW. Fig. 4.5 shows the dynamic responses of LPA-LPB and GEN-EXC when the DFIG-based wind turbines operate at different operating points. The time domain simulation indicates that the TI of the T-G unit in GEN1 has worse damping as the DFIG-based wind turbines operate from the

sub-synchronous speed range to the super-synchronous speed range. The eigenvalue analysis (Table 4.4) also confirms the trend.

All the eigenvalues in Table 4.4 have positive real parts, and this means that Mode 2 is excited under different operating points. As the output power of each DFIG-based increased from 0.75 MW to 1.5 MW, the damping ratio of Mode 2 decreases, and the oscillation frequency of Mode 2 changes slightly. The trend of the eigenvalues for Mode 2 under different operating points confirms the results of time domain simulation. Meanwhile, the change rate of damping ratio is nonlinear with the increase of operating point of the DFIG. This phenomenon attributes to that the damping provided by the DFIG changes nonlinearly with operating point of itself.

Table 4.3 Operating point of a DFIG-Based wind turbine

Operation Point	Sub-synchronous Speed		Super-synchronous Speed	
Wind Speed (m/s)	8.654	9.525	10.260	10.903
Output Power (MW)	0.75	1	1.25	1.5
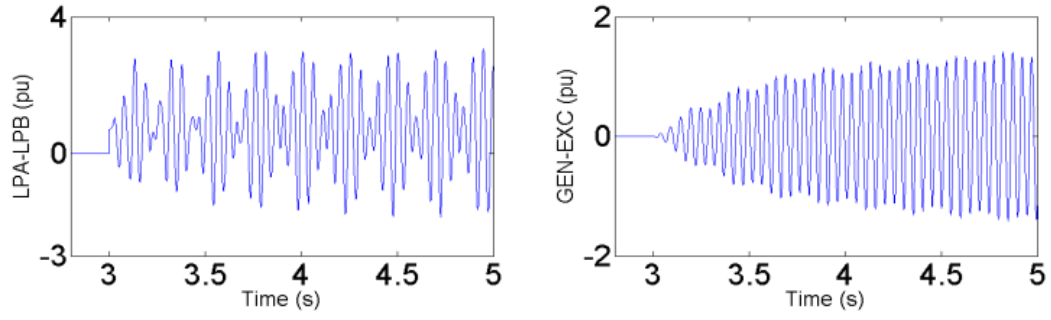
(a) 0.75 MW
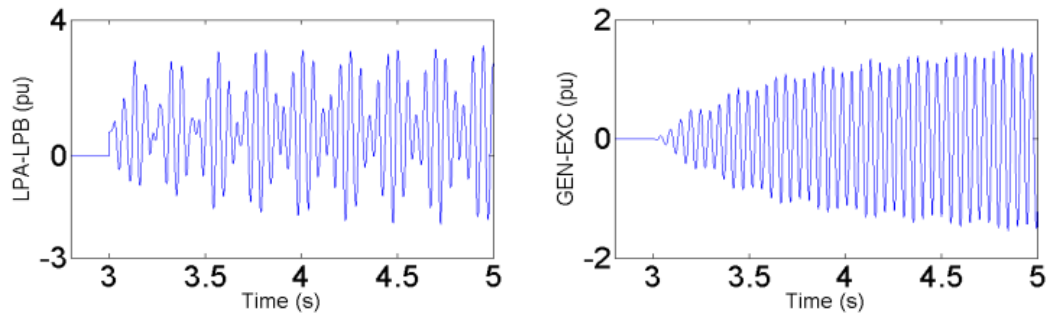
(b) 1 MW
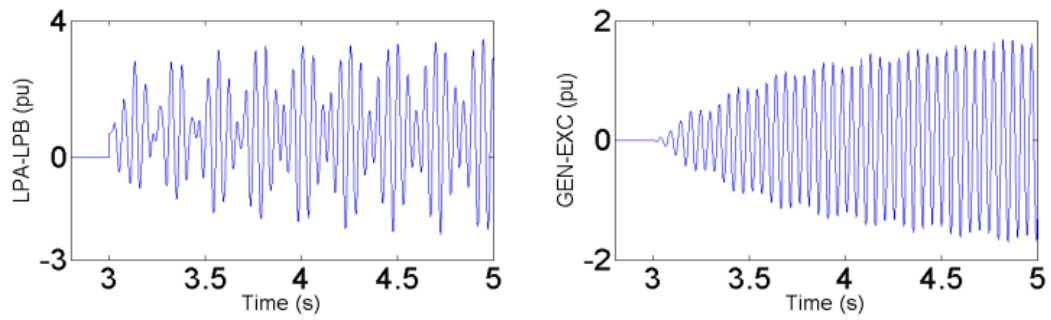
(c) 1.25 MW
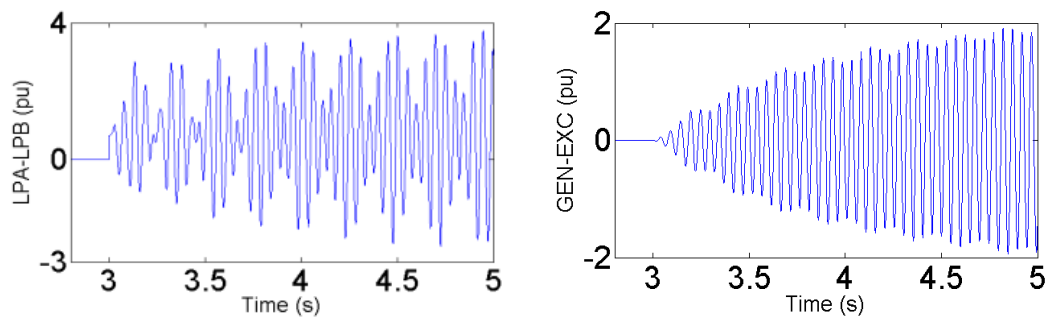
(d) 1.5 MW

Fig. 4.5 Torsional response of Mode 2 under different operating point

Table 4.4 Torsional Mode 2 at different operating point

Operating Point	Eigenvalue (Mode 2)	Damping	Frequency (*Hz*)
0.75 MW	0.42±127.46i	-0.330%	20.286
1 MW	0.46±126.59i	-0.363%	20.147
1.25 MW	0.50±127.72i	-0.391%	20.327
1.5 MW	0.56±127.84i	-0.438%	20.346

4.6 Results of Induction Generator Effect

In this section, the induction machine effect (IGE) of the proposed test benchmark system is analysed when some T-G units in GEN 2 are replaced by a DFIG-based wind farm. To exclude the effect of TI and focus on the IGE, the torsional dynamics of conventional T-G unit in GEN 1 are ignored in the following eigenvalue analysis and time domain simulation. To excite the IGE in the test benchmark system, the resistance of the transmission line R_{TL} is reduced to 0.00645 *pu*. The per-unit base values for this data can be referred to Appendix A.1 in this thesis. The IGE is an oscillation of network, and it can be examined by the eigenvalues of the network mode [2]. In the time domain simulation, the IGE can be observed through the dynamic response of the voltage of the series capacitor in the transmission. In the following study, the condition of system fault is the same as that in the research of TI. Initially, the compensation level of the series capacitive compensated transmission line is 74.2%, which is the same as in the IEEE FBM.

4.6.1 Impact of compensation level

The IGE of the test benchmark system is a purely electrical interaction. The dynamics of IGE is largely dependent on the compensation level of the series compensated transmission line. Under different compensation level, the impact of the DFIG-based wind farm on the IGE may be different.

In this part, the influence of the compensation level on the IGE of the test benchmark system is evaluated. During the following study, the compensation level of the series compensated transmission line decreases from 74.2% to 10% in both Case 1 and Case 2. In Case 2, two 75-MW T-G units in GEN 2 are replaced by a 150 MW DFIG-based wind farm, and the output power of each wind turbines in the DFIG-based wind farm is 1.5 MW. The control parameter K_{p2} in the DFIG-based wind turbine is set to 0.05. This control parameter is a feasible parameter obtained from theoretical calculations [29][35]. Fig. 4.6 demonstrates dynamic responses of the capacitor voltage after the system fault for both Case 1 and Cass 2 with different compensation level of the transmission line.

In the time domain simulations, the dynamic responses of the voltage of the series capacitor indicate that the DFIG-based wind farm makes the IGE of test benchmark system even worse when the compensation level of the transmission line is comparatively high. However, as the compensation level of the transmission line

(a) 72.4%

(b) 70%

(c) 30%

(d) 10%
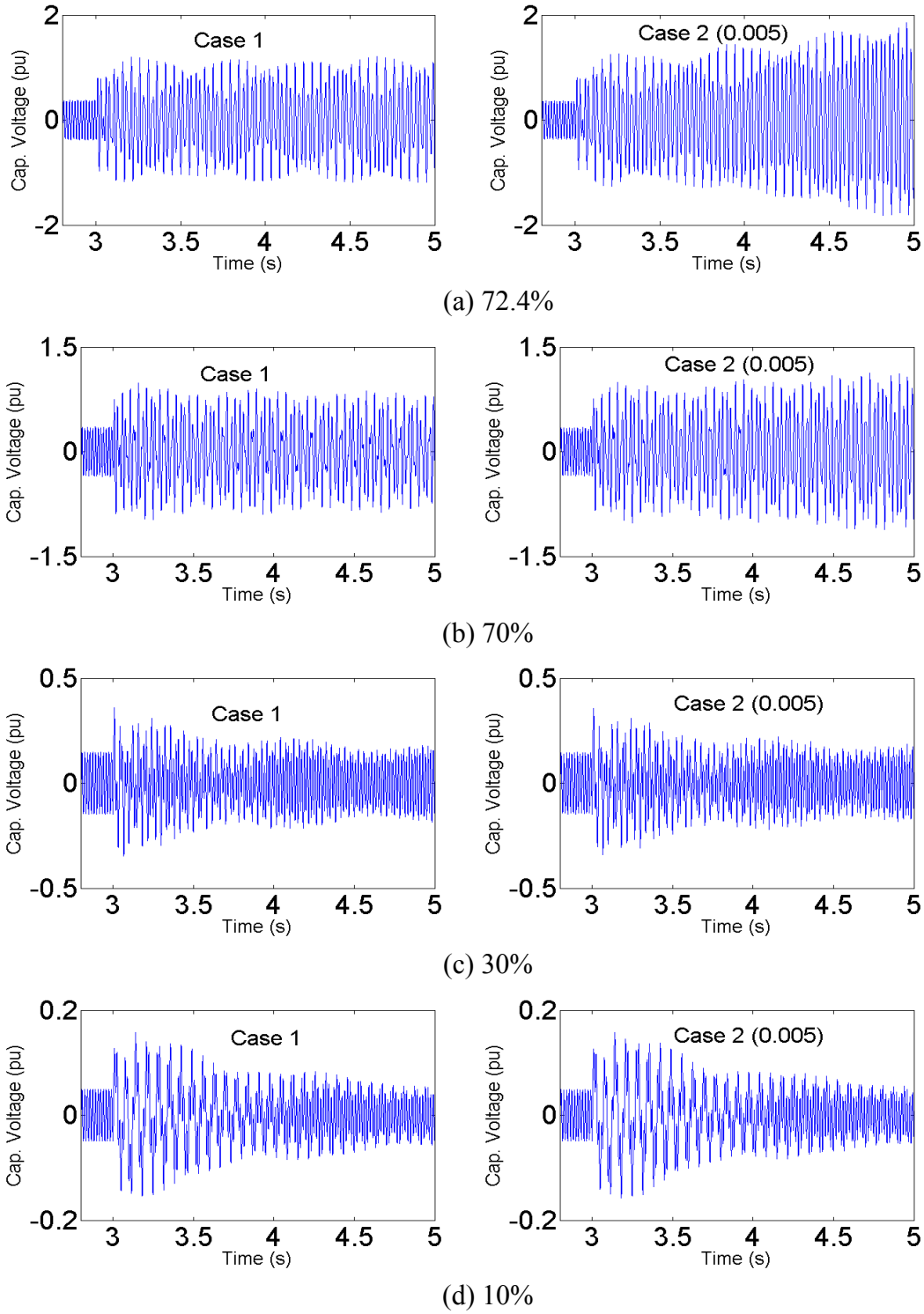
Fig. 4.6 Dynamic response of the voltage of series capacitor in Case 1 and Case 2 (K_{p2}= 0.005)

99

(a) 72.4%

(b) 70%

(c) 30%

(d) 10%
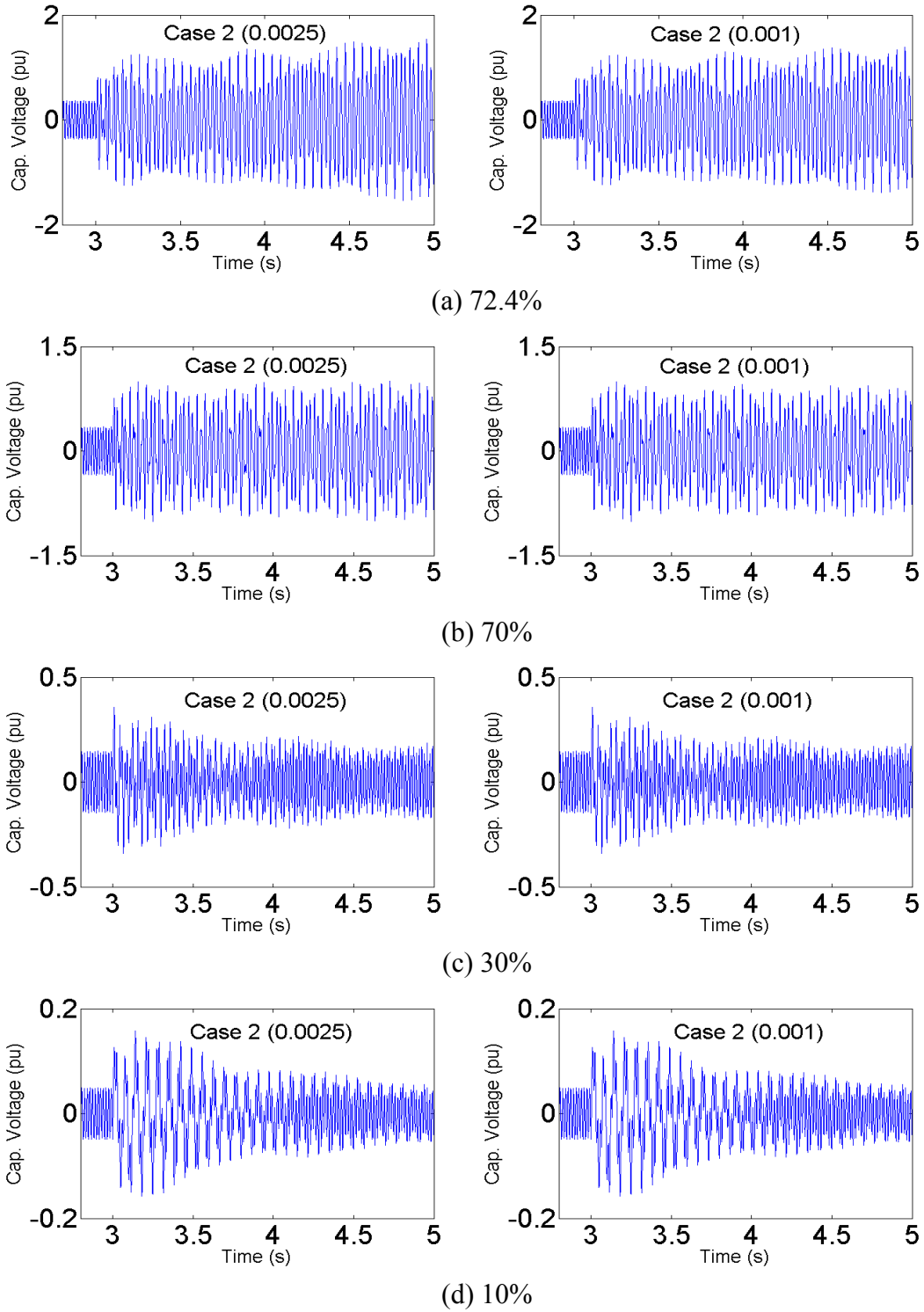
Fig. 4.7 Dynamic response of the voltage of series capacitor in Case 2 under different

control parameters

decreases, the DFIG-based wind farm manifests a positive impact on the IGE of the test benchmark system. In summary, the compensation level of the transmission line determines whether the DFIG-based wind farm will have a negative or positive effect on the IGE of test benchmark system.

Then, the control parameter K_{p2} in the DFIG-based wind turbine is reduced from 0.05 to 0.001. Fig. 4.6 and Fig. 4.7 show the dynamic responses of the voltage of the series capacitor under different control parameter. From these time domain simulations, it can be concluded that dynamic responses of the capacitor voltage improve with the decreasing control parameter K_{p2}. However, no matter how small the control parameter K_{p2} is, the trend of the influence of compensation level will not change. The eigenvalue analysis is also conducted for the above cases and confirms the conclusion of time domain simulation. Fig. 4.8 summarises the trend of the eigenvalues for both Case 1 and Case 2 under different compensation level with different control parameters.
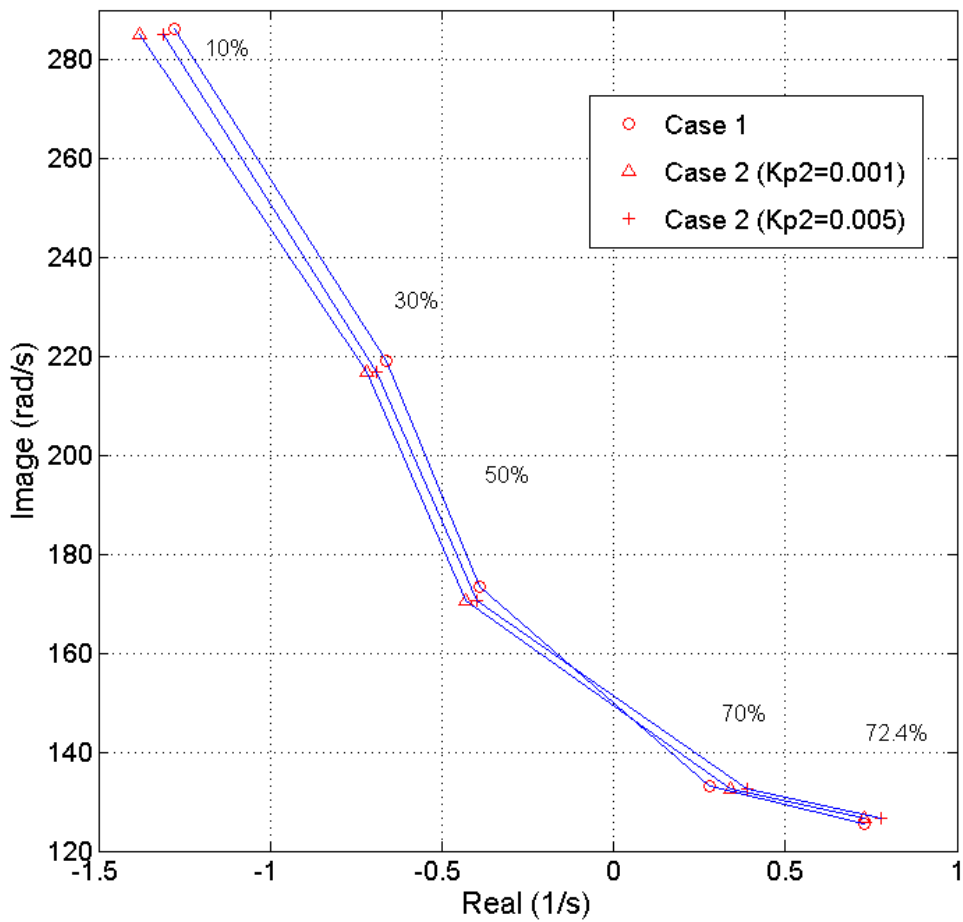
Fig. 4.8 Eigenvalue of network mode under different compensation level for Case 1 and Case 2 with various control parameters

4.6.2 Impact of Wind Farm Scale

This part will investigate the influence of wind farm scale on the IGE of test benchmark system. In the following study, the DFIG-based wind farm in Case 2 includes 100 wind turbines at the beginning, and the output power of each DFIG-based wind turbine is fixed at 1.5 MW. Then, the number of DFIG-based wind turbines gradually increases

(a) 72.4%

(b) 70%

(d) 30%

(e) 10%
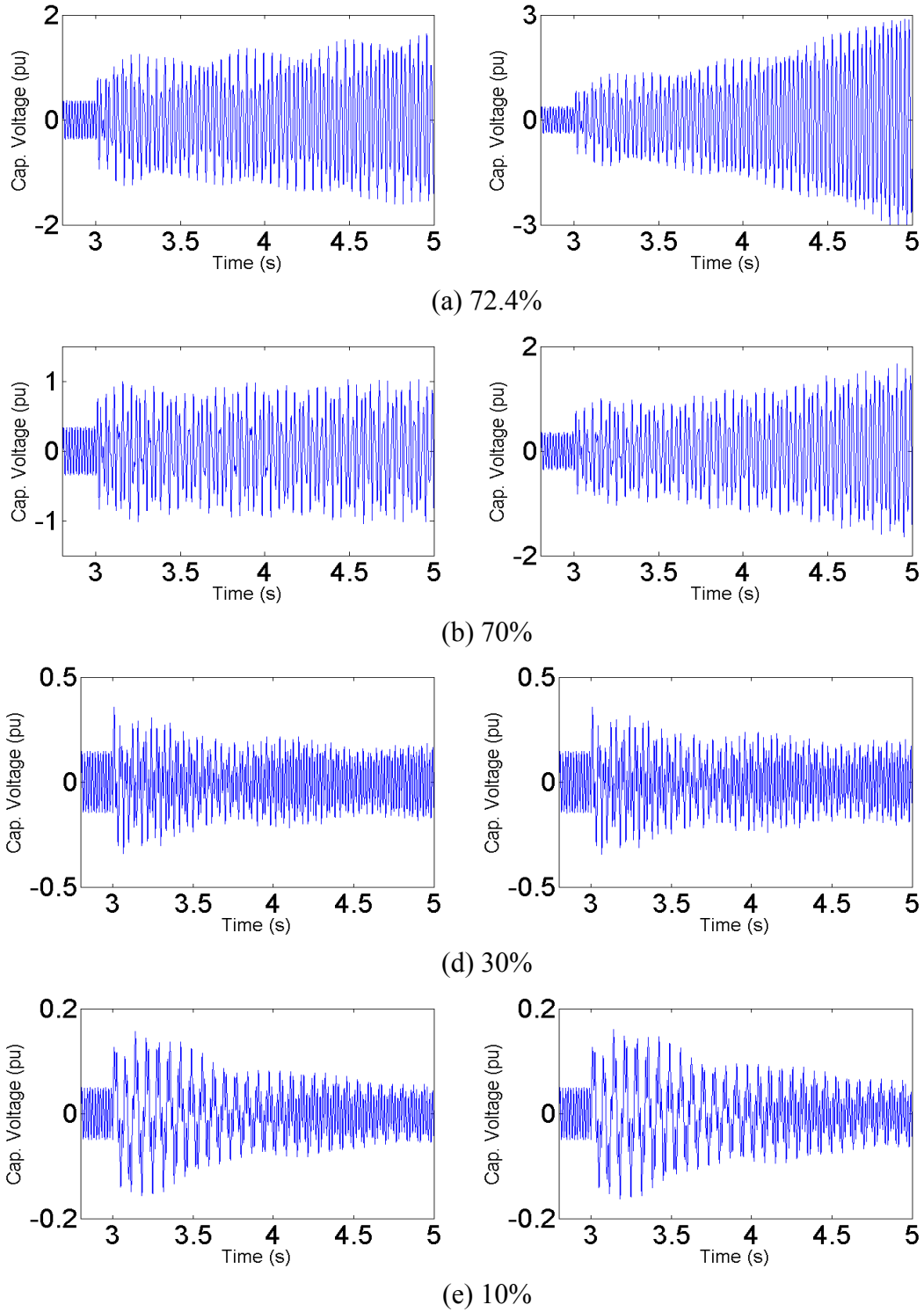
Fig. 4.9 Dynamic response of series capacitor voltage in Case 2 (225 MW) and Case 2 (300 MW)

from 100 to 200, and the number of replaced T-G units in GEN 2 increases from 2 to 4 accordingly. The control parameter K_{p2} of the DFIG-based wind turbine is fixed at 0.0025 during the following study.
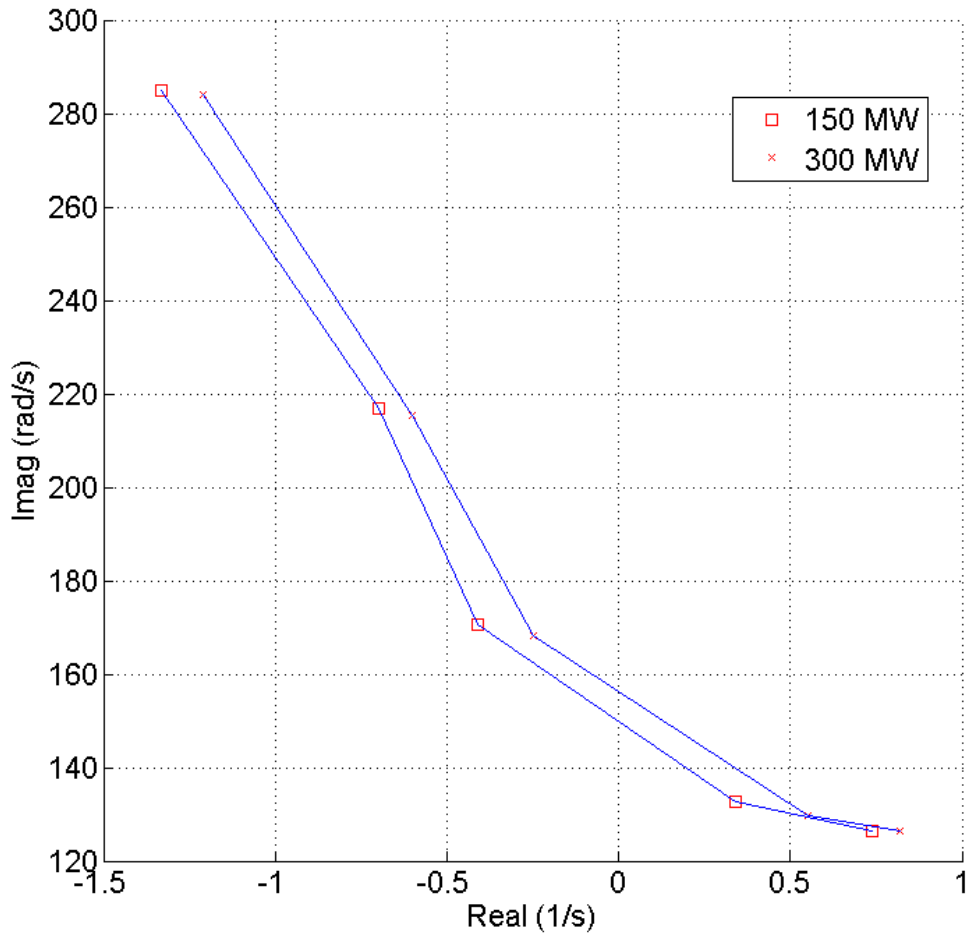
Fig. 4.10 Network resonance mode under different compensation level for Case 2 with increased wind farm scale

Fig. 4.7 and Fig. 4.9 show the dynamic responses of the voltage of the series capacitor when the scale of wind farm increase from 150 MW to 300 MW. From the time domain

simulation, the steady-state dynamics of the capacitor voltage become worse with increased wind farm scale at all compensation level. This indicates that the damping of IGE in the test benchmark system will be worse when more conventional T-G units are replaced by the DFIG-based wind farm. The result of the eigenvalues analysis also supports the time domain simulation, as shown in Fig. 4.10.

4.7 Summary

With vast utilisation of wind energy, the dynamics of wind farms will affect the conventional T-G unit in power systems. This chapter has examined the influence of the DFIG-based wind farm on the SSR of the conventional T-G units. The DFIG-based wind farm is proposed to replace several conventional T-G units with equivalent capacity. The influences of the wind farm on the SSR of conventional T-G units have been evaluated from the aspects of the TI and IGE. Based on the IEEE FBM, a new test benchmark system has been proposed for the evaluation. Then, the mathematical model of the proposed test benchmark system was presented, and the eigenvalue analysis was conducted based on this detailed model. The time domain simulations were also conducted in the PSCAD/EMTDC to verify the results of the eigenvalue analysis. The conclusions are presented from the TI and IGE as follows.

The replacement of conventional T-G units by a DFIG-based wind farm has a negative impact on the TI, and the influence can be summarised as follows,

(1) The damping of torsional oscillation becomes worse with increased wind farm scale.

(2) The inner PI controller of rotor-side converter has a significant influence on the TI. The smaller proportional gain of inner PI controller will improve the damping of torsional oscillation.

(3) The higher the operating point of the DFIG-based wind turbine, the less damping for the torsional oscillation of the conventional T-G unit.

On the other hand, the influence of the replacement on the IGE of T-G units mainly depends on the compensation level of the series compensated transmission line. At the high compensation level, when the system is excited to cause the IGE, the DFIG-based wind farm will make the IGE even worse. At the comparative low compensation level, if the system can maintain the stability against the fault, the DFIG-based wind farm can enhance the damping of oscillation. Meanwhile, the IGE of a system will become worse if more conventional T-G units are replaced by the DFIG-based wind farms.

CHAPTER 5 SMALL SIGNAL STABILITY OF WIND FARMS INTEGRATED VIA FFTS

5.1 Introduction

With the increased scale of offshore wind farms, the long distance transmission for wind power becomes a challenge. The fractional frequency transmission system (FFTS) provides a relatively new solution to increase the transmission capacity for offshore wind farms. The FFTS can achieve higher transmission capacity through the decrease of transmission frequency. However, when the offshore wind farms are integrated via the FFTS, the dynamic performance of such a system will be different from that of wind farms with a traditional AC transmission system.

In this chapter, the research focuses on the damping performance of wind farms with the FFTS. The wind farms consist of the doubly fed induction generators (DFIG), and they are proposed to be connected to the main grid via the FFTS. To analyse the damping performance, the mathematical model of wind farms with the FFTS is established, and then the eigenvalue analysis is carried out to evaluate the small signal stability of such a system. To confirm the results of eigenvalue analysis, the time domain simulations are carried out in both the single machine infinite bus (SMIB) and

the multi-machine system. Besides, the power electronic device, the cycloconverter, provides the potential for the FFTS to improve the damping of power systems. So, this chapter also proposes a feedback control loop on the cycloconverter to improve the damping performance of the FFTS with wind farms. The effectiveness of the proposed controller is also verified through the time domain simulations.

This chapter is organized as follows. In Section 5.2, the basic principle of the FFTS and the configuration of the studied systems are introduced. The detailed dynamic models of the studied systems are depicted in Section 5.3. Section 5.4 conducts the eigenvalue analysis for the studied systems. Section 5.4 proposes a feedback control loop on the cycloconverter to improve the damping performance of wind farms with the FFTS. The time domain simulations are demonstrated in Section 5.5 to verify the results of the eigenvalue analysis and the performance of the proposed feedback controller. Section 5.6 summarises the content of this chapter and provide the conclusion of this research.

5.2 Research Scenario

In this chapter, the offshore wind farm is supposed to include 100 2-MW, 0.69-kV DFIG-based wind turbines. The standard frequency is 60 Hz instead of UK standard 50 Hz. The reason is that most available cases for DFIG-based wind turbine use the 60 Hz (USA standard frequency).

Traditionally, the power generated by the offshore wind farm is delivered through the conventional AC transmission system. The transmission frequency is the nominal frequency (60 Hz). The configuration of such a system is shown as Fig. 5.1 (a).

In this chapter, the FFTS is proposed to transmit the power from offshore wind farms. The offshore wind farm directly produces 20 Hz (1/3 of 60 Hz) AC power, and the power is delivered through the 20 Hz transmission system. The cycloconverter acts as the interface between the FFTS (20 Hz) and the nominal power grid (60 Hz). It can increase the power frequency from 20 Hz to 60 Hz. The configuration of the wind farm with the FFTS is shown as Fig. 5.1 (b).

For comparison, the following studies are conducted in two cases as presented:

Case 1: the offshore wind farm is connected with the main grid through a conventional AC transmission system. The length of the transmission line is 100 *km*, and the nominal voltage is 230 *kV*. The frequency of the whole system is 60 *Hz*.

Case 2: the offshore wind farm directly generates AC power at 20 Hz, and it is linked with the low frequency side of cycloconverter through a 100 *km* 230 *kV* transmission line. The high frequency side of the cycloconverters is connected with the main grid with standard frequency (60 Hz).
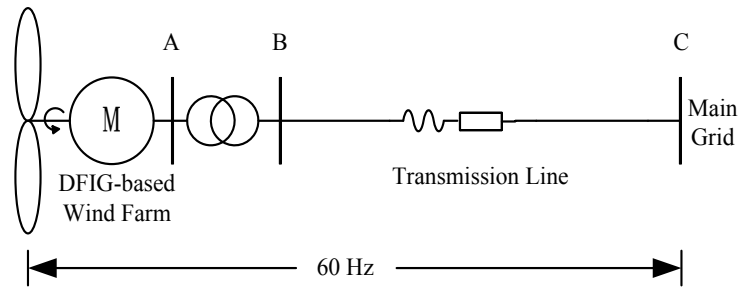
(a) Wind farm with standard AC system (Case 1)
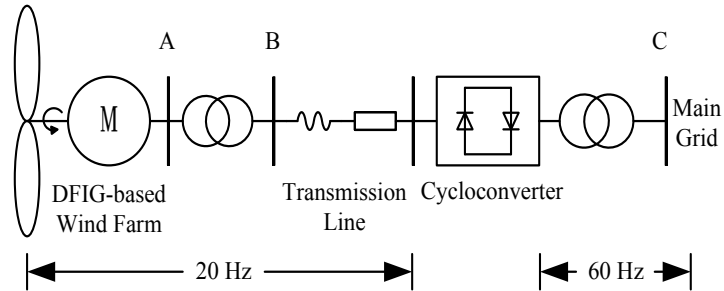
(b) Wind farm with FFTS (Case 2)

Fig. 5.1 Configuration of the studied systems

5.3 Modelling of the Studied Systems

In Case 1 and Case 2, the major electrical components include the DFIG-based offshore wind farms, the cycloconverter and the transmission line. In the following, the models of each electrical component will be introduced.

5.3.1 Modelling of DFIG-based Wind Farm

The offshore wind farm consists of 100 DFIG-based wind turbines, and its model is obtained by aggregating 100 wind turbines into a single DFIG-based wind turbine. The parameters of each wind turbines is summarised in Appendix. In chapter 3, the structure

and mathematical model of the DFIG-based wind turbine have been introduced in detail, so they will not be discussed here further.

In general, the overall mathematical model of a DFIG-based wind turbine can be summarised by,

$$\dot{x}_{\ldots} \quad \ldots \quad x_{wt}, z_{wt}, u_{wt}) \tag{5.1}$$

$$z_{wt} = g_{wt}(x_{wt}, u_{wt}) \tag{5.2}$$

where $x_{wt} = [\omega_t, \theta_{tw}, \omega_r, i_{ds}, i_{qs}, E'_d, E'_q, x_1, x_2, x_3, x_4, v_{DC}, x_5, x_6, x_7, i_{dg}, i_{qg},]^T$, $z_{wt} = [v_{dr}, v_{qr}, v_{dg}, v_{qg}]^T$, $u_{wt} = [v_{ds}, v_{qs}]^T$; ω_t is the angle speed of the wind turbine; θ_{tw} is the shaft twist angle; ω_r is the angle speed of induction machine, and $\omega_r = \omega_5$; i_{ds} and i_{qs} are the d and q axis stator currents, respectively; E'_d and E'_q are the d and q axis voltages behind the transient reactance, respectively; x_1, x_2, x_3 and x_4 are the intermediate variables of the controller for rotor side converter; v_{DC} is the DC capacitor voltage; x_5, x_6 and x_7 are the intermediate variables of the controller for grid side converter; i_{dg} and i_{qg} are the d and q axis currents of the grid-side converter, respectively; v_{dr} and v_{qr} are the d and q axis rotor voltages, respectively; v_{dg} and v_{qg} are the d and q axis voltages of the grid-side converter, respectively; v_{ds} and v_{qs} are the d and q axis stator voltages, respectively.

Although the general model of the DFIG is almost the same in Case 1 and Case 2, the base frequency in each case is different. In Case 1, the DFIGs generate power at the

111

standard frequency (60 Hz). However, the DFIGs in Case 2 produce AC power directly at 20 Hz. The reduced frequency in Case 2 may lead to the changes of parameters in the DFIG-based wind turbine.

The inertia constant of the drive train is affected significantly by the reduced transmission frequency. In this thesis, the drive train of the DFIG-based wind turbine is modeled as a two-mass system as shown in Fig. 5.2.
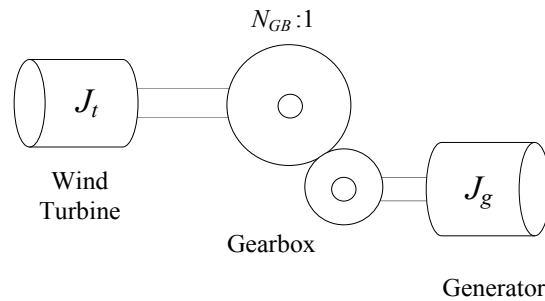
Fig. 5.2 Two-mass model of drive train

So, the total moment of inertia of the drive train can be obtained by [86],

$$J = \frac{J_t}{\left(N_{GB}\right)^2} + J_g \tag{5.3}$$

where J is the total moment of inertia of the drive train; J_t is the moment of inertia of the wind turbine; J_g is the moment of inertia of the generator; N_{GB} is the gearbox ratio.

Based on (5.3), the total inertia constant of the drive train can be obtained as,

$$H = H_t + H_g = J_t \frac{(\omega_b)^2}{2S(N_{GB})^2} + J_g \frac{(\omega_b)^2}{2S} \qquad (5.4)$$

where ω_b is the angular velocity of the base frequency; H is the total inertia constant of drive train; H_t is the inertia constant of the wind turbine; H_g is the inertia constant of the generator; S is the nominal apparent power of the generator.

In Case 2, the DFIG-based wind turbines generate power at 20 Hz, which is 1/3 of the standard frequency. Consequently, the base frequency and the gearbox ratio in Case 2 both decrease to 1/3 of those in Case 1. According to (5.4), although the inertia constant of wind turbine H_t is the same in both Case 1 and Case 2, the inertia constant of generator H_g decrease greatly in Case 2. So, the total inertia constant of the drive train in Case 2 is reduced.

5.3.2 Modelling of Cycloconverter

The cycloconverter is the core electrical component in the FFTS. It is a static frequency changer, which can convert AC power at one frequency to power at another frequency. It can also provide bidirectional power flow. Normally, it is used to step down the frequency of power to drive induction and synchronous motors in high power applications. However, in the FFTS, the cycloconverter will step up the frequency of power from the low frequency side to the nominal frequency of the grid. This requires

the cycloconverter to operate in its inversion mode, and this kind of application was first proposed in [20].

A three phase cycloconverter is formed by an array of 36 thyristor switches as shown in Fig. 5.3. In each phase, two three phase six-pulse converters, named P-Group and N-Group (also referred to as Positive-Group and Negative-Group), are connected back-to-back.
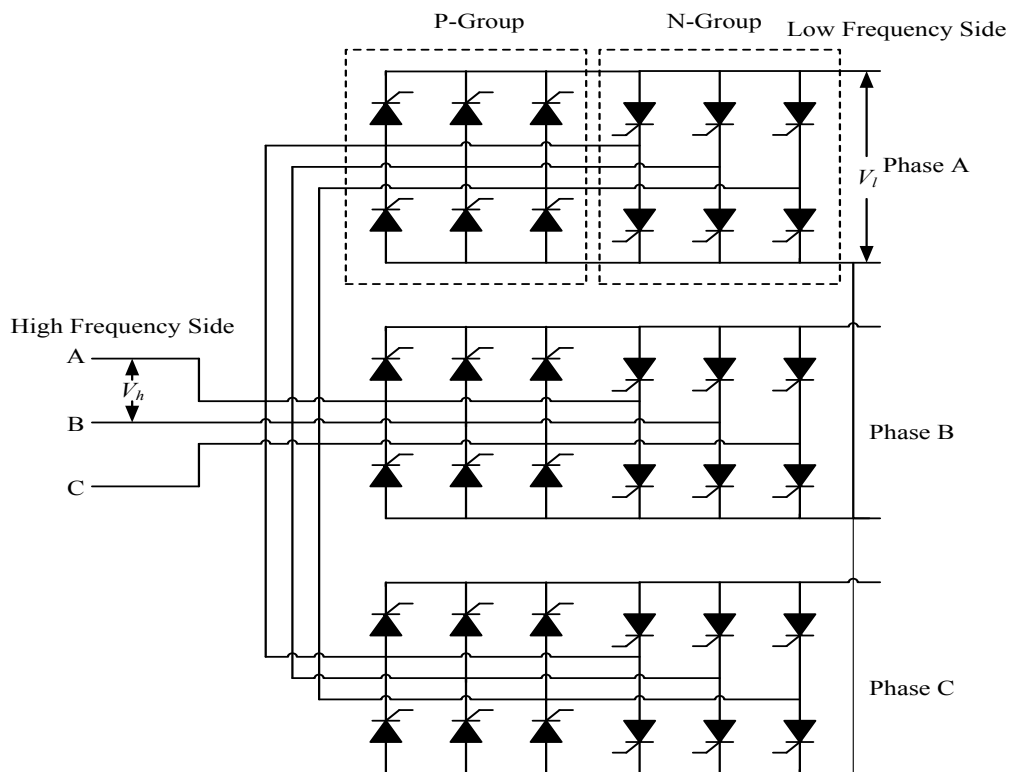
Fig. 5.3 Structure of a three phase cycloconverter

Basically, cycloconverters has two operation modes: circulating current mode and circulating current-free mode. To avoid the short circuit, the circulating current mode

for a cycloconverter needs an intergroup reactor (IGR), and the IGR increases the size
and cost of the cycloconverter. Although the circulating current-free mode may cause
the zero distortion, it has the advantages of less power losses and higher efficiency. In
the FFTS, the cycloconverter applies the circulating current-free mode. In summary,
we have the following assumptions for the cycloconverter in the FFTS:

(1) The cycloconverter is operated in the non-circulating current mode, or blocking
mode

(2) Control algorithm for the cycloconverter is assumed to be the cosine-wave crossing
method

Ideally, the mathematical model of a 6-pulse cycloconverter can be represented by
[119],

$$V_l = \frac{3\sqrt{2}}{\pi} V_h \cos\alpha \tag{5.5}$$

$$P_l = P_h \tag{5.6}$$

$$\cos\theta_h = 0.843 \cos\theta_l \cos\alpha \tag{5.7}$$

where α is the firing angle; V_l is the rms value of the line-to-neutral voltage at the low
frequency side; V_h is the rms value of the line-to-line voltage at the standard frequency
side; θ_h and θ_l are the power factor angle at the standard frequency side and the low
frequency side, respectively.

Dynamically, the cycloconverter can be treated as a time-delay element, and the time-delay is caused by the uncontrolled time of the thyristors [120]. It is obvious that the delayed time is random, and its average value can be demonstrated as,

$$T_s = \frac{1}{2mf_1} \tag{5.8}$$

where f_1 is the frequency of the standard power, and m is pulse number of a commutation cycle.

The equation (5.5) can be rewritten as

$$V_l = \frac{3\sqrt{2}}{\pi} V_h \cos\alpha \bullet 1(t - T_s) \tag{5.9}$$

where the black spot in the above equation means multiply.

The Laplace transform of equation (5.9) can be obtained as,

$$V_l(s) = \frac{3\sqrt{2}}{\pi} V_h e^{-T_s s} \cos\alpha \tag{5.10}$$

The time delay element can also be represented by

$$e^{T_s s} = 1 + T_s s + \frac{1}{2!} T_s^2 s^2 + \frac{1}{3!} T_s^3 s^3 + \cdots \tag{5.11}$$

Ignoring the high order terms in equation (5.11), equation (5.10) can be approximated as,

$$V_l(s) = \frac{3\sqrt{2}}{\pi} V_h \frac{\cos\alpha}{1+T_s s} \qquad (5.12)$$

Then, the equation (5.12) in the time domain can be transformed as,

$$\frac{dV_l}{dt} = -\frac{V_l}{T_s} + \frac{3\sqrt{2}}{\pi T_s} V_h \cos\alpha \qquad (5.13)$$

5.3.3 Transmission Line

The voltage equation of the transmission line is given by

$$V_s \angle \varphi_1 - V_l \angle \varphi_2 = (jX_{TL} + R_{TL})(-\boldsymbol{I}_s - \boldsymbol{I}_g) \qquad (5.14)$$

where $V_s \angle \varphi_1$ is the terminal voltage of the stator; $V_l \angle \varphi_2$ is the terminal voltage at the low frequency side of the cycloconverter; X_{TL} is the combined reactance of the transmission line and the transformer; R_{TL} is the combined resistance of the transmission line and the transformer.

In the stator oriented *d-q* reference frame, the above equation can be transformed as

$$\begin{bmatrix} v_{ds} \\ v_{qs} \end{bmatrix} = \begin{bmatrix} \cos(\varphi_1 - \varphi_2) \\ -\sin(\varphi_1 - \varphi_2) \end{bmatrix} V_l - \begin{bmatrix} R_{TL} & -X_{TL} \\ X_{TL} & R_{TL} \end{bmatrix} \left(\begin{bmatrix} i_{ds} \\ i_{qs} \end{bmatrix} + \begin{bmatrix} i_{dg} \\ i_{qg} \end{bmatrix} \right) \qquad (5.15)$$

5.4 Eigenvalue Analysis and Time Domain Simulation

In the following eigenvalue analysis, the main grid in Case 1 and Case 2 are supposed to be an infinite bus for the sake of simplicity. The linearised dynamic equations of the

DFIG-based wind farm are derived from the mathematical model at a steady state operating point. These linearized equations can be written in state space form as,

$$\Delta \dot{x}_{wt} = A_{wt} x_{wt} + B_{wt} \Delta u_{wt} \tag{5.16}$$

The above model includes 17 state variables and 2 inputs. The state variables consist of 3 drive train states, 4 states of the induction generator, 4 controller states of the rotor-side controller, the voltage of the DC-link capacitor, 3 controller states of the grid-side converter and 2 states for the currents of the grid-side controller. The 2 inputs are the d and q axis voltage of the stator.

Based on equation (5.13), the linearized equation of cycloconverter can be derived as

$$\Delta \dot{x}_{cyc} = A_{cyc} \Delta x_{cyc} \tag{5.17}$$

The linearized equation of the transmission line can be obtained by equation (5.15) as

$$\Delta u_{wt} = C_1 \Delta x_{wt} + C_2 \Delta x_{cyc} \tag{5.18}$$

Based on (5.18), the inputs in (5.16) can be eliminated. Then, the completed state space model for Case 2 can be represented by,

$$\Delta \dot{x} = A x \tag{5.19}$$

where $\Delta x = [\Delta x_{wt}, \Delta x_{cyc}]^{T}$.

The mathematical model for Case 1 can also be obtained if the state of cycloconverter is removed from equation (5.19).

In the following, the eigenvalue analyses are carried out for both Case 1 and Case 2. The wind speed for both cases is 12 *m/s*, and the output power of each DFIG-based wind turbine is 2 MW. The wind farm is obtained by aggregating 100 2-MW DFIG-based wind turbines into an equivalent one. The parameters of a single DFIG-based wind turbine are given in Appendices.

Table 5.1 demonstrates the eigenvalues for Case 1 and Case 2. From Table 5.1, all eigenvalues in both cases have negative real parts indicating a stable operating condition of the DFIG-based wind farm in both cases. The damping ratios of dominant states in Case 2 decrease compared with those in Case 1. This means the damping performance of the FFTS with wind farms is worse than that of the conventional AC system with wind farms.

Table 5.1 Eigenvalues of DFIG-based wind farm with FFTS and standard AC system

Dominant States	Case 1 (60 Hz)	Damping	Case 2 (20 Hz)	Damping
i_{ds}, i_{qs}	$-79.54 \pm 383.67i$	20.30%	$-26.50 \pm 193.22i$	13.60%
i_{dg}, i_{qg}	$-1.35 \pm 377.30i$	0.04%	$-0.03 \pm 128.16i$	0.02%
E_d', E_q'	$-4.56 \pm 17.66i$	25.00%	$-0.70 \pm 13.11i$	5.33%
ω_r	$-6.05 \pm 18.58i$	31.00%	$-2.41 \pm 13.58i$	17.10%
v_{DC}	$-1.09 \pm 7.49i$	14.40%	$-0.16 \pm 4.40i$	3.63%

The reason for less damping of the FFTS with wind farm is that the inertia constant of the drive train in DFIG is reduced significantly. According to the previous model analysis, the transmission frequency for the DFIG model in Case 1 and Case 2 is different. According to (5.4), if the transmission frequency is 1/3 of the standard frequency in the FFTS, the total inertia constant of the drive train in DFIG is reduced significantly. The reduced inertia constant decreases the damping of the FFTS with wind farms.

5.5 Dynamic Damping Improvements for FFTS

From previous eigenvalue analysis, it is concluded that the FFTS decreases the damping of DFIG-based wind farm significantly. To improve the damping performance, the better control design [33] for DFIG and the DFIG damping controller [88] are two established methods. However, both two approaches are based on a single or a single aggregated DFIG model. In practice, the DFIG-based wind turbines in a wind farm often operate under different conditions. So, the general effectiveness of these two approaches in multiple DFIG system needs further discussion.

This chapter proposes to add additional control loop on the cycloconverter to improve the damping of FFTS. The cycloconverter is a thyristor phase–controlled converter, and it is possible to apply a feedback controller on it to improve the damping performance of the FFTS. The feedback controller on the cycloconverter can manipulate the overall

dynamic performance of the DFIG-based wind farm, no matter with conditions of individual DFIG. In the following simulations, the general effectiveness of this controller will be confirmed through the simulations in both the single DFIG system and the multiple DFIG system.
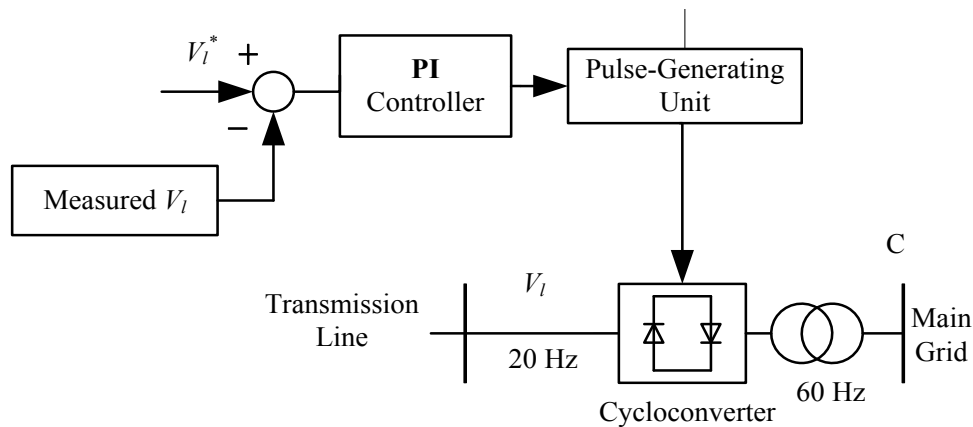
Fig. 5.4 Feedback control loop for cycloconverter

As mentioned before in this chapter, the cycloconverter applies cosine-wave crossing method, which is an open-loop control originally. To improve the damping performance, a feedback controller for the cycloconverter is implemented as Fig. 5.4. The feedback signal chooses the RMS voltage of the low frequency side of cycloconverter V_l, and the proposed feedback controller is adopted to track the control reference. Due to the fast transient of cycloconverter, the proposed controller chooses the proportional-integral (PI) strategy. The PI controller has the advantages of simple structure and fast response, and it is very suitable to control the power electronic devices. To verify the effectiveness, the proposed feedback controller is tested in both SMIB and multi-machine system through time domain simulations.

5.6 Dynamic Simulations

The time domain simulations are conducted in PSCAD/EMTDC to verify the results of eigenvalue analysis and the proposed controller on the cylcoconverter. The DFIG-based wind farm in the following simulations is obtained by aggregating serveral 2-MW DFIGs into an equivalent DFIG. Dynamic simulations are carried out in a single machine infinite bus (SMIB) and a multi-machine system, respectively. The dynamic responses of the systems are compared between Case 1 and Case 2.

5.6.1 Simulations on SMIB System

In this part, the dynamic simulations are carried out in SMIB to observe the dynamic responses in the following three cases:

Case 1 and Case 2: as described in Section 5.2. The main grid is replaced by an infinite bus.

Case 3: a feedback control loop is added to cycloconverter in Case 2.

1) Dynamic Responses against Disturbances

To study the dynamic performance of Case 1 and Case 2, a three-phase ground fault is applied to excite the dynamic responses. The reason to apply three-phase ground fault is that it will lead to a large fault current, and the damage caused by it is usually more severe. So, the three phase ground fault is usually chosen as a large disturbance to

verify the stability of a power system when small signal stability is studied [33] [118]. On the other hand, the purpose of three ground fault in this thesis is to excite the oscillations of power systems, and then the damping performance can be compared between different systems. Other types of fault are no more necessary.

In the following simulations, the three-phase ground fault happens at Bus B in both cases as shown in Fig. 5.1, and the duration for this fault is 0.025 s.

Fig. 5.5 shows the dynamic responses of the active power, reactive power, rotor speed, DC-link voltage, the active power of grid side converter and the reactive power of the grid side converter against the fault in Case 1 and Case 2. The state responses of the DFIG-based wind farm with the FFTS (Case 1) and the standard AC system (Case 2) demonstrate that both systems can restore to the steady state after the fault with the support of the stiff grid. It also can be seen that the damping of the DFIG-base wind farm with the FFTS decrease significantly.
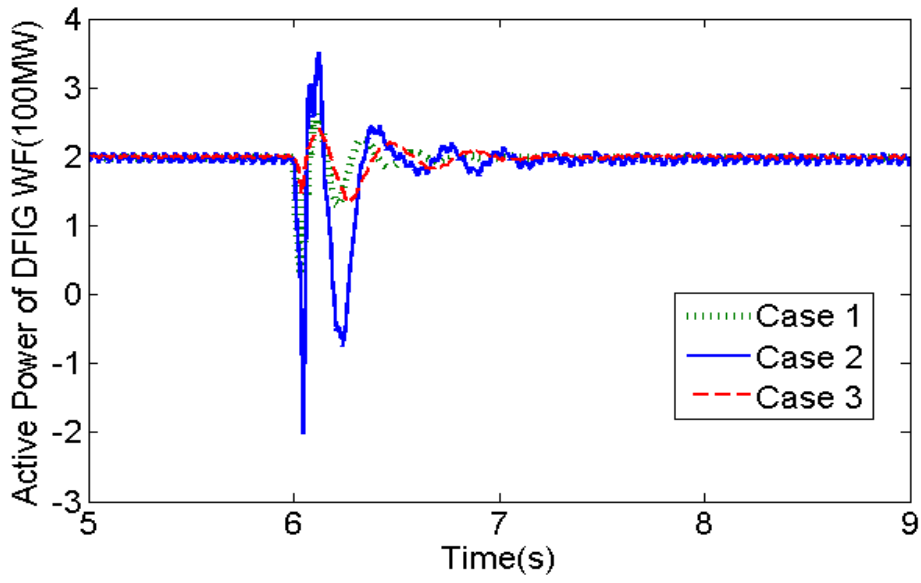
(a)
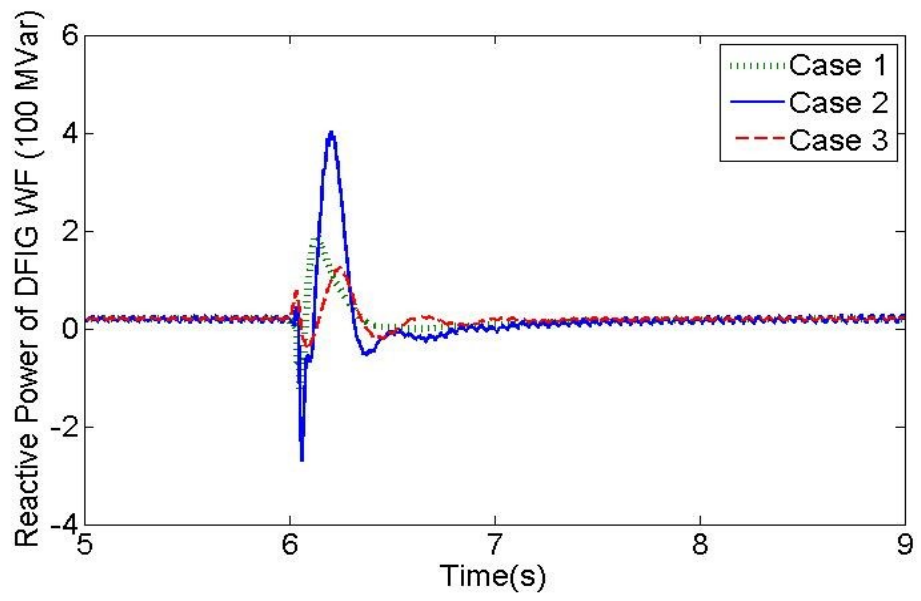
(b)
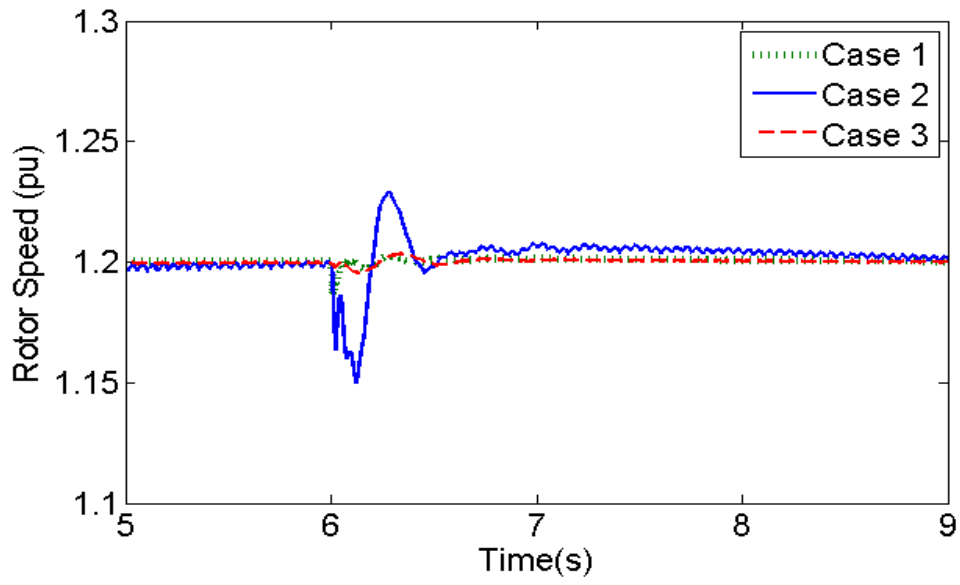
(c)
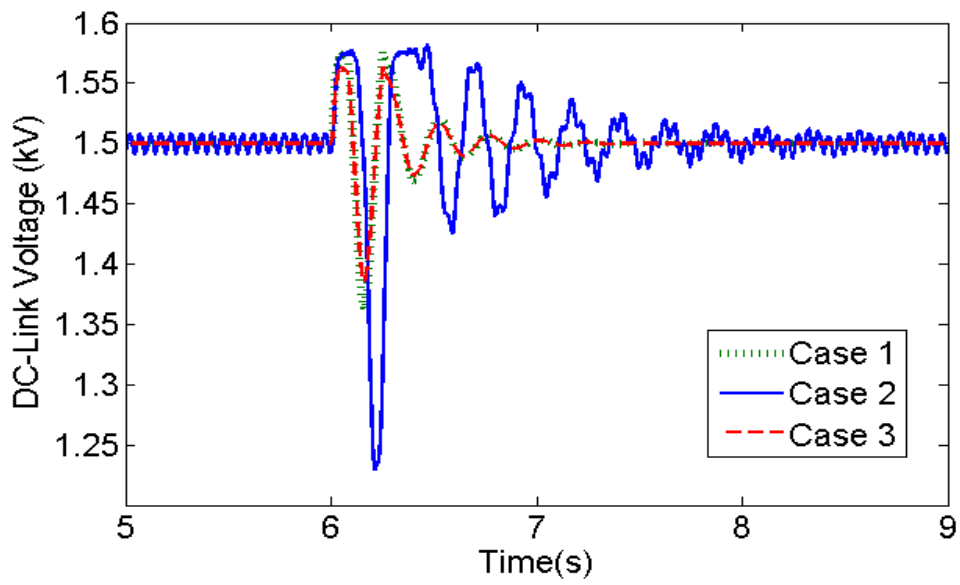
(d)
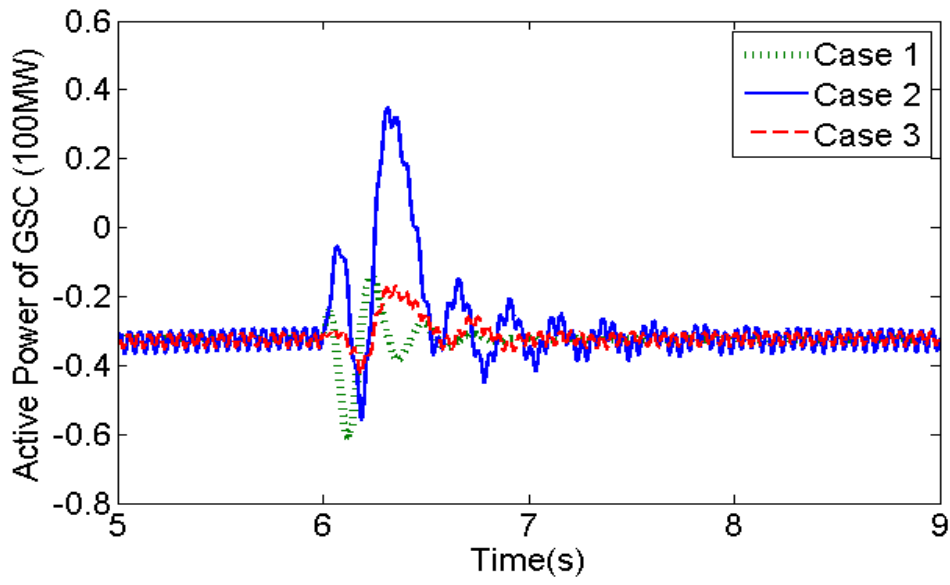
(e)
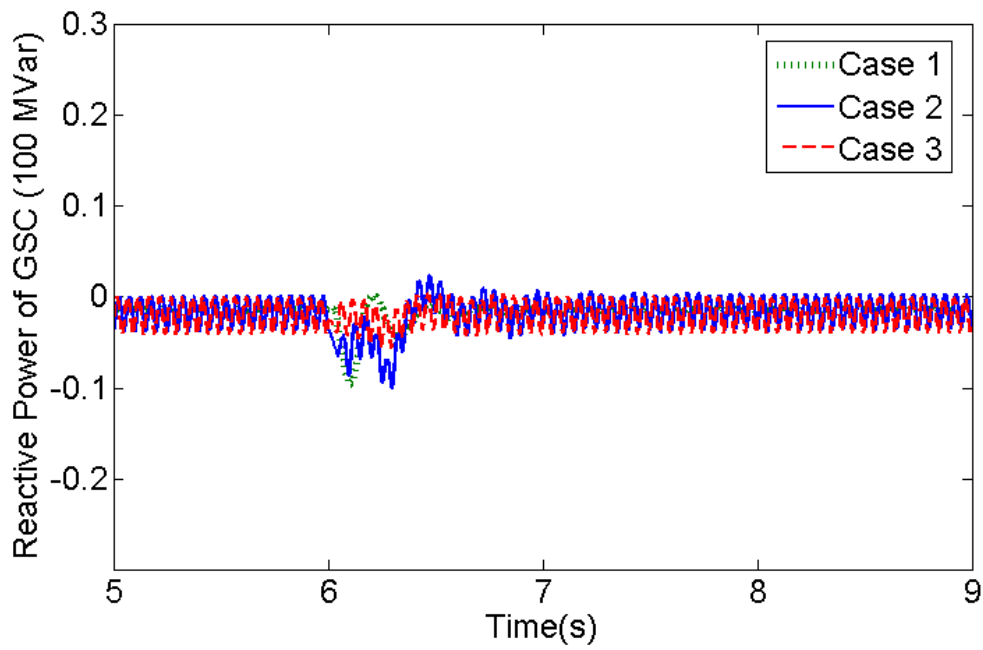
(f)

Fig. 5.5 Dynamic responses for Case 1, 2 and 3 in SMIB under fault

126

It also can be observed from Fig. 5.5 that the simulation results for the FFTS with wind farms (Case 2) contain 20 Hz frequency noises. These high frequency noises are attributed to the nature of the FFTS. Due to the reduced transmission frequency of the FFTS, the response time of the FFTS increases under the same conditions compared with that of the conventional AC system.

However, these high frequency noises cannot be removed in the above case studies due to the reason of comparison. The damping performance of the DFIG is very sensitive to the control parameters [33][35]. For comparison, the control parameters for DFIGs in both conventional AC system and FFTS should remain the same to exclude their influence on the damping performance.

Furthermore, these noises will not affect the study of small signal stability between the FFTS and conventional AC systems. This chapter focuses on the small signal stability of FFTS, which mainly concerns the low frequency oscillations (0.1~2 Hz) [23]. So, some high frequency noises in the FFTS will not affect the evaluation of damping performance between the FFTS and conventional AC system.
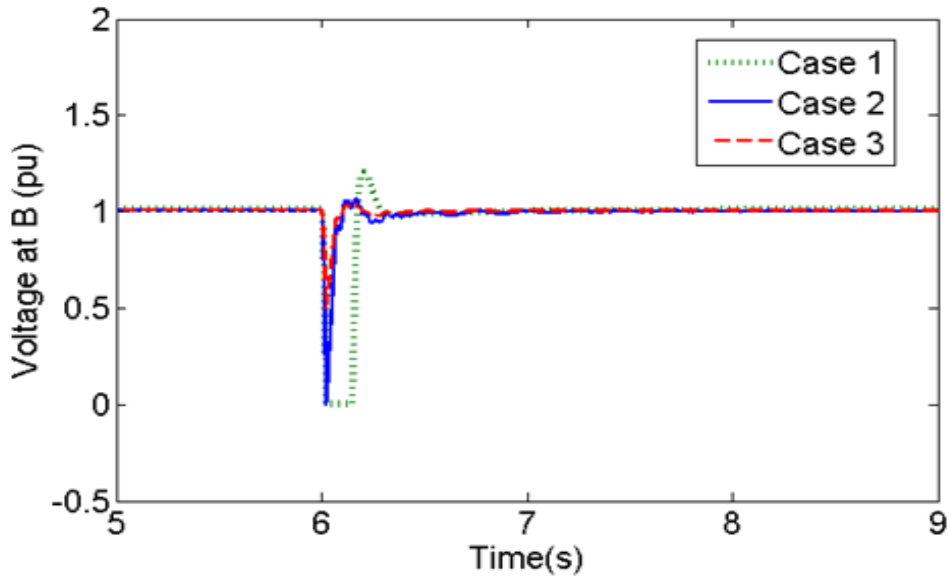
Fig. 5.6 Voltage dynamics at Bus B for Case 1, 2 and 3 under fault

Fig. 5.6 demonstrates the voltage responses at Bus B in Case 1 and 2 after the fault. The voltage fluctuation at Bus B in the FFTS is improved compared with that in the traditional AC system. The improved voltage dynamics is attributed to the reduced reactance of the transmission line in the FFTS.

2) Damping Improvement for FFTS

From previous time domain simulations, it is found that the FFTS reduces the damping of wind farms significantly compared with the standard AC system. To improve the damping performance, an additional feedback controller on cycloconverter is proposed as Fig. 5.4, and its effectiveness is also confirmed through the dynamic simulations in the SMIB. In Case 3, the applied fault is the same as that in Case 1 and Case 2.

Fig. 5.5 compares the dynamic responses of the active power, reactive power, rotor speed, DC-link voltage, the active power of grid side converter and the reactive power of the grid side converter in Case 3 with those in Case 1 and Case 2. With the feedback controller on cycloconverter, the damping performance of the wind farm with FFTS is improved significantly, and it is even better than the wind farm with standard AC system. The simulation results indicate the feedback controller on the cycloconverter can overcome the problem of less damping in the FFTS.

Fig. 5.6 shows the voltage profile at Bus B in Case 3 with those in Case 1 and 2. The voltage dynamics can be further improved with the proposed feedback controller on the cycloconverter.

5.6.2 Simulations in Multi-Machine System

For further study, the four-machine system is used to verify the results of small signal stability analysis and the proposed controller. The four-machine system as shown in Fig. 5.7 is symmetric, and it is composed of two identical areas connected by a comparatively weak tie. Each area includes two machine units with equal power output. The details of this four-machine system can be found in [22].

Furthermore, the DFIG-based wind farm in previous section is divided into two separate wind farms: WF1 and WF2. Each wind farm includes 50 DFIG, but the wind speed is different for each wind farm. The wind speed is 10.903 m/s for WF1, and the

output power for each DFIG-based wind turbine is 1.5MW. The WF2 is under 12 m/s

wind speed, and the output power for each DFIG is 2MW.
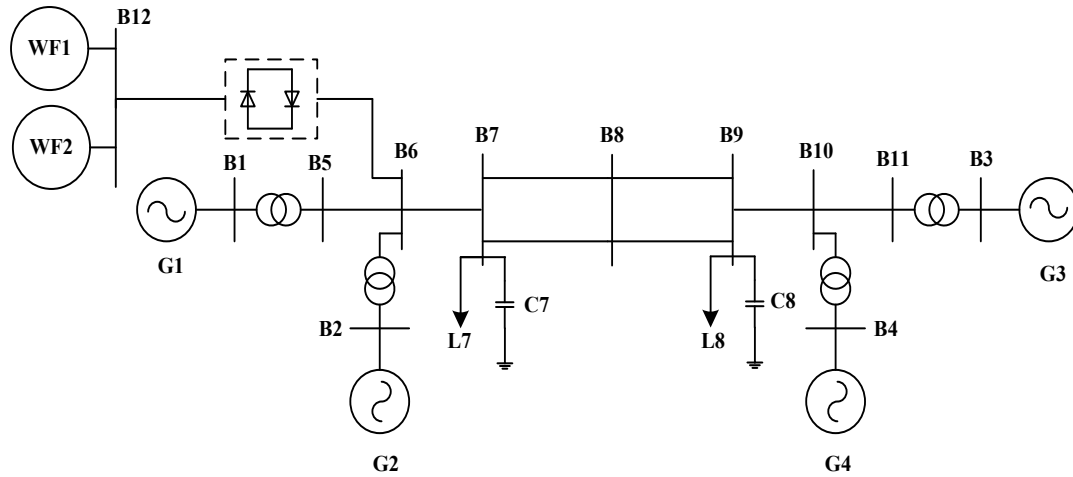
Fig. 5.7 Configuration of the simulations in four-machine system

For comparison, the dynamic simulations are carried out in three cases as the following:

Case 4:   WF1 and WF2 are connected to Bus B6 (as in Fig. 5.7) through a 100 *km* 230

kV standard AC transmission line.

Case 5: the power generated by WF1 and WF2 is delivered to the four-machine system

through a 100 *km* 230 *kV* low frequency transmission line. The low frequency side of

the cycloconverter is connected to Bus B12, and the high frequency side is linked with

B6 in the four-machine system.

Case 6: based on Case 5, the proposed feedback controller for the cycloconverter is

implemented as shown in Fig. 5.4.

In Case 4, 5 and 6, the total output power of WF1 and WF2 is 175 MW. Consequently, the output of G1 is reduced by 175 MW to guarantee the overall output from G1 and wind farms remain at 900 MW.

1) Dynamic Responses against Disturbances

The three-phase ground fault is applied at Bus B8 as shown in Fig. 5.7. The reason to choose the three-phase ground fault has been explained in Section 5.6.1. The fault starts at 6.0 s in Case 4, 5 and 6, and the duration of this fault is 0.1 s.

Fig. 5.8 shows the dynamic responses of the active power, reactive power of the WF1 and WF2 against the fault in Case 4 and Case 5. The simulation results in the four-machine system also demonstrate that the damping of the DFIG-based wind farms with the FFTS decrease obviously compared with that of wind farm integrated through traditional AC system. The simulation result in the four-machine system is the same as that in SMIB.

The 20 Hz frequency noises in the FFTS can also be observed in Fig. 5.8. The technical justification for these noises has been provided in Section 5.6.1.
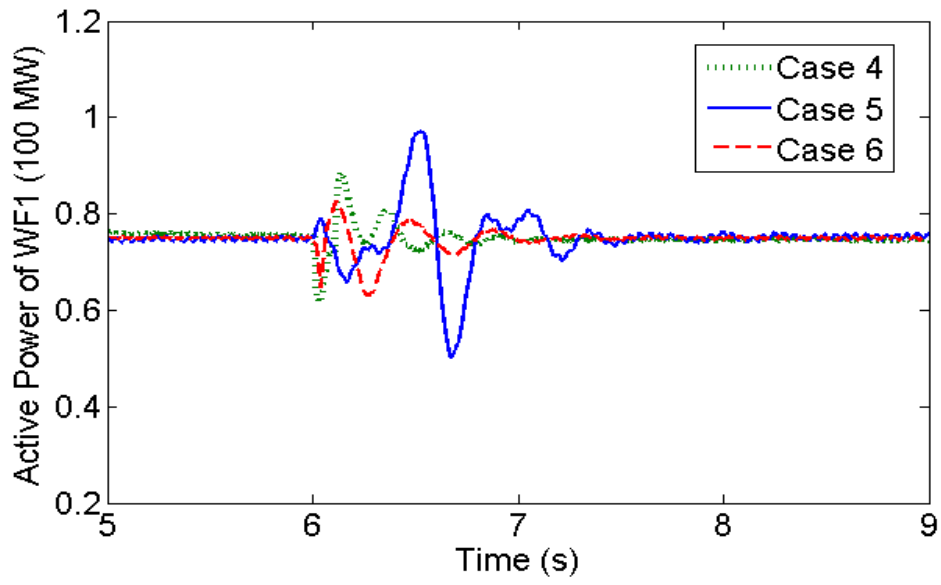
(a)
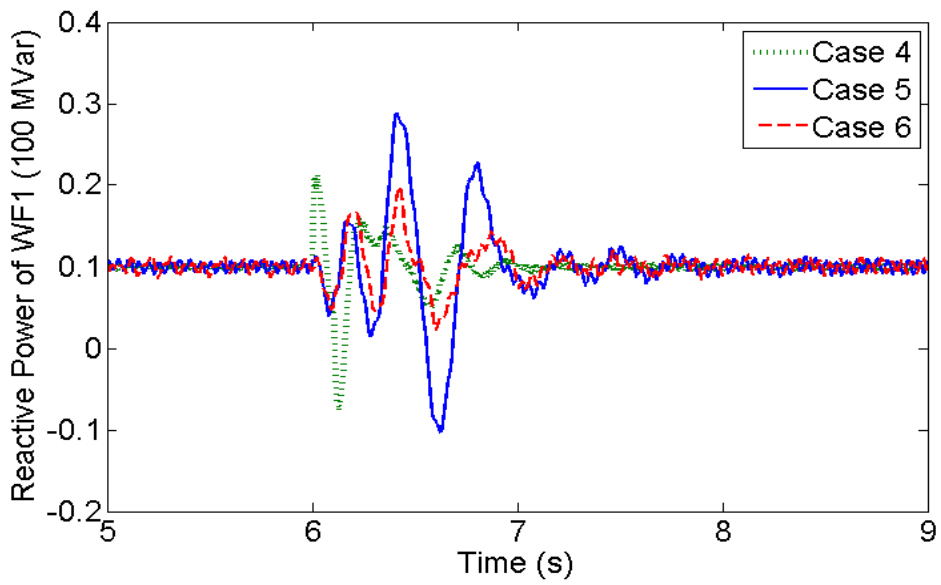
(b)
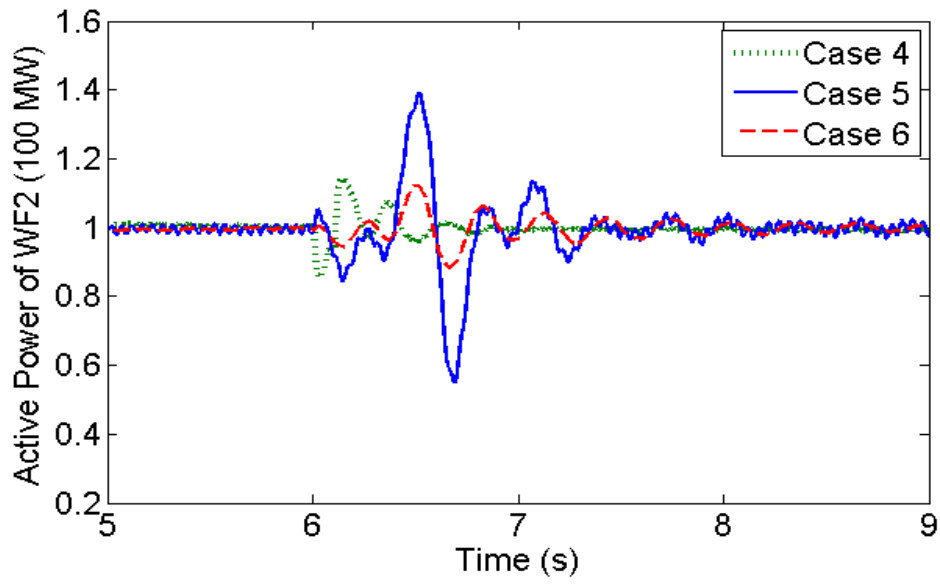
(c)
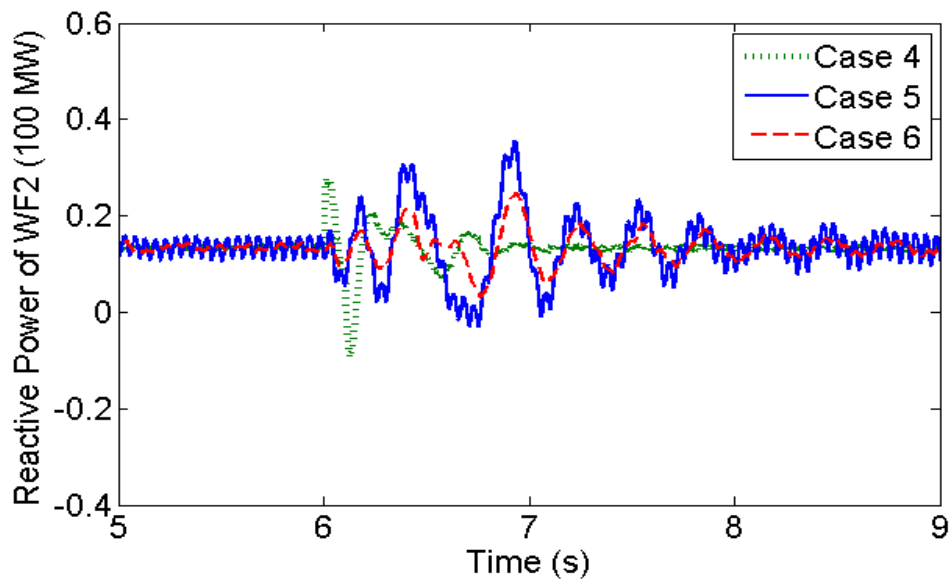
(d)

Fig. 5.8 Dynamic responses for Case 4, 5 and 6 in the four-machine system

Fig. 5.9 demonstrates the voltage responses at Bus B12 in Case 4 and Case 5, and it also

shows that the voltage response is improved in the FFTS.
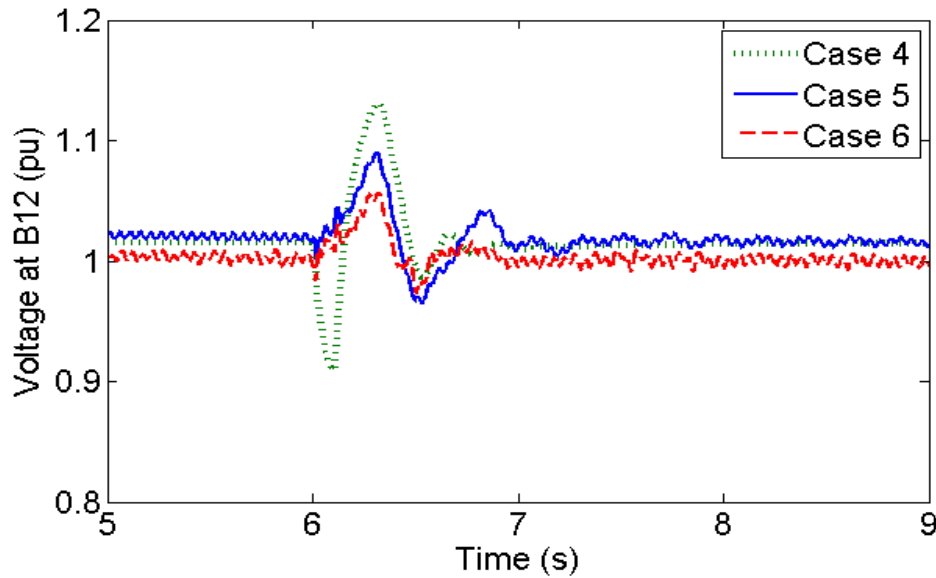
Fig. 5.9 Voltage responses at Bus B12 for Case 4, 5 and 6 under fault

2) Damping Improvement for FFTS

The general effectiveness of the proposed feedback controller on the cycloconverter is

also demonstrated in the four-machine system.

Fig. 5.8 shows the dynamic responses of the active power, reactive power in WF1 and

WF2 against the fault in Case 6. The dynamic responses in Case 6 demonstrate that the

feedback controller on the cycloconverter can greatly improve the damping of the wind

farm with FFTS. Meanwhile, with the support from the cycloconverter, the damping

performance of the wind farms with FFTS can perform even better than that of the wind farms with traditional AC transmission system.

5.7 Summary

This chapter has applied the FFTS to transmit the power from the DFIG-based offshore wind farms to the main grid. The small signal stability model of the FFTS with DFIG-based wind farms has been presented in detail. Based on the above model, eigenvalue analysis has been carried out to study the damping performance of the DFIG-based wind farm with the FFTS. To verify the results of the eigenvalue analysis, dynamic simulations have also been conducted in the SMIB and four-machine system. Both eigenvalue analysis and dynamic simulations have indicated that the damping of the DFIG-based wind farms is significantly decreased by applying the FFTS in comparison to the wind farms with the traditional AC transmission system. However, this chapter has proposed to add a feedback control loop on the cycloconverter to overcome this problem. With the help of this feedback controller, the damping of the DFIG-based wind farms with the FFTS can be performed even better than that of wind farms with the traditional AC system.

CHAPTER 6 GRID INTERCONNECTION VIA THE FRACTIONAL FREQUENCY TRANSMISSION SYSTEM

6.1 Introduction

The fractional frequency transmission system (FFTS) can significantly increase the transmission distance and capacity through the reduced transmission frequency. Due to the above advantages, the FFTS is not only suitable for integrating large scale offshore wind energy, but also has the potential to be applied in inter-area grid interconnection.

The inter-area oscillations between interconnected synchronous generators are inherent phenomena in power systems. In a large interconnected system, different areas in this system are often connected together by tie lines. Previous research [106] has found that the decrease of tie line impedance can improve the damping performance of the inter-area oscillations. So, for the purpose of damping improvement, it is better to find a method to reduce the impedance of the tie lines. The FFTS is a choice to cope with this problem. If the tie lines apply the FFTS technique, the impedance of the tie lines can be reduced through lowering the transmission frequency.

Although previous research also proposed to apply HVDC to interconnect power systems, the operation of the multi-terminal HVDC system is still in early development [20]. The FFTS does not face this challenge. It can easily form a network as the conventional AC system. Consequently, this chapter proposes to use the FFTS as a substitute for the conventional AC tie lines. The eigenvalue analysis and time domain simulations demonstrate that the application of FFTS as the tie lines improves the damping of the inter-area oscillations. Furthermore, the FFTS can also achieve power flow control through the frequency changer-cycloconverter.

This chapter is organized as follows. In Section 6.2, the configuration of the studied systems is introduced. The mathematical models for the major electrical components in the studied systems are presented in Section 6.3. Section 6.4 conducts the eigenvalue analysis and time domain simulation to demonstrate the influence of the FFTS on inter-area oscillations of power systems. Section 6.5 proposes a power flow controller for the FFTS, and its effectiveness is also verified through time domain simulations. The conclusion is summarised in Section 6.6.

6.2 The Studied Systems

6.2.1 Two-area System

The inter-area oscillations are very complex in large interconnected power systems. To concentrate the study of inter-area oscillations, the two-area system was proposed as

the standard benchmark system [106]. Although the size of this two-area system is small, it can imitate the inter-area oscillations in the actual power system. The configuration of the two-area system is shown as Fig. 6.2. It is a symmetric system and consists of two identical areas. The two areas are interconnected by a comparatively weak tie. Each area includes two T-G units with equal power output. The parameters for this two-area system can be found in [22].

This two-area system is operating under the condition that 400 MW power is transferred from Area 1 to Area 2 through two tie lines. In this system, there are three electro-mechanical modes of oscillation: two inter-machine modes for each area and one inter-area mode. When the inter-area mode is excited, the synchronous generators in Area 1 will swing against the synchronous generators in Area 2.

6.2.2 Two-area System with FFTS

This chapter proposes to apply the FFTS to interconnect power systems. The conventional AC tie lines between different areas are replaced by the FFTS. The general configuration of the FFTS in system interconnections is shown as Fig. 6.1.

In Fig. 6.1, Area 1 is interconnected with Area 2 through the FFTS. The FFTS includes two cycloconverters (C1 and C2) located at two terminals. The C1 and C2 are linked by a low frequency transmission line, in which the transmission frequency is 20 Hz. C1 is responsible for converting the 60 Hz AC power to the 20 Hz AC

power. C2 increases the transmission frequency of the AC power from 20 Hz to 60 Hz. The power flow through the FFTS can also be reversed. In this chapter, the reason to choose 60 Hz instead of UK standard 50 Hz is that the two-area system [22] [116] in the following research adopts the 60 Hz as its base frequency. So, this chapter chooses 60 Hz standard frequency.

Through the FFTS interconnection, the electrical length between the Area 1 and Area 2 is significantly reduced. Thus, the inter-area oscillation between these two utility grids can be improved.
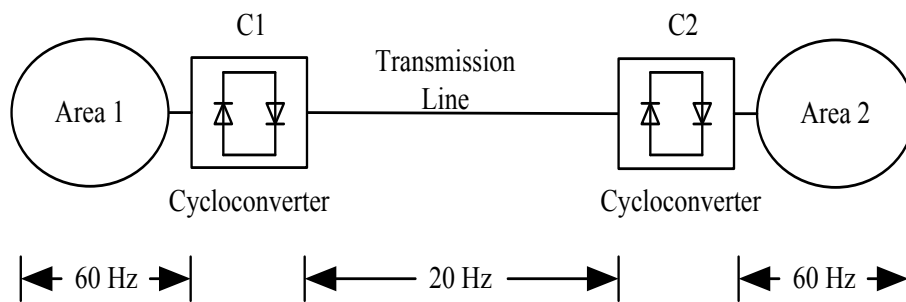
Fig. 6.1 Structure of the FFTS in system interconnections

For further study, the FFTS is adopted as the tie lines in the two-area system. The following three cases are established for comparison.

Case 1: The original two-area system is shown as Fig. 6.2.

Case 2: One of the tie lines between Area 1 and Area 2 is substituted by the FFTS (as shown in Fig. 6.3)

Case 3: Both of the two tie lines between Area 1 and Area 2 are replaced by the FFTS

(as shown in Fig. 6.4)
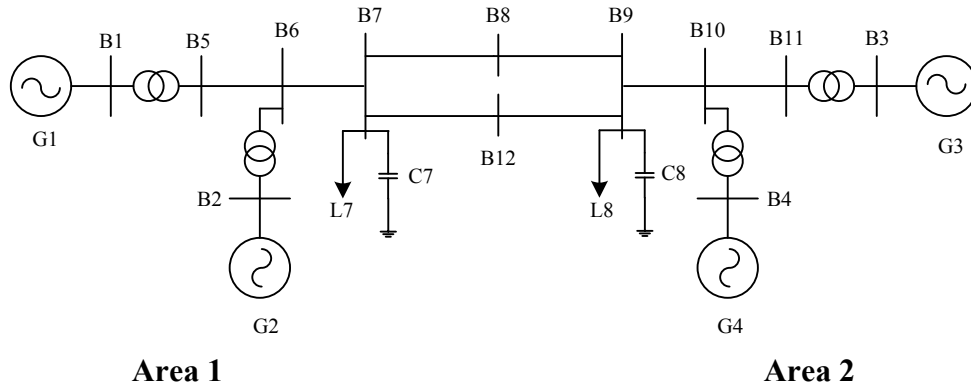
Fig. 6.2 Two-area system (Case 1)
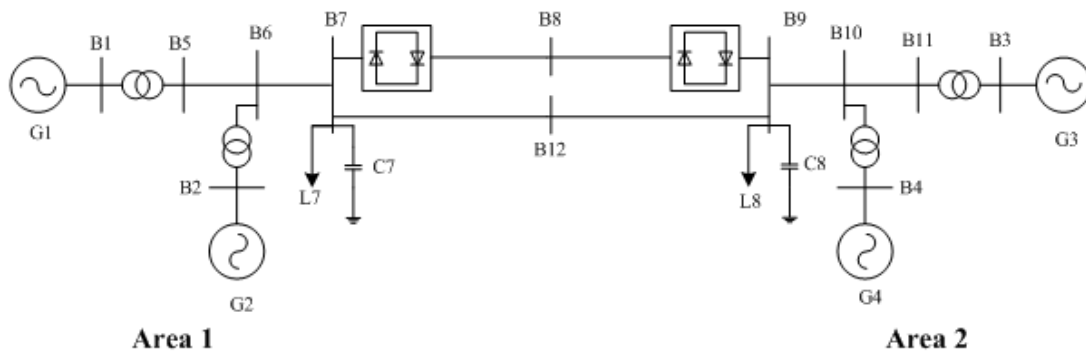
Fig. 6.3 Configuration of Case 2
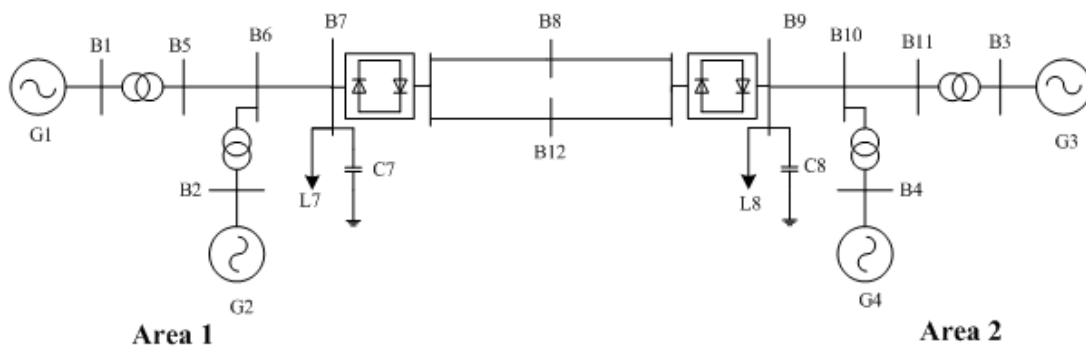
Fig. 6.4 Configuration of Case 3

6.3 Modelling of Studied Systems

In this section, the mathematical models of major electrical components in the two-area system with FFTS will be presented.

6.3.1 Synchronous Machine

The generators in the two-area system are the synchronous machines. The small signal stability model for the synchronous machine has been introduced in Chapter 3. This model is a 6th order dynamic model with six differential equations and two algebraic equations. The compact form of the model for a single synchronous machine is given by,

$$\dot{x}_{gi} \quad \quad x_{gi}, i_{gi}, u_{gi}) \tag{6.1}$$

$$i_{gi} = h_g\left(x_{gi}, v_{gi}\right) \tag{6.2}$$

where $i=1, 2, \dots, 4$; $x_{gi} = [\delta_i, \Delta\omega_i, E'_{qsi}, E'_{dsi}, \varphi_{1di}, \varphi_{2qi}]^T$, $i_{gi} = [i_{di}, i_{qi}]^T$, $u_{gi} = [T_{mi}, v_{fdi}]^T$; $v_{gi} = [\theta_i, V_i]^T$; δ_i is the angular position of rotor; $\Delta\omega_i$ is the speed deviation of rotor; E'_{ds} and E'_{qs} are the d and q axis induced transient electromagnetic force, respectively; φ_{1d} and φ_{2q} are the subtransient induced electromagnetic force; i_{di} and i_{qi} are the d and q axis stator currents, respectively; T_{mi} is the mechanical torque, v_{fdi} is the field voltage; θ_i is the angle of terminal voltage of synchronous machine; V_i is the magnitude of terminal voltage of synchronous machine.

6.3.2 Excitation System

Each synchronous machine in the two-area system includes an excitation system. The dynamics of the excitation system will influence the small signal stability of the overall system, and thus its dynamics should be considered in the modelling process. The excitation system is a thyristor exciter with high transient gain. The mathematical model of the excitation system is given by [135],

$$\dot{v} = \frac{v}{T_{Ai}} + \frac{K_{Ai}}{T_{Ai}}\left(V_{refi} - V_i\right) \tag{6.3}$$

where T_{Ai} is the time constant of regulator; K_{Ai} is the transient gain of regulator; V_{refi} is the voltage reference of excitation system.

6.3.3 Cycloconverter

In previous chapter, the model of cyclconverter considers the delay element. Under ideal condition, the cycloconverter can be modelled as an amplifier with linear gain characteristics. For the sake of simplicity, the cycloconverter in this chapter is demonstrated by an algebraic equation as (5.5).

6.3.4 Networks

In the small signal stability analysis, the transients of the networks are not considered. For a lumped radial network, the mathematical model can be represented by equation

(3.62) and (3.63) in Chapter 3. In the two-area system, the networks can be modelled by the node equations as,

$$\boldsymbol{i} = Y_{NET}\boldsymbol{V} \qquad (6.4)$$

where $\boldsymbol{i}$ is the vector of currents injection into the networks; $\boldsymbol{V}$ is the vector of bus voltages in the networks; Y_{NET} is the admittance matrix of the networks.

6.4 Eigenvalue Analysis and Time Domain Simulation

6.4.1 Eigenvalue Analysis

The first step to conduct eigenvalue analysis is to obtain the state-space model of the overall system. The overall state-space model of the studied systems can be derived by combining the linearized dynamic equations of all the electrical components.

The linearized dynamic equations for a single synchronous machine with excitation system can be obtained the mathematical model at a steady operating point. The linearized model can be written in state-space form as,

$$\Delta \dot{\boldsymbol{x}} \quad \quad \boldsymbol{x} + B_{1i}\Delta \boldsymbol{i}_{gi} + C_{1i}\Delta \boldsymbol{v}_{gi} \qquad (6.5)$$

$$D_{1i}\Delta \dot{\boldsymbol{x}} \quad \quad \boldsymbol{i}_{gi} + D_{3i}\Delta \boldsymbol{v}_{gi} = 0 \qquad (6.6)$$

where $\boldsymbol{x}_i = \left[\boldsymbol{x}_{gi}, v_{fdi} \right]^T$.

143

Then, the model of four synchronous machines with excitation systems can be represented in the state-space form as

$$\Delta \dot{x} \quad . \quad x \quad \cdot B_1 \Delta i_g + C_1 \Delta v_g \tag{6.7}$$

$$D_1 \Delta \dot{x} \quad \_ \quad i_g + D_3 \Delta v_g = 0 \tag{6.8}$$

where $\Delta x = [\Delta x_1, \cdots, \Delta x_4]^T$, $\Delta i_g = [\Delta i_{g1}, \cdots, \Delta i_{g4}]^T$, $\Delta v_g = [\Delta v_{g1}, \cdots, \Delta v_{g4}]^T$.

The linearized equation of the interconnected networks transmission line can be demonstrated as

$$\Delta i_g = Y_{NET} \Delta v_g \tag{6.9}$$

Based on equation (6.7), (6.8) and (6.9), the overall state-space model for two area system is represented by,

$$\Delta \dot{x} \quad x \tag{6.10}$$

In this chapter, the cycloconverter is modelled by an algebraic equation. So, the mathematical model of the two-area system with the FFTS (Case 2 and 3) can also be represented by equation (6.10).

For comparison, the eigenvalue analyses are carried out for Case 1, 2 and 3. There are three operating points for Case 1, 2 and 3, shown as Table 6.1. Table 6.2 shows the eigenvalue for the inter-area oscillation in Case 1, 2 and 3. From the eigenvalues in

144

Table 6.2, the damping ratio and frequency of the inter-area mode increases as more conventional AC tie lines are replaced by the FFTS under the same operating point. Furthermore, when the power flow of the tie lines increases from 200 MW to 600 MW in the same case, the damping ratio of the inter-area mode reduces and the frequency of inter-area mode changes slightly. The above results indicate that the damping performance of the inter-area mode can be improved when the FFTS is utilised as AC tie line in multi-area system.

Table 6.1 Operating points for Case 1, 2 and 3

Operating Points	Active power from Area 1 to Area 2 (MW)
1	200
2	400
3	600

Table 6.2 Eigenvalues of inter-area oscillations in Case 1, 2 and 3 under different operating points

Studied Case	Inter-area Mode	Frequency (Hz)	Damping Ratio
Case 1 (200 MW)	-0.33 ± 3.66i	0.58	0.089
Case 2 (200 MW)	-0.49 ± 4.44i	0.71	0.112
Case 3 (200 MW)	-0.59 ± 4.79i	0.76	0.121
Case 1 (400 MW)	-0.30 ± 3.65i	0.58	0.082
Case 2 (400 MW)	-0.44 ± 4.44i	0.71	0.099
Case 3 (400 MW)	-0.51 ± 4.85i	0.78	0.105
Case 1 (600 MW)	-0.17 ± 3.52i	0.56	0.048
Case 2 (600 MW)	-0.24 ± 4.34i	0.69	0.056
Case 3 (600 MW)	-0.31 ± 4.80i	0.76	0.064

6.4.2 Time Domain Simulation

To verify the result of eigenvalue analysis, the time domain simulations are conducted in PSCAD/EMTDC. The simulation platform for Case 1, 2 and 3 are established. To excite the inter-area oscillations, a three-phase ground fault happens at Bus B8 in the above three cases. The fault starts at 6.0s, and its duration time is 0.1s.

Fig. 6.5 (a), Fig. 6.6 (b) and Fig. 6.7 (c) demonstrate the active power transferred from Area 1 to Area 2 in Case 1, 2 and 3 under different operating points. The dynamic responses of the active power also indicate that the damping performance of inter-area oscillations can be improved if the conventional AC tie line is replaced by the FFTS. The results of this dynamic simulation can confirm the eigenvalue analysis.

Fig. 6.5 (a), Fig. 6.6 (b) and Fig. 6.7 (c) shows the voltage profiles at Bus B7 in Case 1, 2 and 3 under different operating points. The dynamic responses of voltage indicate that the FFTS can improve the voltage fluctuation. This improvement is also attributed to the reduced impedance of the transmission line in the FFTS.
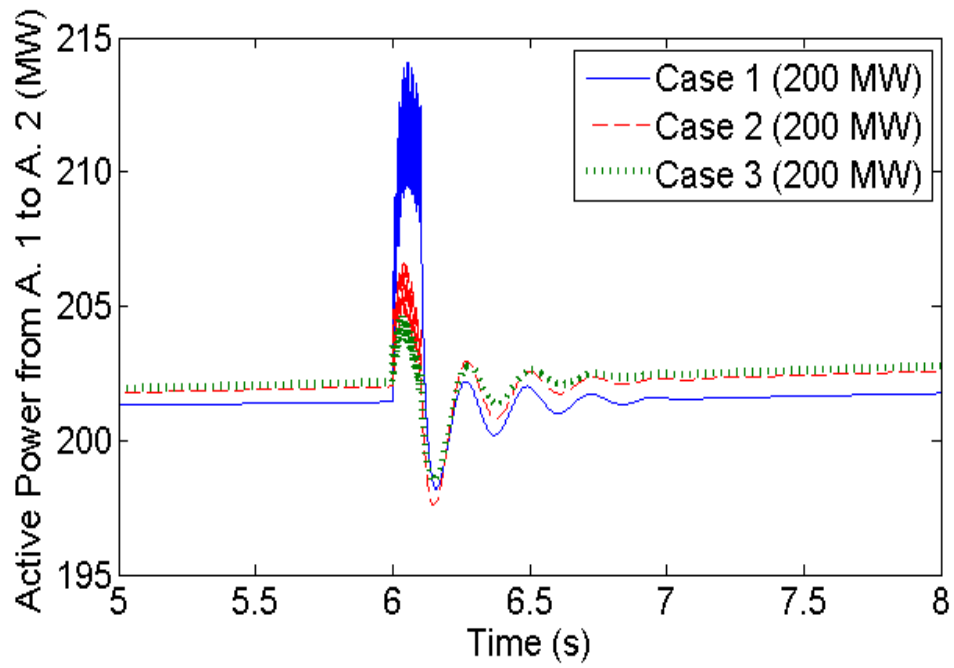
(a) Active power from Area 1 to Area 2
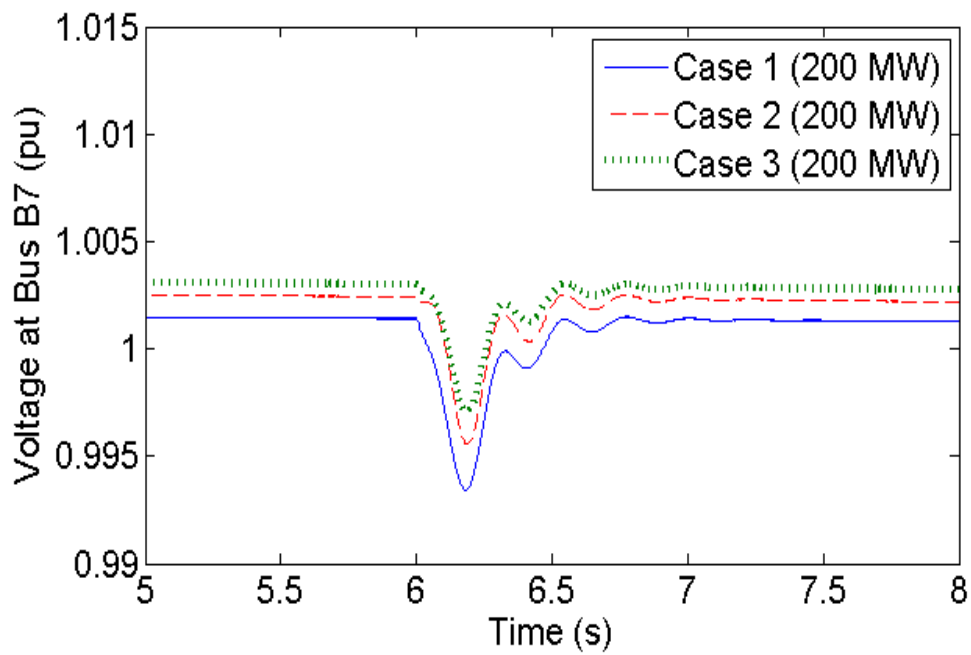
(b) Voltage profile at Bus B7

Fig. 6.5 Dynamic responses in Case 1, 2 and 3 (Operating point 1)
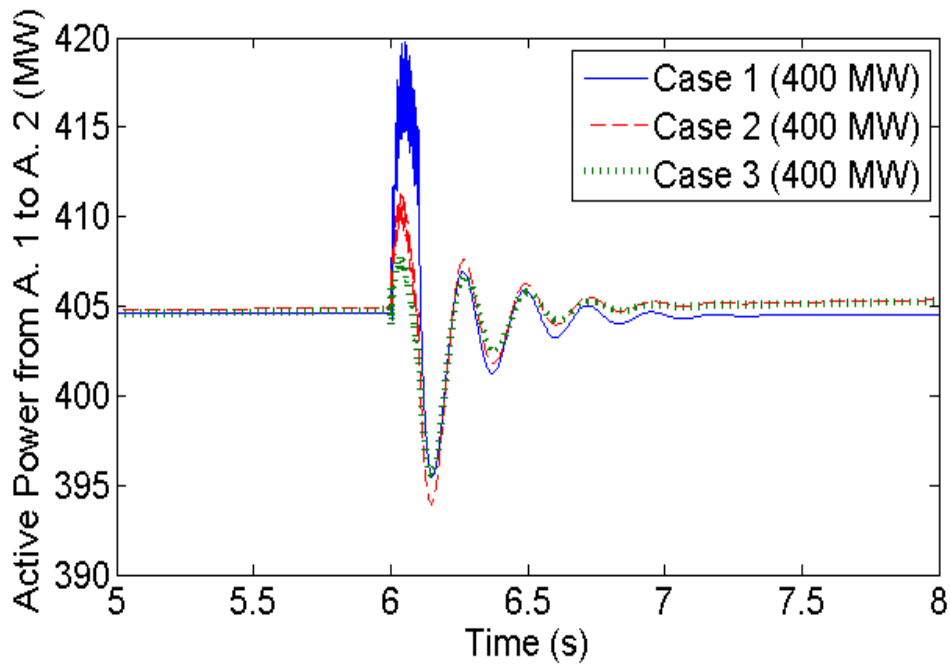
(a) Active power from Area 1 to Area 2
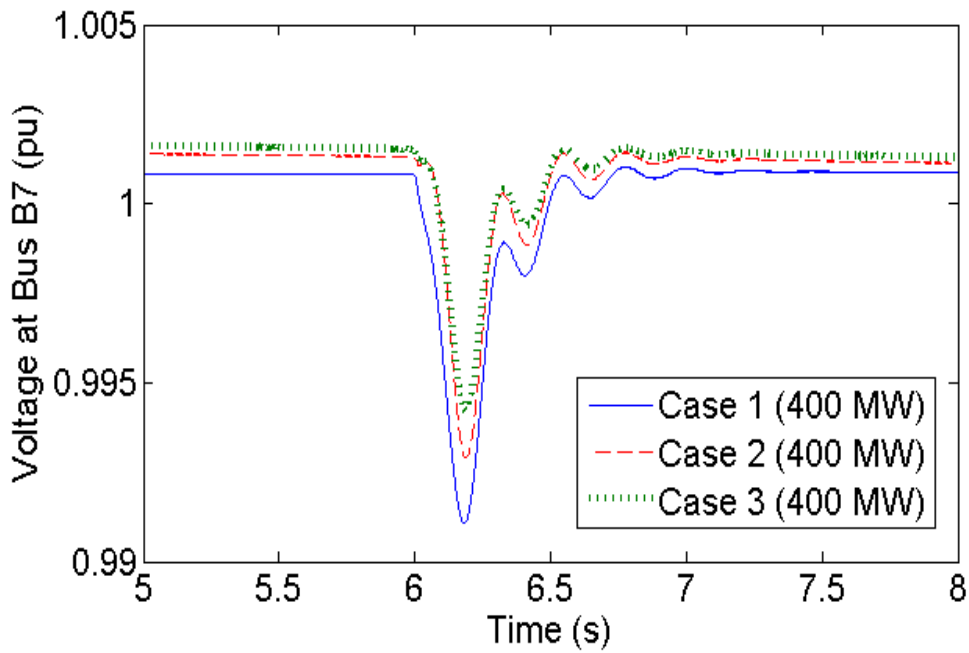
(b) Voltage profile at Bus B7

Fig. 6.6 Dynamic responses in Case 1, 2 and 3 (Operating point 2)

148
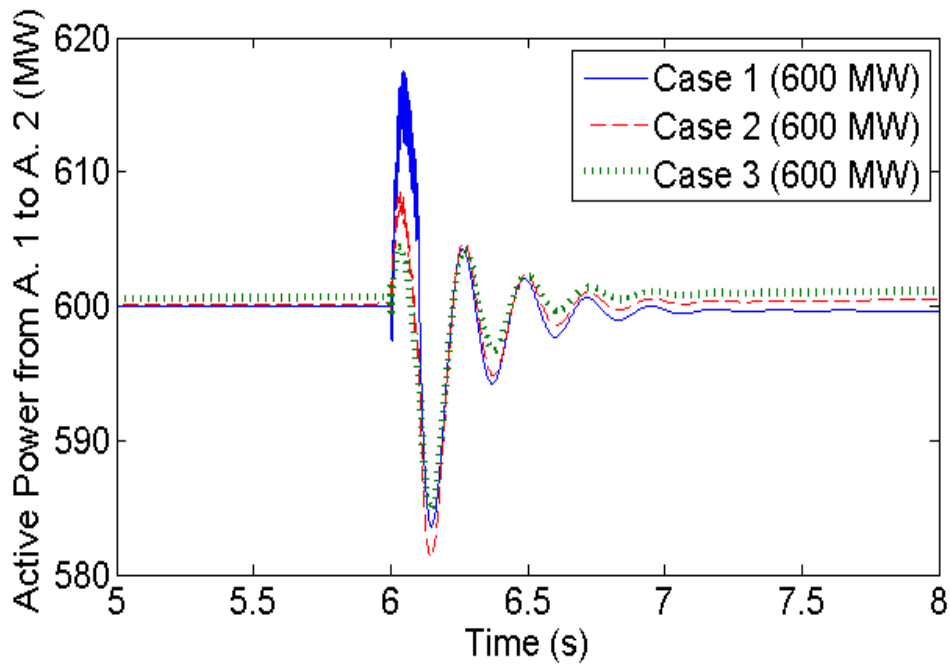
(a) Active power from Area 1 to Area 2
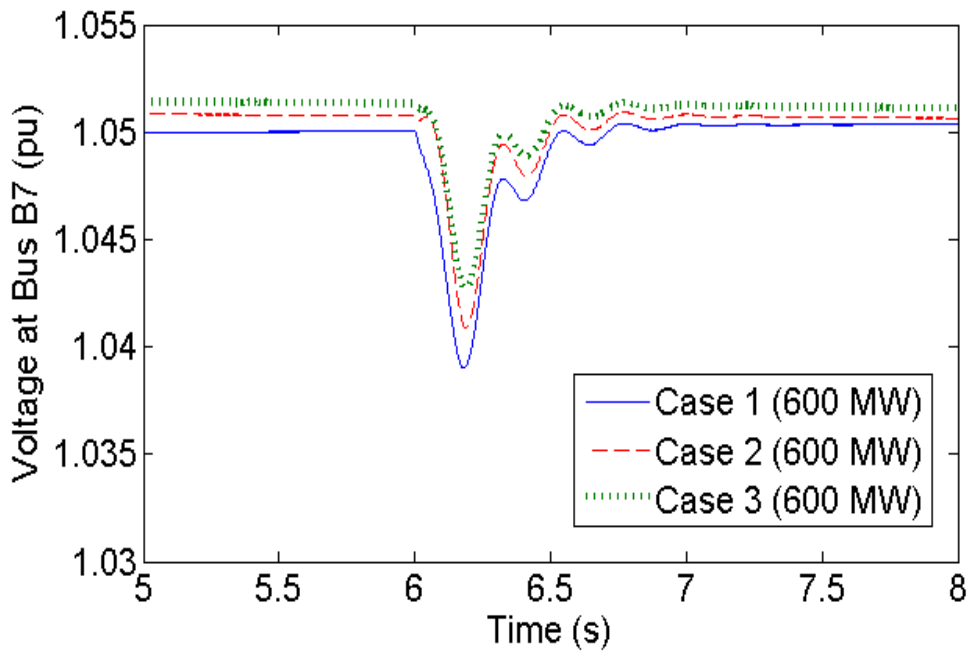
(b) Voltage profile at Bus B7

Fig. 6.7 Dynamic responses in Case 1, 2 and 3 (Operating point 1)

6.5 Power Flow Control via Cycloconverter

In the FFTS, the cycloconverters originally operate as the static frequency changer. Under this circumstance, the cycloconverter cannot control the power flow through the FFTS. In this section, the additional controller is proposed to be implemented on the cycloconverter to achieve power flow control.

The structure of FFTS for system interconnections is shown as Fig. 6.1. There are two cycloconverters at each terminal of the FFTS. The cycloconverter is a thyristor phase–controlled converter, and it is possible to design a feedback controller on it to achieve power flow control. For the sake of simplicity, only one cycloconverter is controlled, and the other cycloconverter remains as the static frequency changer.
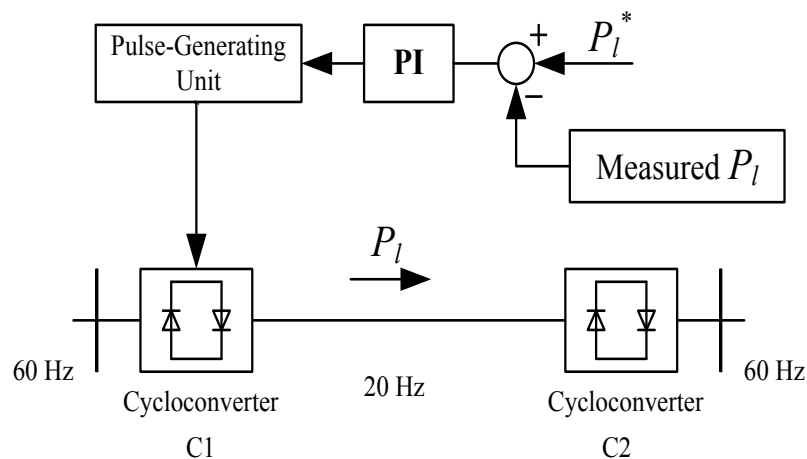
Fig. 6.8 Power flow controller for FFTS

The power flow controller on the cycloconverter is implemented as Fig. 6.8. The active power through the FFTS is chosen, and the proportional-integral (PI) controller is applied to track the control reference.

To verify the effectiveness of power flow controller, Case 4 is established as follows,

Case 4: the proposed power flow controller (as Fig. 6.8) is implemented in Case 2.

For comparison, time domain simulations for Case 2 and Case 4 are both conducted. In the following simulations, Case 2 and Case 4 are at the Operating point 2, which means 400 MW power is transferred from Area 1 to Area 2. Since there is no power flow controller, the power transferred through the FFTS and the conventional AC tie line is distributed according to the impedance of transmission lines. Consequently, the power flows through the FFTS is 300 MW, and the power flows through the conventional AC tie lines is 100 MW.

After the implementation of power flow controller on one cycloconverter in the FFTS, the power transferred through the FFTS can be regulated. If the total power transmitted from Area 1 and Area 2 remain the same, the power flows through the conventional AC tie line will change accordingly. In the following simulation, the control reference for the power transferred through the FFTS is set to 250 MW initially. Then, the control reference is changed to 350 MW at 6 s during the simulation.
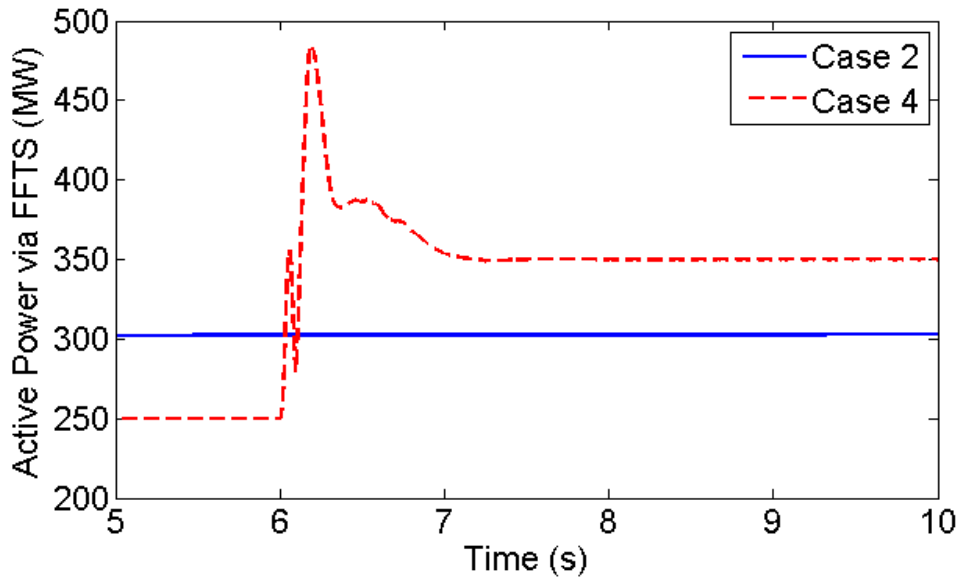
Fig. 6.9 Active power via FFTS in Case 2 and Case 4

Fig. 6.9 shows the active power transmitted through the FFTS in Case 2 and 4. The simulation result indicates that the power flow controller on the cycloconverter can successfully regulated the power flow through the FFTS. In Case 4, the power flow controller maintains the active power through the FFTS at 250 MW before 6 s. After the change of control reference, the power flow controller demonstrates its ability to track the new control reference.

Fig. 6.10 demonstrates active power transmitted through the conventional AC tie line in Case 2 and 4. In Case 4, since the total power from Area 1 and Area 2 remains the same, the power through the conventional AC tie line is changed accordingly during the simulation. Before 6 s, the active power through the conventional AC tie line is 150 MW, and the active power changes to 50 MW after 6 s.
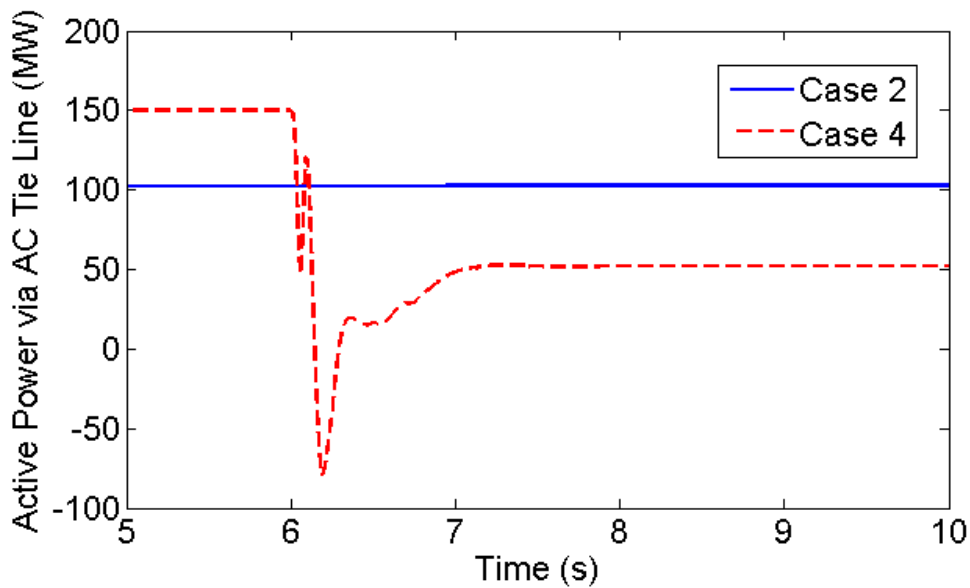
Fig. 6.10 Active power via conventional AC tie line in Case 2 and Case 4

6.6 Summary

This chapter has proposed to apply the FFTS in system interconnection. Through the FFTS, the electrical length between different areas can be reduced significantly, and thus the damping of the inter-area oscillations can also be improved. To study the benefits of the FFTS, it has been utilised to replace the conventional AC tie lines in the two-area system. The dynamic model of the two-area system with the FFTS was presented. Based on the model, the eigenvalue analysis has been conducted to investigate the influence of the FFTS on the inter-area oscillations. Then, the result of the eigenvalue analysis was confirmed through the time domain simulation. Both the eigenvalue analysis and the time domain simulations demonstrated that the damping of

the inter-area oscillation can be improved through utilisation of the FFTS. Furthermore, with additional control on the cycloconverter, the FFTS achieved the power flow control in the two-area system.

CHAPTER 7 CONCLUSION AND FUTURE RESEARCH WORK

7.1 Conclusion

The low carbon economy has become one of the most discussed issues around the world. The utilisation of renewable energy is a solution to reduce carbon emissions. Among all renewable energies, wind energy is the most widely utilised at present. With the rapid development of wind energy, large scale wind farms are integrated into power grids and provide power to meet the energy demands. Under certain circumstances, large scale wind farms are even considered to replace some conventional T-G units. Although the replacement of T-G units can reduce air pollution and protect the environment, the dynamics of the conventional power systems may be affected by the inclusion of wind energy. Previous research focused on the impact of wind energy on the small signal stability of conventional power systems. In this thesis, the influence of wind energy on conventional power systems is evaluated from the subsynchronous resonance (SSR) perspective.

On the other hand, the long distance transmission of wind energy also becomes a technical issue. In the early days, wind farms were often constructed onshore. As many

wind energy resources are located offshore, more offshore wind farms are developed to obtain energy. To cope with the long-distance delivery, the fractional frequency transmission system (FFTS) is proposed as a new solution to transmit the energy from offshore wind farms. Through reducing the transmission frequency, the capacity of the transmission line can be increased several fold. The FFTS is also very suitable to deliver offshore wind energy. The gearbox of wind turbines can be reduced in the FFTS, and the investment and maintenance costs are lower compared with the HVDC. In this thesis, a DFIG-based wind farm is proposed to be integrated in the main grid via FFTS. The dynamic performance, especially the small signal stability, of the FFTS with wind farms is the focus of this research. The damping performance of FFTS is compared with that of the conventional AC transmission system with wind farms. The method to improve the damping of FFTS is also discussed.

The FFTS can also be used in system interconnections. Through the reduced transmission frequency, the electrical length between areas is greatly decreased. Another benefit of the FFTS in grid interconnections is that it can easily form a network as the conventional AC system. Furthermore, the FFTS has the potential to control the power flow.

The main conclusions of this thesis can be summarised as follows,

1. The influence of DFIG-based wind farms on the subsynchronous resonance (SSR) of conventional power systems was systematically examined. To evaluate the impact, a new test system was modified from the IEEE first benchmark model (FBM). The SSR model of the modified test system was also presented. Based on the SSR model, the eigenvalue analysis was conducted, and the simulation platform for the test system was established in PSCAD/EMTDC. The impacts of the wind farms on the SSR of the conventional T-G unit were evaluated from the torsional interaction (TI) and induction generator effect (IGE), and the conclusions can be summarized as follows:

1) When the conventional power plants were replaced by an equivalent DFIG-based wind farm, the TI of the remaining T-G unit will become worse. The TI of the T-G unit was also found to be affected by three factors related to the wind farm: the scale of the wind farm, the rotor side controller and the operating point of the DFIG-based wind turbine. The conclusion can be expressed as follows,

- The larger the scale of wind farm, the less damping for the TI of the T-G unit.

- The inner current PI controller for the rotor side converter (RSC) in the DFIG-based wind turbine has a significant influence on the TI of the conventional T-G unit. It was found that the smaller proportional gain of the PI controller, the torsional dynamics of the T-G unit will have better damping performance.

- Under different wind speeds, the operating point of a DFIG-based wind turbine was different. The higher the rotating speed of a DFIG led to more severe torsional oscillation of the T-G unit.

2) The impact of wind energy on the IGE mainly depends on the compensation level of the series compensated transmission line. When the compensation level was high enough to excite the IGE of the test benchmark, the DFIG-based wind farm made the instability even worse. When the compensation level is low and the system can maintain the stability after the fault, the damping of IGE was improved by the DFIG-based wind farm. In addition, the IGE was also influenced by the scale of the wind farm. As more conventional power plants are substituted by DFIG-based wind farms, the damping of IGE will become worse.

2. A novel transmission system, the fractional frequency transmission system, was proposed to deliver the electricity from offshore wind farms. With the vast development of offshore wind farms, the long distance transmission of the wind energy has become a technical issue. In particular, when the transmission distance exceeded 50 km, the charging reactive current in the submarine cable reduces the amount of active current over the distance until it becomes technically impossible or economically not reasonable. The FFTS provided another technical option to solve this problem. Through the reduced transmission frequency, the FFTS can significantly increase the transmission capacity. In this thesis, a DFIG-based wind farm was integrated to the

main grid through FFTS. The wind farm directly generated electricity at 1/3 of the standard transmission frequency, and then the electricity was transmitted through the low frequency transmission line to the main grid. To analyse the dynamics, the small signal stability model of the FFTS with the DFIG-based wind farm was presented. Then the eigenvalue analysis is carried out to evaluate the damping performance of such a system. To confirm the results of the eigenvalue analysis, the time domain simulations were carried out in both the single machine infinite bus (SMIB) and the multi-machine system. The damping performance of the FFTS with wind farms can be concluded as follows,

1) Both the eigenvalue analysis and time domain simulations indicated that the FFTS with the wind farm had a worse damping performance than the traditional AC transmission system with the wind farm.

2) To improve the damping performance of the FFTS with wind farms, a feedback controller was proposed for the FFTS. This controller was implemented on the cycloconverter. With the support of this controller, the damping of wind farms with the FFTS was greatly improved and is even better than that of the wind farms with the traditional AC transmission system.

3. The FFTS was also proposed to be utilised in system interconnections. The FFTS can effectively reduce the impedance of tie lines between different areas. The model for the

FFTS in the two-area system was presented. The dynamics of such a system was studied, and the conclusions can be summarised as follows,

1) The damping performance of the inter-area oscillations in the multi-area system can be improved through the FFTS. The eigenvalue analysis and dynamic simulations were both carried out in the two-area system, and their results confirmed the above conclusion.

2) The power flow between different areas can also be controlled through the FFTS. In the FFTS, the cycloconverter originally operated as a static frequency changer. However, it is a thyristor phase–controlled converter and has the potential to control the power flow through the FFTS. This thesis proposed a power flow controller for the FFTS, and this controller was verified through the dynamic simulation on PSCAD/EMTDC.

7.2 Future Research Work

Based on the research work presented in this thesis, future studies can be continued in the following aspects:

1. In the SSR study, the DFIG-based wind farm is often represented by an aggregated single DFIG-based wind turbine. However, the wind turbines in a wind farm are operating under different conditions, and the aggregated model of wind farm will not

reflect the dynamic effects of distributed generation sources. Future research can be conducted to investigate the SSR of DFIG-based wind turbines under unequal conditions.

2. This thesis proposed to deliver the power from offshore wind farm through the FFTS, and the small signal stability analysis has been conducted for the above system. However, the transient stability and frequency stability of the FFTS with wind farms need further investigation. Furthermore, the harmonics introduced by the cycloconverters also need detailed analysis.

3. In Chapter 6, the power flow controller for the FFTS in system interconnections has been proposed. This was a preliminary design for power control, and the power flow controller was only implemented on one cycloconverter of the FFTS. Further coordinated control for both cycloconverters in the FFTS can be designed to achieve better performance.

APPENDIX

A.1 Parameters for the New Test Benchmark System in Chapter 4

A.1.1 Parameters of the IEEE First Benchmark System

1) Per-unit base values

P_b=892.4 *MVA*, V_b=539 *kV*, ω_b=376.99 *rad/s*

2) Multi-mass of turbine-generator unit

Inertia constant (*s*):

H_1=0.092897, H_2=0.155589, H_3=0.858670, H_4=0.884215, H_5=0.868495

Spring constants (*pu torque/rad*):

K_{12}=19.303, K_{23}=34.929, K_{34}=52.038, K_{45}=70.858, K_{56}=2.822

3) Generator parameters

Generator power output: P_o=0.9 *pu*

Generator power factor: *pf*=0.9 (lagging)

Stator armature resistance: R_a=0

d-axis (*pu*):

X_l=0.13, X_{ad}=1.66, X_{fd}=0.04, X_{1d}=0.00573, R_{fd}=0.00105, R_{1d}=0.003713

q-axis (*pu*):

X_l=0.13, X_{aq}=1.58, X_{1q}=0.1045, X_{2q}=0.2449, R_{1q}=0.005257, R_{2q}=0.01819

4) Series compensated transmission line

R_{TL}= 0.0187 *pu*, X_{TL}= 0.7 *pu*, X_c=0.371 *pu*

A.1.2 Parameters of a T-G Unit in GEN 2

Rated power: 89.24 *MVA*, Rated voltage: 15.01 *kV*

Stator armature resistance: 0

d-axis (*pu*):

X_l=0.13, X_{ad}=1.66, X_{fd}=0.04, X_{1d}=0.00573, R_{fd}=0.00105, R_{1d}=0.003713

q-axis (*pu*):

X_l=0.13, X_{aq}=1.58, X_{1q}=0.1045, X_{2q}=0.2449, R_{1q}=0.005257, R_{2q}=0.01819

A.1.3 Parameters of a DFIG-based Wind Turbine

1) Per unit system

S_b= 2.2 *MW*, V_b= 0.69 *kV*

2) Wind turbine

V_w=10.903 m/s, C_p=0.4382, R= 37.049 m, ρ=1.225 kg/m^3, H_t= 1 s

3) The induction machine of DFIG:

Stator resistance : R_s=0.00462 pu

Mutual inductance : L_m= 4.348 pu

Stator self-inductance : L_{ss}= 4.450 pu,

Rotor self-inductance : L_{rr}= 4.459 pu,

Rotor resistance : R_r= 0.006007 pu,

Inertia constant : H_g=0.5 s

4) AC-DC-AC converter:

C= 0.11 F, v_{DC}=1.5 kV, L_g= 0.3 pu, R_g= 0.003 pu

5) Control parameter:

K_{p1}=0.5, T_{i1}=2, K_{p2}=0.0025, T_{i2}=0.005, K_{p3}=0.5, T_{i3}=2, K_{p4}=1.5, T_{i4}=0.075, K_{p5}=1,

T_{i5}=0.02

A.2 Parameters for the Case study in Chapter 5

A.2.1 Parameters of a DFIG-Based Wind Turbine

1) Per unit system:

S_b= 2.2 *MW*, V_b= 0.69 *kV*

2) Wind Turbine:

V_w=12 *m/s*, C_p=0.4382, R= 37.049 *m*, ρ=1.225 *kg/m³*, H_t= 1 *s*

3) The induction machine of DFIG:

R_s=0.00462 *pu*, L_m= 4.348 *pu*, L_{ss}= 4.450 *pu*, L_{rr}= 4.459 *pu*, R_r= 0.006007 *pu*, H_g=0.5 *s*

4) AC-DC-AC Converter:

C= 0.11 *F*, v_{DC}=1.5 *kV*, L_g= 0.3 *pu*, R_g= 0.003 *pu*

5) Control parameter:

K_{p1}=0.5, T_{i1}=0.4, K_{p2}=0.025, T_{i2}=0.075, K_{p3}=0.5, T_{i3}=0.4, K_{p4}=1, T_{i4}=0.05, K_{p5}=0.8,

T_{i5}=0.032

A.2.2 Parameters of the transmission line

Length of the transmission line: 100 *km*

Line-to-line RMS voltage: 230 kV

Combined resistance of the transformer and transmission line: R_{TL}= 5 Ω

Combined inductance of the transformer and transmission line: L_{TL}= 0.13 H

LIST OF PUBLICATIONS & OUTCOMES

1. **Jing Li**, Xiao-Ping Zhang, "Impact of increased wind energy generation on the subsynchronous resonance of turbine-generator units," *Journal of Modern Power Systems and Clean Energy* (under second round review)

2. **Jing Li**, Xiao-Ping Zhang, "Small signal stability analysis of fractional frequency transmission systems with offshore wind farms," *IEEE Transactions on Sustainable Energy* (under third round review)

3. **Jing Li**, Xiao-Ping Zhang, "Grid interconnections via fractional frequency transmission system," *IEEE Transactions on Power Systems* (submitted)

4. Qiang Ling, **Jing Li**, and Haojiang Deng "Robust Speed Tracking of Networked PMSM Servo Systems with Uncertain Feedback Delay and Load Torque Disturbance," *Journal of Applied Mathematics* 2012 (ISSN: 1110-757X (Print))

5. **Jing Li**, Qiang Ling, and Daxin Wang, "Robust Controller Design for Network-based PMSM Servo Systems with Transmission Delay," *Proceedings of the 30th Chinese Control Conference*, 2011.6: 6568-6572

6. **Jing Li**, Qiang Ling, and Huihui Gu,"Robust Speed Tracking of Networked PMSM Servo Systems with Uncertain Delay," *Proceedings of the 23rd IEEE Chinese Control and Decision Conference*, 2011.5: 2140-2145

REFERENCES

[1] B. Fox, Q. Flynn, L. Bryans, N. Jenkins, D. Milborrow, M. O'Malley, R. Watson, and O. Anaya-Lara, *Wind Power Integration: Connection and System Operational Aspects*. The Institution of Engineering and Technology, 2007.

[2] E. Commission, Communication from the commission: energy efficiency: delivering the 20% target. November 2008.

[3] REN21, *Renewables 2014: Global Status Report* , p.13, 2014.

[4] REN21, *Renewables 2011: Global Status Report* , p.11, 2011.

[5] The World Wind Energy Association, *2014 Half-year Report*. WWEA, pp. 1-8, 2014.

[6] The European Wind Energy Association, *Wind in power: 2014 European Statistics*. Feb. 2015.

[7] Wind Power Statistics. Available: http://www.thewindpower.net/statistics_countries_en.php , retrieved 10 Sep. 2015.

[8] *UK Wind Energy Database*. Available: http://www.renewableuk.com/en/renewable-energy/wind-energy/uk-wind-energy-database/index.cfm , retrieved 10 Sep. 2015.

[9] A. Jha, "UK overtakes Denmark as world's biggest offshore wind generator," *The Guardian*, London, Oct. 2008.

[10] *World's largest offshore wind farm set to open off Kent coast*. Available: http://www.theguardian.com/business/2010/sep/12/thanet-wind-farm-energy retrieved 6 Jan. 2016.

[11] O. James, R. Mike, A.-B. Hezlin, "Will British weather provide reliable electricity," *Energy Policy*, vol. 36, pp. 2312-2325, June 2008.

[12] M. Mokhtari, J. Khazaei, and D. Nazarpour, "Sub-synchronous resonance damping via doubly fed induction generator," *Electrical Power and Energy Systems*, 53, 2013.

[13] S. O. Faired, I. Unal, and D. Rai et al, "Utilizing DFIG-based wind farms for damping subsynchronous resonance in nearby Turbine-Generator," *IEEE Transactions on Power Systems*, vol. 28, no. 1, pp. 452-459, Feb. 2013.

[14] ENTSOE, "Offshore transmission technology," *European Network of Transmission System Operators for Electricity*, 2011.

[15] Q. Nan, Y. Shi, X. Zhao and A. Vladislav, "Offshore wind farm connection with low frequency AC transmission technology," *Power and Energy Society General Meeting*, 2009, pp. 1-8.

[16] X. Wang and X. Wang, "Feasibility study of fractional transmission system," *IEEE Transactions on Power Systems*, vol. 11, no.2, pp. 962-967, May 1996.

[17] L. Ning, X. Wang, Y. Teng et al, "Experiment on wind power grid integration via fractional frequency transmission system," *Proceedings of the CSEE*, vol. 31, no. 21, July 2011.

[18] W. Fischer, R. Braun and I. Erlich, "Low frequency high voltage offshore grid for transmission of renewable power," *3rd IEEE PES Innovative Smart Grid Technologies Europe*, Berlin, 2012, pp. 1-6.

[19] Power Systems Engineering Research Center, "Low frequency transmission," *Final Project Report,* Oct. 2012.

[20] X. Wang, C. Cao and Z. Zhou, "Experiment on fractional frequency transmission system," *IEEE Transactions on Power Systems*, vol. 21, no. 1, pp. 372-377, Feb. 2006.

[21] IEEE/CIGRE Joint Task Force on Stability Terms and Definitions, "Definition and classification of power system stability," *IEEE Transactions on Power Systems*, vol. 19, no. 3, pp. 1387-1401, Aug. 2004.

[22] P. Kundur, *Power System Stability and Control*. New York: McGraw-Hill, 1994

[23] X.-F. Wang, Y. Song, M. Irving, *Modern Power Systems Analysis*. Springer, 2008.

[24] Z. Saad-Saoud, N. Jenkins, "Simple wind farm dynamic model," *IEE Proceedings-Generation, Transmission, Distribution*, vol. 142, no. 5, pp. 545-548, Sep. 1995.

[25] L. Holdsworth, X.G. Wu, J.B. Ekanayake, and N. Jenkins, "Comparison of fixed speed and doubly-fed induction wind turbines during power system disturbances," *IEE Proceedings-Electric Power Applications*, vol. 150, no. 3, pp. 343-352, May 2003.

[26] D. J. Trudnowski, A. Gentile, J. M. Khan and E. M. Petritz, "Fixed-speed wind-generator and wind-park modeling for transient stability studies," *IEEE Transactions on Power Systems*, vol. 19, no.4, pp. 1911-1917, Nov. 2004.

[27] F. Wu, X.-P. Zhang, and P. Ju, "Modeling and control of the wind turbine with the direct drive permanent magnet generator integrated to power grid," *Third International Conference on Electric Utility Deregulation and Restructuring and Power Technologies*, 2008, pp. 57-60.

[28] H. Lin, and Q. Chao, "The study of reduced-order model of the direct-drive permanent magnet generator," *2011 International Conference on Electrical and Control Engineering (ICECE)*, 2011, pp. 907-910.

[29] R. Pena, J. C. Clare, G. M. Asher, "Doubly fed induction generator using back-to-back PWM converters and its application to variable speed wind-energy generation," *IEE Proceedings-Electric Power Applications*, vol. 143, no. 3, pp. 231-241, May 1996.

[30] J. B. Ekanayake, L. Holdsworth, X. Wu, N. Jenkins, "Dynamic modeling of doubly fed induction generator wind turbines," *IEEE Transactions on Power Systems*, vol. 18, no.2, pp. 803-809, May 2003.

[31] Y. Lei, A. Mullane, G. Lightbody and R. Yacamini, "Modeling of the wind turbine with a doubly fed induction generator for grid integration studies," *IEEE Transactions on Energy Conversion*, vol. 21, no.1, pp. 257-264, Mar. 2006.

[32] I. Erlich, J. Kretschmann, J. Fortmann, S. Mueller-Engelhardt, and H. Wrede, "Modeling of wind turbines based on doubly-fed induction generators for power system stability studies," *IEEE Transactions on Power Systems*, vol. 22, no. 3, pp. 909-919, Aug. 2007.

[33] F. Wu, X.-P. Zhang, K. Godfrey, and P. Ju, "Small signal stability analysis and optimal control of a wind turbine with doubly fed induction generator," *IET Gen., Transm., Distrib.*, vol. 1, no. 5, pp. 751-760, Sep. 2007.

[34] B. C. Pal, and F. Mei, "Modelling adequacy of the doubly fed induction generator for small-signal stability studies in power systems," *IET Renewable Power Generation*, vol. 2, No. 3, pp. 181-190, Sep. 2008

[35] L. Yang, G.Y. Yang, Z. Xu, Z.Y. Dong, K.P. Wong, and X. Ma, "Optimal controller design of a doubly-fed induction generator wind turbine system for small signal stability enhancement," *IET Generation, Transmission and Distribution*, vol. 4, no. 5, pp. 579-597, 2010

[36] L. Yang, Z. Xu, J. Østergaard, and Z. Y. Dong et al., "Oscillatory stability and eigenvalue sensitivity analysis of a DFIG wind turbine system," *IEEE Transactions on Energy Conversion*, vol. 26 , no. 1, pp. 328-339, Mar. 2011.

[37] J. G. Slootweg, W. L. Kling, "The impact of large scale wind power generation on power system oscillations," *Electric Power Systems Research*, vol. 67, pp. 9-20, 2003.

[38] E. Hagstrøm, I. Norheim and K. Uhlen, "Large-scale wind power integration in Norway and impact on damping in the Nordic Grid," *Wind Energy*, vol.8, pp. 375-384, July, 2005.

[39] E. Muljadi, C. P. Butterfield, B. Parsons, and A. Ellis, "Effect of variable speed wind turbine generator on stability of a weak grid," *IEEE Transactions on Energy Conversion*, vol. 24 , no. 3, pp. 1426-1434, Aug. 2009.

[40] D. Thakur, N. Mithulananthan, "Influence of constant speed wind turbine generator on power system oscillation**,"** *Electric Power Components and Systems*, vol. 37, iss. 5, 2009

[41] D. Gautam, V. Vittal, and T. Harbour, "Impact of increased penetration of DFIG-based wind turbine generators on transient and small signal stability of power systems," *IEEE Transactions on Power Systems*, vol. 24 , no. 3, pp. 1426-1434, Aug. 2009.

[42] P. He, F. Wen, G. Ledwich, and Y. Xue, "Small signal stability analysis of power systems with high penetration of wind power," *Journal of Modern Power System and Clean Energy*, vol.1, no.3, pp. 241-248, 2013.

[43] IEEE Committee Report by Subsynchronous Resonance Working Group of the System Dynamic Performance Subcommittee, "Reader's guide to

subsynchronous resonance," *IEEE Transactions on Power Systems*, vol. 7, no. 1, pp. 150-151, Feb. 1992.

[44] H. M. Rustebakke, C. Concordia, "Self-excited oscillations in a transmission system using series capacitors," *IEEE Transactions on Power Apparatus and Systems*, vol. PAS-89, no. 7, pp. 1504-1512, Sep./Oct. 1970.

[45] D. N. Walker, C. E. J. Bowler, R. L. Jackson, and D. A. Hodges, "Results of subsynchronous resonance test at Mohave," *IEEE Transactions on Power Apparatus and Systems*, vol. PAS-94, no. 5, pp. 1878-1889, Sep./Oct. 1975.

[46] R. G. Farmer, and A. L. Schwalb, "Navajo project report on subsynchronous resonance analysis and solution," *IEEE Transactions on Power Apparatus and Systems*, vol. PAS-96, no. 4, pp. 1226-1232, July/Aug. 1977.

[47] E. W. Kimbark, "How to improve system stability without risking subsynchronous resonance," *IEEE Transactions on Power Apparatus and Systems*, vol. PAS-96, no. 5, pp. 1608-1618, Sep./Oct. 1977.

[48] L. A. Kilgore, D. G. Ramey, and M. C. Hall, "Simplified transmission and generation system analysis procedures for subsynchronous resonance problems," *IEEE Transactions on Power Apparatus and Systems*, vol. PAS-96, no. 6, pp. 1840-1846, Nov./Dec. 1977.

[49] IEEE Subsynchronous Resonance Task Force of the Dynamic System Performance Working Group, Power System Engineering Committee, "First benchmark model for computer simulation of subsynchronous resonance," *IEEE Transactions on Power Apparatus and Systems*, vol. PAS-96, no. 5, pp. 1565-1572, Sep./Oct. 1977.

[50] IEEE Subsynchronous Resonance Working Group of the Dynamic System Performance Subcommittee, Power System Engineering Committee, "Second benchmark model for computer simulation of subsynchronous resonance," *IEEE Transactions on Power Apparatus and Systems*, vol. PAS-104, no. 5, pp. 1057-1066, May 1985.

[51] IEEE Subsynchronous Resonance Working Group of the System Dynamic Performance Subcommittee, Power System Engineering Committee, "Proposed terms and definitions for subsynchronous oscillations," *IEEE Transactions on Power Apparatus and Systems*, vol. PAS-99, no. 2, pp. 1326-1334, March/April1980.

[52] IEEE Committee Report, "Second supplement to a bibliography for the study of subsynchronous resonance between rotating machines and power systems," *IEEE Transactions on Power Apparatus and Systems*, vol. PAS-104, no. 2, pp. 830-834, Feb. 1985.

[53] IEEE Subsynchronous Resonance Working Group of the System Dynamic Performance Subcommittee, Power System Engineering Committee, "Terms, definitions and symbols for subsynchronous oscillations," *IEEE Transactions on Power Apparatus and Systems*, vol. PAS-104, no. 6, pp. 1326-1334, June

1985.

[54] IEEE Committee Report, "Third supplement to a bibliography for the study of subsynchronous resonance between rotating machines and power systems," *IEEE Transactions on Power Systems*, vol. 6, no. 2, pp. 321-327, May 1991.

[55] IEEE Committee Report by Subsynchronous Resonance Working Group of the System Dynamic Performance Subcommittee, "Reader's guide to subsynchronous resonance," *IEEE Transactions on Power Systems*, vol. 7, no. 1, pp. 150-151, Feb. 1992.

[56] P. M. Anderson, B. L. Agrawal, and J. E. Van Ness, *Subsynchronous Resonance in Power System*. New York: IEEE Press, 1990.

[57] H. Ghasemi, G. B. Gharehpetian, S. A. Nabavi-Niaki, and J. Aghaei, "Overview of subsynchronous resonance analysis and control in wind turbines," *Renewable and Sustainable Energy Reviews*, vol. 27, pp. 234-243, 2013.

[58] L. Fan, R. Kavasseri, Z. L. Miao, and C, Zhu, "Modeling of DFIG-based wind farms for SSR analysis," *IEEE Transactions on Power Delivery*, vol. 25, no. 4, pp. 2073-2082, Oct. 2010.

[59] E. H. Larsen, and D. H. Baker, "Series compensation operating limits-a new concept for subsynchronous resonance stability analysis," *IEEE Transactions on Power Apparatus and Systems*, vol. PAS-99, no. 5, pp. 1855-1863, Sept./Oct. 1980.

[60] R. A. Achilles, and A. R. Ramirez, "An in-depth analysis of critical parameters affecting loading SSR countermeasures," *IEEE Transactions on Power Apparatus and Systems*, vol. PAS-104, no. 2, pp. 357-367, Feb. 1985.

[61] N. Uchida, and T. Nagao, "A new eigen-analysis method of steady-state stability studies for large power systems: a matrix method," *IEEE Transactions on Power Systems*, vol. 3, no. 2, pp. 706-714, May 2013.

[62] B. L. Agrawal, and R. G. Farmer, "Use of frequency scanning techniques for subsynchronous resonance analysis," *IEEE Transactions on Power Apparatus and Systems*, vol. PAS-98, no. 2, pp. 341-349, March/April 1979.

[63] H. W. Dommel, "Digital computer solution of electromagnetic transients in single-and multi-phase networks," *IEEE Transactions on Power Apparatus and Systems*, vol. PAS-88, pp. 388-399, April 1969.

[64] G. Gross, and M. C. Hall, "Synchronous machine and torsional dynamics simulation in the computation of electro-magnetic transient," *IEEE Transactions on Power Apparatus and Systems*, vol. PAS-91, no. 4, pp.1074- 1086, July/Aug. 1978.

[65] IEEE Committee Report, "Countermeasure to subsynchronous resonance problem," *IEEE Transactions on Power Apparatus and Systems*, vol.PAS-99, no. 5, pp. 1810- 1818, Sep./Oct. 1980.

[66] N. G. Hingorani, "A new scheme for subsynchronous resonance damping of torsional oscillations and transient torques-Part I," *IEEE Transactions on Power*

Apparatus and Systems, vol. PAS-100, no. 4, pp. 1852-1855, April 1981.

[67] R. A. Hedin, K. B. Stump, and N. G. Hingorani, "A new scheme for subsynchronous resonance damping of torsional oscillations and transient torques-Part II," *IEEE Transactions on Power Apparatus and Systems*, vol. PAS-100, no. 4, pp. 1856-1863, April 1981.

[68] C. E. J. Bowler, D. H. Baker, N. A. Mincer, and P. R. Vandiveer, "Operation and test of the Navajo SSR protective equipment," *IEEE Transactions on Power Apparatus and Systems*, vol. PAS-97, no. 4, pp. 1030-1035, July/Aug. 1978.

[69] C. E. J. Bowler, J. A. Demcko, L. Menkoft, W. C. Kotheimer, and D. Cordray, "The Navajo SMF type subsynchronous resonance relay," *IEEE Transactions on Power Apparatus and Systems*, vol. PAS-97, no.5, pp. 1489-1495,Sep./Oct. 1978.

[70] S. C. Sun, S. Salowe, E. R. Taylor, and C. R. Mummert, "A subsynchronous oscillation relay-type SSO,"*IEEE Transactions on Power Apparatus and Systems*, vol. PAS-100, no. 7, pp. 3580-3589, July 1981.

[71] IEEE Committee Report, "Series capacitor controls and settings as a countermeasure to subsynchronous resonance," *IEEE Transactions on Power Apparatus and Systems*, vol. PAS-101, no. 6, pp. 1281-1287, June 1982.

[72] R. J. Piwko, N. Rostamkolai, E. V. Larsen, D. A. Fisher, M. A. Mobarak, A. E. Poitras, "Subsynchronous torsional interactions with static VAR compensators-concepts and practical implications," *IEEE Transactions on Power Systems*, vol. 5, no. 4, pp. 1324-1332, Nov. 1990.

[73] D. Limebeer and R. Harley, "Subsynchronous resonance of single-cage induction motors," *IEE Proc. Electric Power Applications*, vol. 128, no.1, pt. B, pp. 33–42, Jan. 1981.

[74] R. K. Varma, S. Auddy, and Y. Semsedini, "Mitigation of subsynchronous resonance in a series-compensated wind farm using FACTS controllers" *IEEE Transactions on Power Delivery*, vol. 23, no. 3, pp. 1645-1654, pp. 429-441, July 2008.

[75] M. S. El-Moursi, B. Bak-Jensen, and M. H. Abdel-Rahman, "Novel STATCOM controller for mitigating SSR and damping power system oscillations in a series compensated wind park," *IEEE Transactions on Power Electronics*, vol. 25, no. 2, Feb. 2010.

[76] A. Tabesh, and R. Iranvani, "Small-signal dynamic model and analysis of a fixed speed wind farm-a frequency response approach," *IEEE Transactions on Power Delivery*, vol. 21, no. 2, pp. 778-787, April 2006.

[77] H. T. Ma, P. B. Brogan, K. H. Jensen, and R. J. Nelson, "Sub-synchronous control interaction studies between full-converter wind turbines and series-compensated AC transmission lines," *IEEE Power and Energy Society General Meeting,* 2012.

[78] L. Harnefors, M. Bongiorno, and S. Lundberg, "Input-admittance calculation and shaping for controlled voltage-source converters," *IEEE Transactions on Industrial Electronics*, vol. 54, no. 6, pp. 984-991, Dec. 2007.

[79] A. Ostadi, A. Yazdani, and R. K. Varma, "Modeling and stability analysis of a DFIG-based wind-power generator interfaced with a series-compensated line," *IEEE Transactions on Power Delivery*, vol. 24, no. 3, pp. 1504-1514, July 2009.

[80] Z. Miao, "Impedance-model-based SSR analysis for type 3 wind generator and series-compensated network," *IEEE Transactions on Energy Conversion*, vol. 27, no. 4, pp. 984-991, Dec. 2012.

[81] D. H. R. Suriyaarachchi, U. D. Annakkage, C. Karawita, and D. A. Jacobson,"A procedure to study sub-synchronous interactions in wind integrated power systems,"*IEEE Transactions on Power Systems*, vol. 28, no. 1, pp. 377-384,Feb. 2013

[82] X. Wang, X. Wang and Y. Teng, "Fractional frequency transmission system and its application," *Proceedings of the CSEE*, vol. 32, no. 13, pp. 1-6, May 2005

[83] O. I. Elgerd, *Electric Energy Systems Theory*. New York: McGraw-Hill, 1985.

[84] X. Wang, "The fractional frequency transmission system," in *Proceedings of IEE Japan Power Energy*, Tokyo, Japan, pp.53-58, July 1994

[85] X. Wang, Y. Teng, L. Ning, Y. Meng, and Z. Xu, "Feasibility of integrating large wind farm via fractional frequency transmission system a case study," *International Transactions on Electrical Energy Systems*, vol. 24, Iss.1, pp. 64–74, Jan. 2014.

[86] S.M. Muyeen, M. H. Ali, R. Takahashi, T. Murata, J. Tamura, Y. Tomaki, A. Sakahara and E. Sasano, "Comparative study on transient stability analysis of wind turbine generator system using different drive train models," *IET Renewable Power Generation,* vol.1, no.2, pp. 131–141, 2007.

[87] P. S. Sauer, and M. A. Pai, *Power System Dynamics and Stability*. New Jersey: Prentice Hall, 1994.

[88] Y. Mishra, S. Mishra, M. Tripathy, N. Senroy, and Z. Y. Dong, "Improving stability of a DFIG-based wind power system with tuned damping controller," *IEEE Transactions on Power Systems*, vol. 24, no.3, pp. 650-660, Sept. 2009.

[89] K. Zhang, J. Wang and X. Wang, "Study on Synthesis Stability Control of the Fractional Frequency Transmission System," *Proceedings of the CSEE*, vol. 21, no. 12, Nov. 2005.

[90] P. B. Wyllie, Y. Tang, L. Ran, T. Yang, J. Yu, "Low frequency AC transmission-elements of a design for wind farm connection," *11th International Conference on AC and DC Power Transmission*, 2015.

[91] C. Nguyen Mau, K. Rudion, A. Orths, P. B. Eriksen, H. Abildgaard, and Z. A. Styczynski, "Grid connection of offshore wind farm based DFIG with low frequency AC transmission system," *IEEE Power and Energy Society General*

Meeting, 2012.

[92] Y. Teng, X. Wang, and M. Deng, "Cycloconverter non-conduction fault and related problems in fractional frequency transmission systems," *Automation of Electric Power System*, vol. 32, no. 7, April 2008.

[93] Y. Teng and X. Wang, "Three-phase short-circuit fault on the lower frequency bus of cycloconverter in FFTS," *PSCE '09 Power System Conference and Exposition,* 2009, pp.1-5.

[94] Y. Cho, G. J. Cokkinides, A. P. Meliopoulos, "Time domain simulation of a three-phase cycloconverter for LFAC transmission systems," *2012 Power and Energy Society Transmission and Distribution Conference and Exhibition*, Orlando, Florida, May 2012, pp. 1-7.

[95] L. Ning, X. Wang, Y. Teng, "Experiment on wind power integration grid via fractional frequency transmission system," *4th International Conference on Electric Utility Deregulation and Restructuring and Power Technologies (DRPT)*, 2011.

[96] Y. Cho, G. J. Cokkinides, A. P. Meliopoulos, "Advanced Time Domain Method for Remote Wind Farms with LFAC Transmission Systems: Power Transfer and Harmonics," in *2012 North American Power Symposium*, Urbana, Illinois, Sep. 2012.

[97] Z. Song, X. Wang, Y. Teng et al, "Optimal Control Study for Fractional Frequency Wind Power System," *Asia-Pacific Power and Energy Engineering Conference (APPEEC)*, 2012.

[98] T. Lei, M. Ozakturk, M. Barnes, "Modelling and analysis of DFIG wind turbine system in PSCAD/EMTDC," *6th IET International Conference on Power Electronics, Machines and Drives (PEMD)*, 2012.

[99] T. Lei, M. Barnes, M. Ozakturk, "Doubly-fed induction generator wind turbine modelling for detailed electromagnetic system studies," *IET Renewable Power Generation*, vol. 7, no.2, pp. 180-189, 2013.

[100] Y. Mishra, S. Mishra, F. Li, Z. Y. Dong, and R. C. Banal, "Small-signal stability analysis of a DFIG-based wind power system under different modes of operation," *IEEE Transactions on Energy Conversion*, vol. 24, no. 4, pp. 972-982, Dec. 2009.

[101] M. Parniani, and M. R. Iravani, "Computer analysis of small-signal stability of power systems including network dynamics," *IEE Proceedings-Generation, Transmission and distribution*, vol. 142, no. 6, pp. 613-617, Nov. 1995.

[102] L. M. Fernandez, F. Jurado, and J. R. Saenz, "Aggregated dynamic model for wind farms with doubly fed induction generator wind turbines," *Renewable Energy*, vol. 33, pp. 129-140, 2008.

[103] H. Chen, M. H. Johnson, and D. C. Aliprantis, "Low-frequency AC transmission for offshore wind power, " *IEEE Transactions on Power Delivery*, vol. 28, no. 4, pp. 2236-2244, Oct. 2013.

[104] X. Wang, X. Wei, and Y. Meng, "Experiment on grid-connection process of wind turbines in fractional frequency wind power system," *IEEE Transactions on Energy Conversion*, vol. 30, no. 1, pp. 22-31, March 2015.

[105] P. Achara, and T. Ise, "Operating phase and frequency selection of low frequency AC transmission system using cycloconverters," *2014 International Power Electronics Conference*, 2014, pp. 3687-3694.

[106] M. Klein, G. J. Rogers, and P. Kundur, " A fundamental study of inter-area oscillations in power systems," *IEEE Transactions on Power Systems*, vol. 6, no. 3, pp. 914-921, Aug. 1991.

[107] L. Wang, and D.-N. Truong, "Stability enhancement of DFIG-based offshore wind farm fed to a multi-machine system using a STATCOM," *IEEE Transactions on Power Systems*, vol. 28, no. 3, pp. 2882-2889, Aug. 2013.

[108] L. Fan, and Z. Miao, "Mitigating SSR using DFIG-based wind generation," *IEEE Transactions on Sustainable Energy*, vol. 3, no. 3, pp. 349-358, July 2012.

[109] A. E. Leon, J. M. Mauricio, and J. A. Solsona, "Subsynchronous resonance mitigation using variable-speed wind energy conversion systems," *IET Generation, Transmission and Distribution*, vol. 7, iss. 5, pp. 511-525, 2012.

[110] I. A. Hiskens, "Dynamics of type-3 wind turbine generator models," *IEEE Transactions on Power Systems*, vol. 27, no. 1, pp. 465-474, Sep. 2011.

[111] F. Hughes, O. Anaya-Lara, N. Jenkins, and G. Strbac, "Control of DFIG-based wind generation for power network support," *IEEE Transactions on Power System*, vol. 20, no. 4, pp. 1958-1966, Nov. 2005.

[112] Z. Miao, L. Fan, D. Osborn, and S. Yuvarajan, "Control of DFIG-based wind generation to improve interarea oscillation damping," *IEEE Transactions on Energy Conversion*, vol. 24, no. 2, pp. 415-422, June 2009.

[113] L. Fan, H. Yin, and Z. Miao, "On active/reactive power modulation of DFIG-based wind generation for interarea oscillation damping," *IEEE Transactions on Energy Conversion*, vol. 26, no. 2, pp. 513-521, June 2011.

[114] G. Tsourakis, B. M. Nomikos, and C. D. Vournas, "Contribution of doubly fed wind generators to oscillation damping," *IEEE Transactions on Energy Conversion*, vol. 24, no. 3, pp. 783-791, Sep. 2009.

[115] J. B. Ekanayake, L. Holdsworth, and N. Jenkins, "Comparison of 5th order and 3rd order machine models for doubly fed induction generator (DFIG) wind turbines," *Electric Power System Research*, vol. 67, pp. 207-215, 2003.

[116] X. Wang, X. Wang and Z. Bie, "Integrating wind farm into grid via FFTS," in *Proceedings of 5th Nordic Wind Power Conference*, Bornholm, Denmark, Sep. 2009.

[117] L. Yang, Z. Xu, J. Østergaard, Z. Y. Dong and K. P. Wang, "Advanced control strategy of DFIG wind turbines for power system fault ride through," *IEEE Transactions on Power Systems*, vol. 27, no. 2, May 2012.

[118] F. Wu, X.-P. Zhang, P. Ju, and M. J. H. Sterling, "Decentralized nonlinear

control of wind turbine with doubly fed induction," *IEEE Transactions on Power Systems*, vol. 18, no. 2, May 2008.

[119] B. R. Pelly, *Thyristor Phase-Controlled Converters and Cycloconverters*. New York: Wiley, 1971.

[120] B. K. Bose, *Modern Power Electronics and AC Drives*. New Jersey: Prentice Hall, 2002r.

[121] P. Ledesma, and J. Usaola, "Effect of neglecting stator transients in doubly fed induction generators models," *IEEE Transactions on Energy Conversion*, vol. 19, no. 2, June 2004.

[122] S. Bozhko, R. V. Blasco-Gimenez, R. Li, J. Clare, and G. Asher, "Control of offshore DFIG-based wind farm grid with line-commutated HVDC connection," *IEEE Transactions on Energy Conversion*, vol. 22, no. 1, Mar. 2007.

[123] D. Xiang, L. Ran, J. R. Bumby, P. J. Tavner, and S. Yang, "Coordinated control of an HVDC link and doubly fed induction generation in a large offshore wind farm," *IEEE Transactions on Power Delivery*, vol. 21, no. 1, Jan. 2006.

[124] T. Funnki, and K. Matsuura, "Feasibility of the low frequency AC transmission," *IEEE Power Engineering Society Winter Meeting*, 2000, pp. 2693-2698.

[125] R. Asad and A. Shoulaie, "Determination, simulation and implementation of a novel improved industrial cycloconverter," *International Transactions on Electrical Energy Systems*, 2011.

[126] L. Wang and K.-H.Wang, "Dynamic stability analysis of a DFIG-based offshore wind farm connected to a power grid through an HVDC link," *IEEE Transactions on Power Systems*, vol. 26, no. 3, Aug. 2011.

[127] T. Lei, M. Barnes, and M. Ozakturk, "Doubly-fed induction generator wind turbine modeling for detailed electromagnetic system studies," *IET Renewable Power Generation*, vol. 7, iss. 2, 2013.

[128] L. Fan, Chanxia Zhu, Zhixin Miao, and M. Hu, "Modal analysis of a DFIG-based wind farm interfaced with a series compensated network," *IEEE Transactions on Energy Conversion*, vol. 26, no. 4, Dec. 2004.

[129] B. G. Lamme, "The technical story of the frequencies," *Transactions AIEE*, Jan. 1918.

[130] M. D. Prada, F. Mancilla-David, and J. L. Dominguez-Garcia et al, "Contribution of type-2 wind turbines to sub-synchronous resonance damping," *Electrical Power and Energy Systems*, vol. 55, 2014.

[131] M. Jafarian, A. M. Ranjbar, "The impact of wind farms with doubly fed induction generators on power system electromechanical oscillations," *Renewable Energy*, vol. 50, 2013.

[132] K. Weiland, "New technological challenges operating the 110 kV, 16.7 Hz grid for railway power supply in Germany," *Proceedings of the 20th international conference on electricity distribution*, 2009, pp. 29-33.

[133] A. Pfeiffer, W. Scheidl, M. Eitzmann, and E. Larsen, "Modern rotary converters

for railway applications," *Proceedings of the 1997 IEEE/ASME joint railroad conference*, 2009.

[134] B. K. Bose, M.-H. Kin, and M. D. Kankam, "High frequency ac vs dc distribution system for next generation hybrid electric vehicle," *Proceedings of the IEEE IECON*, Aug. 5-10, 1996, pp. 706–712.

[135] G. Rogers, *Power System Oscillations*, Kluwer Academic Publishers, 2000.

[136] P. Jain, M. Pahlevaninezhad, S. Pan, and J. Drobnik, "A review of high-frequency power distribution systems: for space, telecommunication, and computer applications," *IEEE Transactions on Power electronics*, vol. 29, no. 8, Aug. 2014.